Effect of an Open Water Body on Tsunami Inundation and Forces exerted on a Structure

Reza Arefiseresht

Thesis submitted to the University of Ottawa in partial fulfillment of the requirements for the

Doctorate in Philosophy Civil Engineering

Academic advisors:

Prof. Ioan Nistor and Prof. Abdolmajid Mohammadian

Department of Civil Engineering
Faculty of Engineering
University of Ottawa

To the one who made every difficult day worthwhile,

and every achievement feel complete

My love, Atefeh

Acknowledgements

First and foremost, I would like to express my sincere gratitude to my supervisors, Dr. Nistor and Dr. Mohammadian, whose unwavering guidance, support, and dedication made the completion of this thesis possible. Their expertise, encouragement, and patience throughout this journey have been invaluable, and I am truly fortunate to have had the opportunity to work under their supervision.

I would also like to extend my appreciation to Dr. Elsheikh for his generous assistance during all stages of the experimental setup. His technical knowledge and willingness to help were instrumental in the success of the laboratory work.

My thanks also go to Mr. Lapointe, the laboratory technician, whose practical support and readiness to help at every turn made the experimental work run smoothly.

On a personal note, I am deeply grateful to my parents, whose endless encouragement and belief in me have been a constant source of strength throughout my academic journey. Their support has always been my foundation.

Finally, and most importantly, I wish to dedicate my deepest gratitude to my wife and my son. They endured the long hours, the stress, and the challenges that inevitably come with a journey of this magnitude, and yet they never stopped believing in me. Their love, patience, and sacrifices have meant everything, and this work is as much theirs as it is mine.

Abstract

Tsunamis are highly destructive natural hazards that pose severe risks to coastal communities and infrastructure. Their unpredictable occurrence, long wavelengths, and large flow depths often generate extreme loads that can exceed the resistance of coastal and onshore structures. Recent tsunami events have demonstrated that even engineered buildings and protective systems may suffer significant damage or failure, underscoring the need for effective mitigation strategies capable of reducing flow energy and structural loading before impact. Consequently, both engineered and nature-based countermeasures have been explored to attenuate tsunami energy, protect built infrastructure, and reduce loss of life. Among engineered mitigation measures, water-filled canals located upstream of coastal infrastructure have been identified as a potentially effective yet relatively under-investigated solution. Field observations and recent studies suggest that such canals can modify bore propagation by inducing flow deceleration and redistributing momentum prior to interaction with downstream structures. However, the hydrodynamic interaction between tsunami bores, water-filled canals, and structural elements remains complex and insufficiently understood. This study investigates the effectiveness of rectangular water-filled canals as a tsunami mitigation countermeasure through a combination of laboratory-scale experiments and calibrated numerical simulations. A series of physical experiments was conducted at a 1:10 geometric scale to reproduce tsunami-like bores using a rapid-release gate mechanism, analogous to a dam-break flow. This approach enabled controlled and repeatable generation of bores with well-defined initial conditions. Bore depth time histories were measured at several locations along the flume to capture the evolution of the flow before, and after the canal. A rigid square column was installed downstream of the canal, and a loadcell was used to record horizontal force time histories during bore impact. The canal geometry was systematically varied to evaluate its influence on bore transformation and structural loading. The experimental results indicate that the presence of a water-filled canal significantly alters bore characteristics, most notably by reducing the bore front velocity prior to impact. Under the tested conditions, the canal reduced the peak horizontal force acting on the downstream column compared to the no-canal configuration. To extend the investigation beyond laboratory-scale constraints and to examine a wider range of canal geometries, numerical simulations were performed using the FLOW-3D computational fluid dynamics model. The numerical model was

calibrated against the experimental measurements to ensure accurate reproduction of free-surface evolution, bore propagation, and force response. Following validation, the model was applied at prototype scale to simulate a tsunami-like bore generated by a 4 m-deep dam-break flow interacting with water-filled canals of varying widths and depths. The numerical results corroborate the experimental findings and provide further insight into the role of canal geometry in force mitigation. The simulations demonstrate that horizontal force reduction is strongly dependent on canal dimensions, with canal width exerting a substantially greater influence than canal depth. Maximum force reductions of approximately 40% were achieved for a canal 40 m wide and 4.5 m deep. The results also reveal the existence of performance thresholds for both geometric parameters, beyond which further increases in width or depth result in diminishing returns in terms of force reduction. Analysis of flow fields from the numerical simulations indicates that the canal promotes flow expansion, momentum redistribution, and partial energy dissipation, leading to reduced momentum flux at the downstream structure. Overall, the combined experimental and numerical results demonstrate that rectangular water-filled canals can meaningfully attenuate tsunami bore energy and significantly reduce hydrodynamic forces acting on downstream coastal structures. The findings emphasize the dominant role of canal width in force mitigation and identify practical geometric limits relevant for design. This study provides new insight into bore-canal and bore–structure interactions and supports the consideration of water-filled canals as an effective engineered countermeasure for reducing structural damage in tsunami-prone coastal regions.

Table of Contents

List of Figures

List of Tables

List of Symbols

A_{col}	Vertical projected areas of column (m^2)
A_{wall}	Vertical projected areas of wall (m^2)
A_{beam}	Vertical projected areas of beam (m^2)
A_w	Wetted area of the panel (m^2)
B	Width of structure (m)
b	Size of structure (m)
C_D	Drag coefficient (-)
C_M	Mass coefficient (-)
C_S	Impact coefficient (-)
d_c	Canal depth (m)
d_0	Depth of the impounded water (m)
Fr	Froude number (-)
F_B	Buoyant force (N)
F_D	Total drag force (N)
F_H	Tsunami force (N)
F_I	Impact force (N)
F_S	Tsunami surge force (N)
F_M	Maximum tsunami induced force (N)
g	Gravitational acceleration (m/s^2)
h	Surge height (m)
I_{tsu}	Importance Factor (-)
L	Length of structure (m)
l_1	Distance between the gate and the canal (m)
l_2	Distance between the canal and the column (m)
L_r	Length ratio (-)
R	Design runup elevation (m)
t	Time since gate opening (s)
T_o	Dimensionless gate opening time (-)
t_o	Gate opening time (m)
t_d	Water level drop instant in the impounding reservoir (s)
u	Bore velocity in the direction of wave propagation (m/s)
u_p	Perpendicular component of flood velocity (m/s)
$\dot{u}$	Bore acceleration (m/s^2)
U	Bore front celerity (m/s)
V	Displaced volume of water (m^3)
w_c	Canal width (m)

w/d	Canal aspect ratio (-)
z	Vertical distance from the bed (m)
x, y, z	x-y-z components of position vector (m)
η	Inundation depth (m)
λ	Scale factor (-)
y_s	Minimum fluid weight density (kg/m^3)
θ	Wave angle (°)
ρ	The density of the water (kg/m^3)

List of Acronyms

ADV	Acoustic Doppler Velocimeter
ASCE	American Society Civil Engineers
CCH	City and County of Honolulu building code
FAVOR	Fractional area/volume method
FEMA	Federal Emergency Management Agency
GEJT	2011 Great East Japan Tsunami
ICCE	International Conference on Coastal Engineering
IOT	2004 Indian Ocean Tsunami
LES	Large Eddy Simulation
OpenFOAM	Open Field Operation and Manipulation
PVC	Polyvinyl Chloride
RANS	Reynolds Averaged Navier Stocks
SMBTR	Structural Design Method of Buildings for Tsunami Resistance
SPH	Smoothed Particle Hydrodynamics
US	Ultrasonic Sensor
UVP	Ultrasonic Velocity Profiler
VOF	Volume of Fluid

Chapter 1. Introduction

1.1 Background and Motivation

Tsunamis are among the most destructive natural hazards affecting coastal regions worldwide. Although their occurrence is relatively infrequent, the magnitude of damage caused by these events can be catastrophic, resulting in significant loss of life, destruction of infrastructure, and long-term socio-economic impacts. Tsunamis are typically generated by sudden displacements of large water volumes due to underwater earthquakes, volcanic eruptions, or landslides, leading to the propagation of long-wavelength waves across oceans. When these waves approach shallow coastal areas, they increase in height and energy, often producing high-velocity bores that exert extreme forces on coastal infrastructure. Historical events, such as the 2004 Indian Ocean Tsunami, which claimed over 230,000 lives across multiple countries, and the 2011 Tohoku Tsunami in Japan, which caused widespread destruction of coastal infrastructure and nuclear facilities, highlight the urgent need for effective mitigation strategies.

Coastal infrastructure and communities are particularly vulnerable to the hydrodynamic forces associated with tsunami inundation. The impact of tsunami bores on built infrastructure depends on multiple factors. The tsunami bore induced forces can lead to catastrophic failures of buildings, seawalls, and other coastal infrastructure, endangering human life and resulting in substantial economic losses. Therefore, understanding tsunami-induced loads and developing effective structural and non-structural mitigation strategies is a critical component of disaster risk management in tsunami-prone regions.

Over the past decades, various countermeasures have been developed to reduce tsunami energy before it reaches vulnerable areas. Engineered solutions include seawalls, breakwaters, and water-filled canals, while nature-based measures leverage natural barriers such as mangrove forests, coral reefs, and coastal vegetation. Seawalls and breakwaters primarily aim to reflect or dissipate wave energy, whereas water-filled canals act as an energy sink, reducing the velocity and momentum of incoming bores. Nature-based measures provide additional protection by attenuating wave energy and promoting ecosystem resilience. Despite their effectiveness in specific contexts, these

approaches have limitations. The performance of engineered structures is highly sensitive to geometric configuration, construction quality, and maintenance, while nature-based solutions may require extensive space and long-term ecological management.

Among the engineered measures, water-filled canals have gained attention due to their potential to attenuate tsunami bore forces and protect critical infrastructure. These canals function by temporarily storing and redistributing the energy of incoming inundations, thereby reducing the horizontal forces exerted on downstream structures. Post-tsunami field investigations and preliminary studies have indicated that properly designed canals can significantly reduce the velocity and momentum of tsunami bores. However, a comprehensive understanding of the hydrodynamic interaction between tsunami waves, water-filled canals, and downstream structures is still lacking. Specifically, the influence of canal geometry, bore characteristics, and column location on force reduction has not been systematically investigated in either laboratory experiments or prototype-scale numerical simulations.

Motivated by these knowledge gaps, the present study aims to investigate the effectiveness of rectangular water-filled canals in mitigating the forces exerted by tsunami-like bores on downstream structures. The study combines controlled laboratory experiments at a 1:10 scale with calibrated numerical simulations at the prototype scale using FLOW-3D software. This integrated approach allows for detailed measurement and analysis of the time-history of bore depth, flow velocity, and horizontal forces acting on a square column. By examining the effects of canal width, depth, and relative positioning, this research provides critical insights into the mechanisms by which water-filled canals reduce tsunami energy and protect coastal infrastructure.

The findings of this study are expected to contribute to the broader understanding of tsunami mitigation strategies by addressing key questions that remain unresolved in the current literature. In addition to quantifying force reductions, the research aims to identify geometric thresholds beyond which further modifications of canal dimensions yield minimal additional benefits. These results will inform practical guidelines for the design and implementation of water-filled canals as part of integrated, evidence-based approaches to enhancing coastal resilience. Ultimately, this research supports the development of strategies that can protect human lives, reduce structural damage, and improve the safety and sustainability of coastal communities in tsunami-prone regions worldwide.

1.2 Objectives

This thesis aims to systematically investigate the effectiveness of rectangular water-filled canals as a mitigation strategy for reducing tsunami-like bore forces on coastal structures. To achieve this, both a comprehensive laboratory experimental program and a series of calibrated, prototype-scale numerical simulations using FLOW-3D were conducted. The combined approach provides an in-depth understanding of bore propagation, canal interaction, and bore-structure dynamics, offering guidance for the design of tsunami-resilient coastal infrastructure.

The specific objectives of this thesis are as follows:

i) To evaluate the effectiveness of rectangular water-filled canals in reducing tsunami-like bore forces on a downstream structural column through both experimental measurements and numerical simulations.

ii) To investigate the influence of key parameters, including bore characteristics, canal width, canal depth, and column location, on bore attenuation, force reduction, and flow transformation.

iii) To record and analyze the time-history of bore depth at critical locations (upstream and downstream of the canal, and in front of the column) to assess how canals change bore propagation.

iv) To measure and examine the time-history of horizontal forces acting on a fixed square column, with emphasis on how the presence and geometry of the canal alter impact force characteristics.

v) To conduct real-scale (prototype) numerical simulations to eliminate scaling effects and achieve a realistic representation of tsunami-like bore behavior and its interaction with mitigation canals.

vi) To investigate bore propagation, canal interaction, and bore-structure interaction using synchronized video analysis and numerical flow field visualization.

vii) To quantify the force reduction achieved by various canal geometries and identify threshold dimensions beyond which additional widening or deepening of the canal does not significantly enhance mitigation efficiency.

1.3 Research Questions

This thesis is guided by the following research questions:

- How effective are rectangular water-filled canals in reducing the horizontal forces induced by tsunami-like bores on downstream coastal infrastructure?
- How do key canal geometric parameters, including width and depth, influence bore propagation, energy attenuation, and force reduction on a downstream square column?
- How does the presence of a water-filled canal modify the hydrodynamic characteristics of a tsunami-like bore, including bore depth, velocity, and flow evolution upstream and downstream of the canal?
- What threshold canal dimensions exist beyond which further increases in width or depth result in diminishing returns in terms of force reduction efficiency?
- To what extent can prototype-scale numerical simulations calibrated against laboratory experiments reliably reproduce bore-canal and bore-structure interactions and predict force reduction mechanisms?

1.4 Scope

The scope of this thesis is focused on evaluating the performance of rectangular water-filled canals as engineered mitigation measures to reduce tsunami-like bore forces on coastal structures. The study integrates laboratory experiments at a 1:10 scale and prototype-scale numerical simulations using FLOW-3D to provide a comprehensive understanding of the hydrodynamic interactions between tsunami-like bores, canals, and downstream structures.

Specifically, the thesis addresses:

- The hydrodynamic behavior of tsunami-like bores as they propagate over rectangular water-filled canals and impact rigid square columns.
- The effects of canal geometry, including width, depth, and relative position, on bore attenuation, force reduction, and flow patterns around the column.

- The time-history of bore depth and horizontal force at key locations along the flume or in the numerical domain, providing quantitative measures of mitigation performance.
- The interaction between tsunami bores, mitigation canals, and structural elements, including flow characteristics around the canal as well as the column, and different stages of bore force exerted onto the column.
- The integration of experimental observations and numerical simulations to evaluate real-scale behavior and prepare valuable information to provide design guidance for tsunami-resilient coastal infrastructure.

The thesis does not address: the effects of canal's presence on scouring pattern, debris impact, or long-term maintenance and environmental considerations of mitigation structures. Additionally, only rectangular water-filled canals are considered; other mitigation measures such as seawalls, breakwaters, or nature-based solutions are discussed in the literature review but are not experimentally or numerically modeled.

By defining this scope, the study provides a detailed and focused assessment of rectangular water-filled canals as a practical and effective approach for reducing tsunami-induced forces on coastal structures.

1.5 Contributions and Novelty of the Study

To the best of the author's knowledge, this study is the first to investigate the effectiveness of rectangular water-filled canals as a tsunami mitigation measure by analyzing the time-history of tsunami-like bore forces exerted on a downstream structural column. This thesis makes several significant contributions to the understanding and application of water-filled canals as tsunami mitigation measures:

- Integrated Experimental and Numerical Investigation: Unlike many previous studies that focused solely on either experiments or simulations, this research combines laboratory-scale experiments and prototype-scale numerical simulations using FLOW-3D. This integrated approach provides a more comprehensive understanding of bore-canal-structure interactions.

- Quantitative Assessment of Canal Effectiveness: The study provides detailed measurements of bore depth evolution and horizontal forces on a square column, quantifying the reduction in impact forces achieved by various canal geometries. This enables the identification of optimal width and depth parameters for effective mitigation.
- Identification of Geometric Thresholds: The research reveals thresholds in canal dimensions beyond which further increases in width or depth yield minimal additional force reduction, providing practical guidance for the design of efficient mitigation canals.
- Hydrodynamic Insights into Bore-Canal-Structure Interaction: Through time-history analysis of bore depth, velocity, and horizontal forces, the study elucidates the physical mechanisms underlying force attenuation, highlighting the dominant role of canal width over depth in reducing initial impact forces.
- Design Guidance for Coastal Infrastructure: The findings offer actionable recommendations for engineers designing coastal structures in tsunami-prone areas, supporting evidence-based decisions regarding the implementation of water-filled canals to enhance resilience.

Overall, the novelty of this work lies in its systematic, combined experimental and numerical approach, its focus on detailed force-time histories and bore dynamics, and its provision of practical insights into canal geometry optimization, filling a critical gap in current tsunami mitigation research.

1.6 Limitations of Study

While this research provides meaningful insights, several limitations should be acknowledged.

Laboratory experiments at a 1:10 scale cannot fully replicate turbulence intensity, bore evolution, or energy dissipation patterns found in real events. Similarly, the study examined only a single, rigid square column; other shapes, sizes, or structural arrays may exhibit different responses.

The tsunami conditions used in this study were simplified, consisting of single dam-break bores on a flat bed, or debris-laden flows. Real tsunamis often involve far more complex hydraulic features.

The investigation was limited to rectangular canal geometries. Alternative shapes, such as trapezoidal, stepped, or irregular profiles, may offer improved performance or cost-effectiveness.

Sediment transport, scour around structures, and morphodynamic changes were not considered. These processes can significantly influence real-world performance, especially during extreme events.

Based on observations from recent tsunami events, secondary tsunami bores propagating over an initially wet bed, with greater bore depths, have been shown to be more destructive. The present study considered only dry flat-bed conditions, whereas bore–canal interactions on an initially wet bed will behave quite differently.

The canal in this study was assumed to be fully water-filled, whereas partially filled canals will exhibit different performance in terms of energy dissipation and force reduction.

1.7 Publications and Presentations

1.7.1 Journal Articles

1) **Arefi, R.**, Nistor, I., Mohammadian, A., & Elsheikh, N. (2025). Effects of a rectangular water-filled canal on bore induced horizontal force exerted on a nearshore structure. Published in *Natural Hazards*. https://doi.org/10.1007/s11069-025-07709-y

2) **Arefi, R.**, Mohammadian, A., & Nistor, I. (in preparation). Numerical Analysis of Bore-Induced Forces on Structures: Evaluating the Mitigation Potential of a Water-Filled Canal.

3) **Arefi, R.,** Nistor, I., & Mohammadian, A., (in preparation). Effectiveness of Engineered Tsunami Mitigation Measures: A Review of Current Approaches and Research Needs, Part I: Field Surveys.

4) **Arefi, R.,** Nistor, I., & Mohammadian, A., (in preparation). Effectiveness of Engineered Tsunami Mitigation Measures: A Review of Current Approaches and Research Needs, Part II: Experimental and Numerical Assessment.

1.7.2 Conferences

1) **Arefi, R.**, Nistor, I., & Mohammadian, A. (2024). Experimental study on the effects of a canal on the tsunami bore-induced forces exerted on a column. Extended abstract accepted for oral presentation at the *38th International Conference on Coastal Engineering (ICCE2024)*, Rome.

2) **Arefi, R.**, Nistor, I., & Mohammadian, A. (2025). Reduction of Tsunami-Induced Forces on a Structure Using a Rectangular Mitigation Canal: An Experimental Study. accepted for oral presentation at *Proceedings of the 5th IAHR Young Professionals Congress*, Online.

3) **Arefi, R.**, Mohammadian, A., & Nistor, I. (2025). Numerical Study of the effectiveness of Water-Filled Canals for Reducing Tsunami-Induced Forces on a Nearshore Structure. accepted for oral presentation at *the 9th International Electronic Conference on Water Sciences,* Online.

4) **Arefi, R.**, Mohammadian, A., & Nistor, I. (2025). Coastal Infrastructure Protection Against Tsunami Inundation – Numerical Modelling of a Novel Countermeasure. accepted for oral presentation at *Proceedings of the 6th IAHR Young Professionals Congress,* Online.

5) **Arefi, R.**, Nistor, I., & Mohammadian, A. (2026). Physical and Numerical Modelling of Mitigation Canals for Tsunamis. Extended abstract accepted for oral presentation at the *39th International Conference on Coastal Engineering (ICCE2026)*, Texas.

1.8 Outline of the Thesis

This thesis is organized as follows:

- Chapter 2 (Literature Review) presents a comprehensive critical review of current tsunami mitigation measures, with a particular focus on engineered solutions such as seawalls, breakwaters, and water-filled canals. The chapter synthesizes findings from post-tsunami field investigations, laboratory experiments, and numerical studies, and identifies gaps in the current understanding of bore-canal-structure interactions, providing the rationale for the present study. This chapter is based on a review paper authored by the candidate (Target Journal: *Journal of Waterway, Port, Coastal and Ocean Engineering* (ASCE)).
- Chapter 3 (Laboratory Experiments) describes a series of reduced-scale (1:10) physical experiments conducted to investigate the effectiveness of rectangular water-filled canals in mitigating the horizontal forces exerted by tsunami-like bores on a downstream square column. The chapter details the experimental setup, methodology, measurement techniques, and presents a comprehensive analysis of the results, including the effects of canal width, depth, and column location on force reduction. This chapter is based on one of the candidate's published papers in *Jornal of Natural Hazards* (*Springer*).
- Chapter 4 (Numerical Simulations) presents the development and application of prototype-scale numerical simulations using FLOW-3D to reproduce and extend the experimental observations. The chapter describes the calibration and validation of the numerical model, the analysis of canal geometry effects on flow dynamics and force reduction, and the quantification of bore attenuation under different scenarios by removing some laboratory limitations. This chapter is based on one of the candidate's papers (Target Journal: *Journal of Coastal Engineering* (Taylor and Francis)).
- Discussion integrates the findings from the literature review, experimental results, and numerical simulations. It examines the mechanisms of bore-canal-structure interactions, identifies key parameters influencing mitigation effectiveness, and discusses implications for the design of water-filled canals in tsunami-prone coastal regions. And Conclusions and Recommendations summarize the main findings of the thesis and highlights the novelty and contributions of the research. The chapter also outlines potential directions for future research.

Chapter 2. Literature Review[1]

Abstract

Tsunamis, though infrequent, pose catastrophic threats to coastal communities and infrastructure, underscoring the urgent need for effective mitigation strategies. This review provides a comprehensive evaluation of current engineered countermeasures, specifically seawalls, breakwaters, and water-filled canals, by synthesizing findings from post-tsunami field surveys, physical modeling, and numerical simulations. Evidence from major events, such as the 2011 Tohoku Tsunami, indicates that well-designed structural measures can substantially reduce tsunami wave energy and delay inland inundation, thereby improving the resilience of coastal infrastructure. However, their effectiveness depends heavily on proper geometric configuration, construction quality, regular maintenance, and integration with non-structural measures such as evacuation planning. Recent experimental and numerical investigations have also highlighted the potential of innovative countermeasures, in attenuating bore forces and protecting critical infrastructure. Despite advancements, significant knowledge gaps remain, particularly concerning the long-term reliability, cost-effectiveness, and adaptability of these systems under diverse tsunami conditions. This critical review aims to identify these gaps and outline key priorities for future research and development. The findings contribute to a deeper understanding of structural tsunami mitigation and support the advancement of integrated, resilient strategies for reducing disaster risk in tsunami-prone regions worldwide.

[1] Arefi, R., Nistor, I., & Mohammadian, A., (2026). Effectiveness of Engineered Tsunami Mitigation Measures: A Review of Current Approaches and Research Needs, Part I: Field Surveys.

Arefi, R., Nistor, I., & Mohammadian, A., (2026). Effectiveness of Engineered Tsunami Mitigation Measures: A Review of Current Approaches and Research Needs, Part II: Experimental and Numerical Assessment.

Highlights:

- This review considers findings from field observations, laboratory experiments, and numerical modeling to evaluate the performance of structural tsunami mitigation measures.
- The study focuses on seawalls, breakwaters, and canals, investigating their capabilities in reducing tsunami wave energy and delaying inundation.
- It concluded that the effectiveness of mitigation structures depends on geometry, placement, design quality, and maintenance, especially under extreme tsunami conditions.
- Design guidelines such as ASCE 7-22, FEMA P-646, and Japan's SMBRT are reviewed, highlighting advances and limitations in current tsunami-resistant standards.
- The review identifies critical research needs, including optimization of structural configurations, integration with non-structural measures, and improved validation through real-world data.

Keywords: Tsunami mitigation, Structural countermeasures, Field surveys, Experimental studies, Numerical modelling.

2.1 Introduction

Since the earliest stages of human civilization, coastal and inland regions have experienced differing levels of development. Today, approximately 90% of the world's largest cities are located in coastal areas (Rossetto et al., 2018). The United Nations reports that nearly 60% of these coastal cities are at risk of tsunamis, emphasizing the urgent need for risk-informed urban development and resilient coastal strategies (Sundermann et al., 2019). Coastal regions face growing threats from tsunamis, as tragically demonstrated by the 2004 Indian Ocean Tsunami (IOT) and the 2011 Great East Japan Tsunami (GEJT) (Suppasri et al., 2015). As shown in Figure 1, many countries around the world have experienced devastating tsunami events in recent decades (NOAA/NCEI, 2023). These events highlight the widespread geographic vulnerability to tsunami hazards, particularly in seismically active coastal regions.

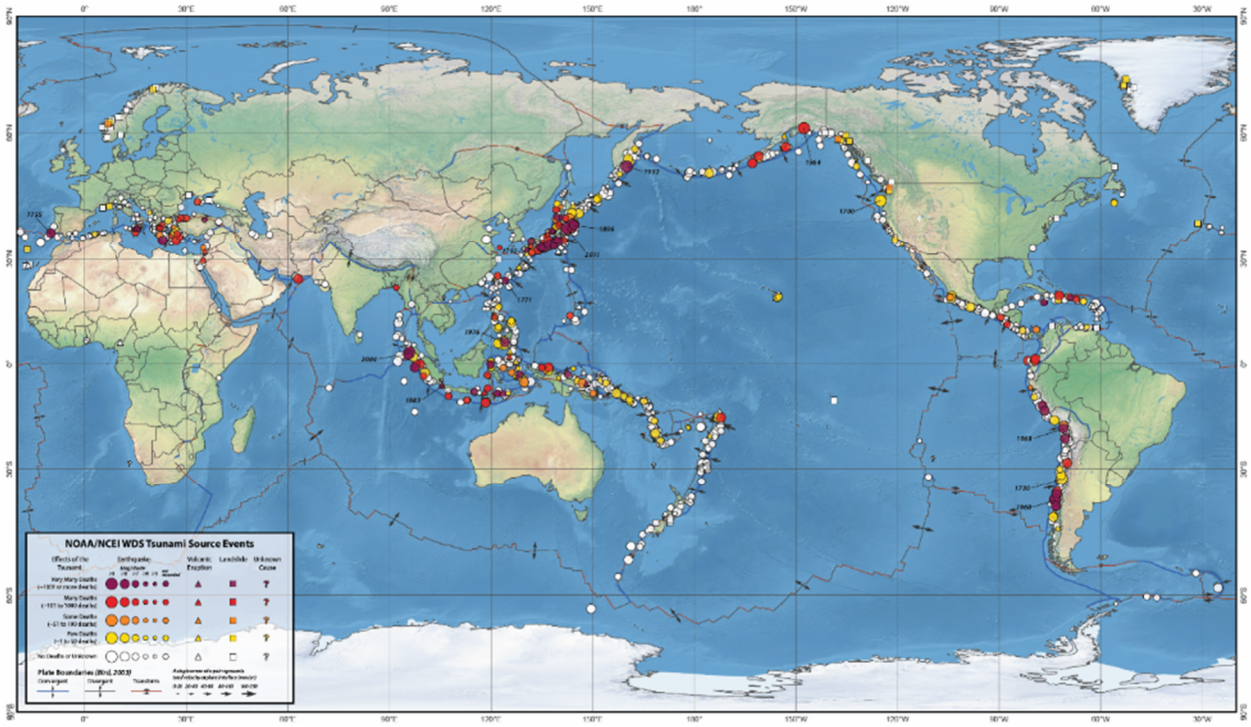

Figure 1: Global tsunami source map produced by NOAA's NCEI, WDS for Geophysics, and the International Tsunami Information Center (ITIC), based on the Global Historical Tsunami Database (1610 B.C.–A.D. 2023). Source: NOAA/NCEI (2023).

These catastrophic events revealed the shortcomings of depending exclusively on structural defenses which, in some cases, failed or created a false sense of security. As a result, strategies have increasingly shifted toward integrated risk management frameworks that blend engineered defenses with non-structural measures such as land-use planning, early warning systems, evacuation protocols, and ecological buffers and multilayer approaches (Tsimopoulou et al. 2015; Samarasekara et al. 2017). Structural countermeasures (such as seawalls and breakwaters) aim to reduce wave energy, while non-structural strategies, including early warning systems and land-use planning, focus on preparedness and risk reduction (Oetjen et al., 2022). However, the effectiveness of these measures varies depending on tsunami characteristics, coastal topography, and the robustness of their design. This review critically examines the performance of structural mitigation techniques by synthesizing evidence from post-tsunami field surveys, laboratory experiments, and computational modeling. It seeks to highlight best practices and identify unresolved challenges in safeguarding coastal infrastructure and communities against tsunami hazards.

2.1.1 Tsunamis

Tsunamis (a term of Japanese origin meaning “harbor wave”) are long-wavelength, high-energy sea waves primarily generated by large-scale disturbances in or near ocean basins (Kusky, 2008). These rare but devastating phenomena can travel vast distances across oceans with minimal energy loss and, upon reaching shallow coastal regions, can transform into towering walls of water capable of causing widespread destruction (Spiridonov et al., 2025). Unlike regular wind-generated waves, tsunamis involve the movement of the entire water column, making them uniquely powerful and destructive when they strike land.

Over the past few decades, awareness of tsunami hazards has increased significantly due to catastrophic events such as the 2004 Indian Ocean Tsunami and the 2011 Great East Japan Earthquake and Tsunami which led to the deaths of nearly 300,000 individuals and inflicted extensive economic and infrastructural damage amounting to billions of dollars (Kajitani et al., 2011; Nandasena et al., 2012). As illustrated in Figure 2, the 2011 Tohoku Tsunami caused extensive destruction along the northeastern coast of Japan. The comparison of Google Earth satellite images before and after tsunami clearly demonstrates the scale of structural damage to coastal infrastructure.

These disasters highlighted the vulnerability of both human settlements and critical infrastructure along coastlines, prompting a global response focused on improved hazard assessment, risk mitigation, and public preparedness (Ferreira et al., 2024). Today, research into tsunami behavior, early warning systems, and resilient infrastructure design continues to evolve, emphasizing the need for international collaboration and informed policy development to reduce future risks (Srinivasa Kumar and Manneela, 2021). The number of academic publications related to tsunami increased significantly after the 2004 Indian Ocean Tsunami. As shown in Figure 3, the number of related studies with the keyword of “tsunami” rose sharply, reflecting a growing global research interest in understanding tsunami hazards, enhancing early warning systems, and advancing effective mitigation strategies.

Figure 2: Google Earth satellite images of the District of Yuriago (a) before and (b) after the 2011 Tohoku Tsunami.

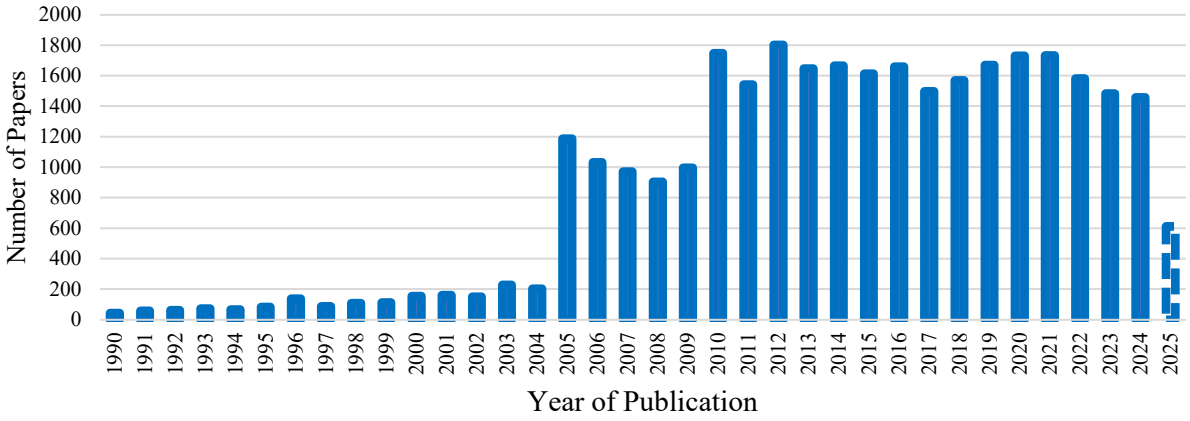

Figure 3: Annual number of published papers including the keyword “tsunami”, showing a significant increase in research activity following the 2004 Indian Ocean Tsunami.

2.1.2 Importance of Mitigation Measures

Tsunamis have caused significant damage to infrastructure and human life worldwide in recent decades (Nistor et al., 2019). The 2004 Indian Ocean Tsunami and the 2011 Great East Japan Tsunami were much stronger than what existing disaster protection systems could handle. They caused serious damage to coastal buildings and communities and had huge financial and environmental effects. Following the Indian Ocean Tsunami, researchers focused on developing early warning systems and evacuation plans to reduce the impact of future events. Since then, various methods have been proposed and implemented to protect coastal infrastructure. These include non-structural measures like planting coastal vegetation, building sand dunes, maintaining lagoons and coral reefs, and structural measures like seawalls, large barriers, floodgates, and specially built evacuation buildings (Oetjen et al., 2022; Tanaka et al., 2024).

Figure 4 presents a satellite image taken after the Tohoku Tsunami, capturing a coastal area in Sendai, Japan, one of the most severely affected regions. The image reveals a combination of tsunami mitigation countermeasures, including seawalls, breakwaters, green belts, and canals. These elements were strategically designed to dissipate tsunami wave energy, delay inland inundation, and protect critical infrastructure from catastrophic failure. In addition, the image highlights several buildings that withstood the destructive forces of the tsunami, providing valuable insight into the performance of various structural and non-structural mitigation measures.

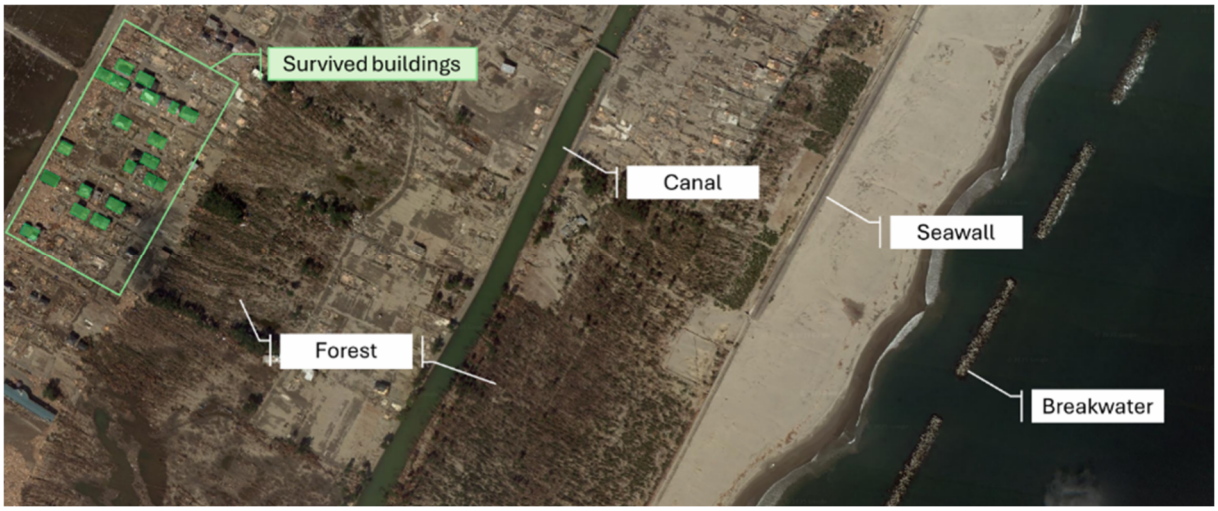

Figure 4: Satellite image of the coastal region in Sendai, Japan, showing structures that withstood the 2011 Japan Tsunami behind various tsunami mitigation countermeasures (Source: Google Earth)

2.1.3 Tsunami Design Guidelines and Standards

While the design of structures in flood-prone areas has been widely studied, few existing codes specifically address the design of onshore civil structures in tsunami-prone regions (Nouri et al., 2010). The increasing awareness of tsunami hazards has led to the development of various national and international guidelines aimed at improving coastal resilience through proper design and mitigation strategies. These guidelines incorporate the latest scientific research and engineering practices to provide comprehensive frameworks for assessing tsunami risks, determining appropriate design loads, and implementing effective structural and non-structural measures (Nistor et al., 2025).

Japan's long history of repeated tsunami events has resulted to the development of comprehensive guidelines, standards, and building codes, as well as a substantial body of academic and industry literature focused on tsunami risk and mitigation since 1950s. In 2000, the Building Technology Research Institute in Japan introduced engineering guidelines for the structural design of tsunami refuge buildings, proposing a method based on experimental studies. The method was updated in 2005 and published as the Structural Design Method of Buildings for Tsunami Resistance (SMBTR) (Okada et al., 2015), which was validated using buildings affected by the 2004 Indian Ocean Tsunami. SMBTR provides detailed formulations for tsunami wave pressure and force calculations, considers buoyancy effects, and acknowledges the influence of surrounding obstacles in reducing tsunami loads on structures (Al-Faesly, 2016).

In the United States, initial provisions addressing tsunami-induced loading were introduced in the 1980s through Hawaii's Building Code. The City and County of Honolulu Building Code (CCH) incorporates specific regulations and design criteria to enhance the resilience of structures against tsunami hazards (CCH, 2013). Recognizing Honolulu's vulnerability to tsunamis, the code mandates rigorous standards for foundation design, structural integrity, and materials to resist hydrodynamic forces and debris impacts. The CCH emphasizes the integration of both structural and non-structural mitigation measures, including elevation requirements and site planning, to reduce the risk to life and property.

In 2011, the Federal Emergency Management Agency (FEMA) released the fourth edition of the Coastal Construction Manual (FEMA P-55, 2011). This document provides guidance for the design and construction of structures in coastal areas vulnerable to damage from natural hazards.

FEMA also has issued comprehensive publications such as FEMA P-646, Guidelines for Design of Structures for Vertical Evacuation from Tsunamis (FEMA P-646, 2019), which provides detailed recommendations for designing evacuation structures that can withstand the extreme forces generated by tsunamis while ensuring the safety and accessibility of occupants. It outlines planning, siting, and structural design criteria to ensure these facilities can withstand tsunami forces, including hydrostatic, hydrodynamic, and debris impact loads.

American Society of Civil Engineers (ASCE) Standard 7-22 (ASCE, 2022) is one of the most widely recognized standards that provides minimum design loads for buildings and other structures, including tsunami-induced forces. ASCE 7-22 outlines detailed methodologies to estimate hydrodynamic pressures, debris impact forces, and erosion effects caused by tsunami inundation, emphasizing the importance of incorporating these forces into structural design to enhance the resilience and survivability of coastal infrastructure. The Tsunami Loads and Effects Subcommittee of the ASCE/SEI 7 Main Committee has prepared a dedicated chapter on tsunami loads and effects, which was introduced in the ASCE/SEI 7-16 standard (Chock, 2016).

Despite these advancements, challenges remain in standardizing tsunami design criteria globally due to regional variations in tsunami characteristics, coastal geomorphology, and socio-economic factors. Continued research and refinement of guidelines are essential to address gaps in knowledge and enhance the effectiveness of engineered mitigation measures worldwide.

2.1.4 Objectives of the Review

Although the effects of tsunami-induced loads on onshore structures have been widely investigated in previous studies (Asakura et al., 2002; Dias et al., 2005; Nouri et al., 2010; Erduran et al., 2025; Triatmadja et al., 2025), relatively few studies have focused on engineered tsunami mitigation countermeasures. This indicates a need for further research to develop a deeper understanding of the effectiveness of such measures in reducing tsunami-induced forces on coastal infrastructure.

The primary objective of this review is to provide a comprehensive evaluation of engineered tsunami mitigation measures, specifically seawalls, breakwaters, and canals, and to assess their effectiveness in reducing tsunami impacts on coastal infrastructure. By systematically reviewing and analyzing findings from field observations, laboratory experiments, and numerical

simulations, this study aims to synthesize current knowledge on structural tsunami mitigation strategies.

A further objective of this review is to identify existing gaps in the literature and to highlight key future research directions and priorities. Ultimately, the review seeks to support the development of more resilient and sustainable coastal infrastructure capable of withstanding future tsunami events.

2.1.5 Scope of the Review

The scope of this review is limited to engineered structural tsunami mitigation measures, including seawalls, breakwaters, and canals, with a particular emphasis on coastal protection strategies that directly interact with tsunami waves. These measures are primarily intended to attenuate wave energy, delay inland inundation, and reduce damage to coastal infrastructure.

In addition to evaluating the performance and limitations of existing structural countermeasures, this review focuses on synthesizing and comparing results reported in the literature regarding their effectiveness in reducing tsunami-induced forces and impacts on coastal infrastructure. The analysis is based on findings from field observations, laboratory experiments, and numerical studies that examine the interaction between tsunami waves and structural mitigation measures. By concentrating on these aspects, the review provides a focused and evidence-based assessment of the current state of knowledge on structural tsunami mitigation.

2.2 Tsunami Hazards and Impacts on Coastal Infrastructure

2.2.1 Generation and Propagation of Tsunamis

Tsunami waves triggered by various reasons which the most common cause is earthquakes, exemplified by the 2004 Indian Ocean tsunami and the 2011 Japan tsunami (Satake, 2015). Tsunamis may also result from non-seismic causes such as underwater landslides (e.g., the 1998 Papua New Guinea event; Tappin et al., 2025), volcanic eruptions (e.g., the 2022 Hunga Tonga eruptions; Xu & Lane, 2025), asteroid or comet impacts (Hills & Goda, 1999), and glacial calving (e.g., the 1958 Lituya Bay mega tsunami; González-Vida et al., 2018). With climate change accelerating glacial retreat, the potential for tsunamis from non-seismic sources is receiving increased attention (Wolper et al., 2021).

As shown in Figure 5, once tsunamis generated, these waves propagate across the ocean at high speeds, often hundreds of kilometers per hour, with long wavelengths and low wave heights in deep water. As they approach shallow coastal areas, the waves slow down and increase in height due to the decreasing water depth, eventually breaking near the shore. This breaking can form a tsunami bore, a turbulent, fast-moving wall of water resembling a tidal bore, or a tsunami surge which is a rapid, continuous flow of water flooding inland. The inundation that follows causes widespread flooding, damaging infrastructure along the coast (Felder and Chanson, 2018; Wüthrich et al., 2019; Harish et al., 2021). Continuous tsunami inundation may last from few minutes to several hours (Sriram et al., 2016; Sundar et al., 2007).

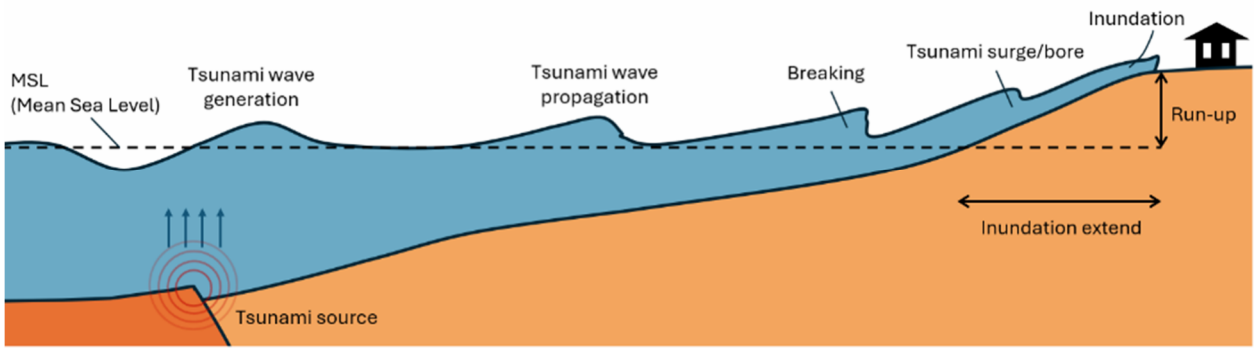

Figure 5: Tsunami generation and propagation toward coastline and its impact to coastal infrastructure

Following the 2011 Great East Japan Tsunami, tsunamis in Japan were classified into two categories of level 1 (L1) and level 2 (L2). L1 tsunamis, with return periods between several decades to around 100 years, are used for disaster prevention and typically cause inundation depths under 7-10 m. (L2) tsunamis, with return periods of few hundred to a few thousand years, are considered for disaster mitigation and can produce much greater inundation depths, often over 10 m and reaching up to 20-30 m. The 2004 Indian Ocean and 2011 Great East Japan tsunamis fall into this category (Takabatake et al., 2020; Muhari et al., 2015).

2.2.2 Interaction of Tsunamis with Coastal Infrastructure

The interaction between tsunami inundation and coastal infrastructure is complex and highly destructive due to the immense energy and momentum carried by tsunami bores. As tsunamis reaching the coast, the waves exert various hydrodynamic and impact forces on structures, including hydrostatic pressure, hydrodynamic drag, uplift, debris impact, and scour at foundations. These forces can lead to partial or complete structural failure, particularly when infrastructure is not designed to withstand such extreme loading conditions (FEMA P-646, 2019; ASCE 7-22,

2022). Structures located near shoreline are vulnerable during tsunami events. Studies of the 2004 IOT and the 2011 GEJT have shown that inadequately designed or maintained infrastructure suffered extensive damage (Leone et al., 2011; Suppasri et al., 2015; Moris et al., 2021). For example, during the GEJT, many reinforced concrete buildings were toppled or displaced due to strong hydrodynamic forces and foundation scour, while bridges were washed away by buoyant uplift and debris impacts (Yeh et al., 2013; Chock et al., 2013a, b).

As shown in Figure 6, the time history of tsunami-induced force on structures typically exhibits multiple phases (Asadollahi et al., 2019). Understanding the different phases of tsunami-induced force time history is crucial, as mitigation countermeasures may influence each phase differently and with varying effectiveness (Arefi et al., 2025). The interaction of front bore with structure, generates an impulsive force, followed by a quasi-steady force during the continuous inundation (Kihara et al., 2021; Harish et al., 2022). The impulsive force phase is characterized by a short-duration, high-magnitude pressure spike, often attributed to air entrainment and strong turbulence at the bore front. During the quasi-steady phase, the hydrodynamic force is governed by the steady interaction of bore height and flow velocity, and the pressure distribution tends to resemble a hydrostatic profile. The transition between these two loading phases is referred to as the transition phase (Nouri et al., 2010; Al-Faesly et al., 2016; Ravindar et al., 2019; Ravindar and Sriram, 2021). Depending on the characteristics of the incoming bore and the geometry of the structure, the maximum force may occur either in the impulsive or quasi-static phase (Bullock et al., 2007; Arikawa, 2011; Kihara et al., 2021; Harish et al., 2022).

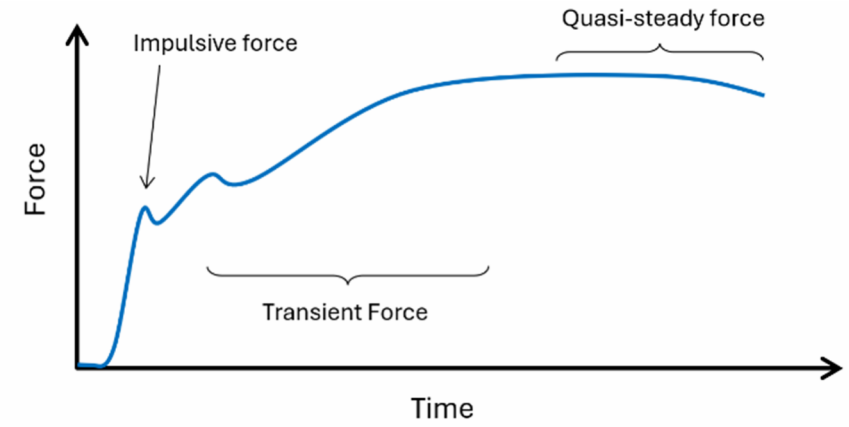

Figure 6: Schematic of the time history of force exerted on structures by tsunami-induced bores

2.2.3 Types of Tsunami Forces and Coastal Infrastructure Failure Mechanisms

Tsunamis exert a wide range of destructive forces onto coastal infrastructure, which vary in magnitude depending on the tsunami characteristics, coastal geometry, and structural design. Because of the significant impact of tsunami-induced forces on structures which is one of the primary causes of failure in coastal infrastructure, many researchers have investigated the interaction between tsunami bores and infrastructure located on affected coastal zones (Shafiei et al., 2016; Ghodosipour et al., 2019; Harish et al., 2025). One of the earliest studies in this field was conducted by Cumberbatch (1960), who analytically examined the forces exerted by tsunami waves on a vertical wall.

ASCE 7-22 (2022) categorizes tsunami-induced forces on structures into two main types: hydrostatic and hydrodynamic loads. Hydrostatic loads include buoyancy forces, unbalanced lateral hydrostatic force, residual water surcharge load on floors and walls, and hydrostatic surcharge pressures on foundation. Hydrostatic forces result from water pressure acting on submerged or partially submerged structures. These are relatively straightforward to calculate but can be substantial in the case of deep inundation. Hydrodynamic drag, caused by the horizontal motion of the wave, applies large forces along the flow direction. Buoyant forces, including uplift, occur when the water level rises around or under structures, potentially dislodging poorly anchored elements such as slabs or lightweight buildings.

Tsunami-induced structural damage to coastal infrastructure arises from multiple factors, including hydrostatic and hydrodynamic forces, impacts from floating debris, the fire spread through floating debris and flammable liquids, as well as soil erosion leading to slope instability or foundation failure (FEMA P-646, 2020). Hydrostatic and hydrodynamic loads can directly damage infrastructure by exerting forces on buildings, potentially causing them to slide, overturn, or collapse entirely (Chock et al., 2013a). Another critical failure mechanism arises from debris impact loads, which can be highly impulsive and difficult to predict. Large floating objects like cars, shipping containers, or even small boats can strike buildings with devastating force. These impacts were widely observed in Japan during the GEJT (Yeh et al., 2013). Scour and erosion at the base of structures, further compromise their stability by removing supporting soil. Breakage or overturning due to loss of bearing capacity is often the result. According to Kian et al. (2022), unanticipated scour depths during tsunami runup were responsible for the collapse of several

bridge superstructures in coastal Japan. Figure 7 illustrates various examples of infrastructure failure that occurred during past tsunami events.

Figure 7: various examples of infrastructure failure that occurred during past tsunami events; (a) Overturned reinforced concrete/steel building in Onawaga, March 2011; (b) breached coastal protection dyke near Hachinohe, Japan, March 2011; (c) debris impact on a column, Banda Aceh, December 2004; (d) damaged costal protection revetment, near Hachinohe, Japan, March 2011 (courtesy of Ioan Nistor)

2.3 Classification of Mitigation Countermeasures

Tsunami defence strategies can be classified into structural, non-structural, and hybrid approaches (Green-Grey which means combination of non-structural and structural measures). Structural measures focus on physical deflection or dissipation of wave energy, non-structural strategies emphasize preparedness and planning, and hybrid solutions integrate both types to

achieve more resilient, adaptable outcomes for coastal communities. Figure 8 presents an overview of existing tsunami countermeasure options.

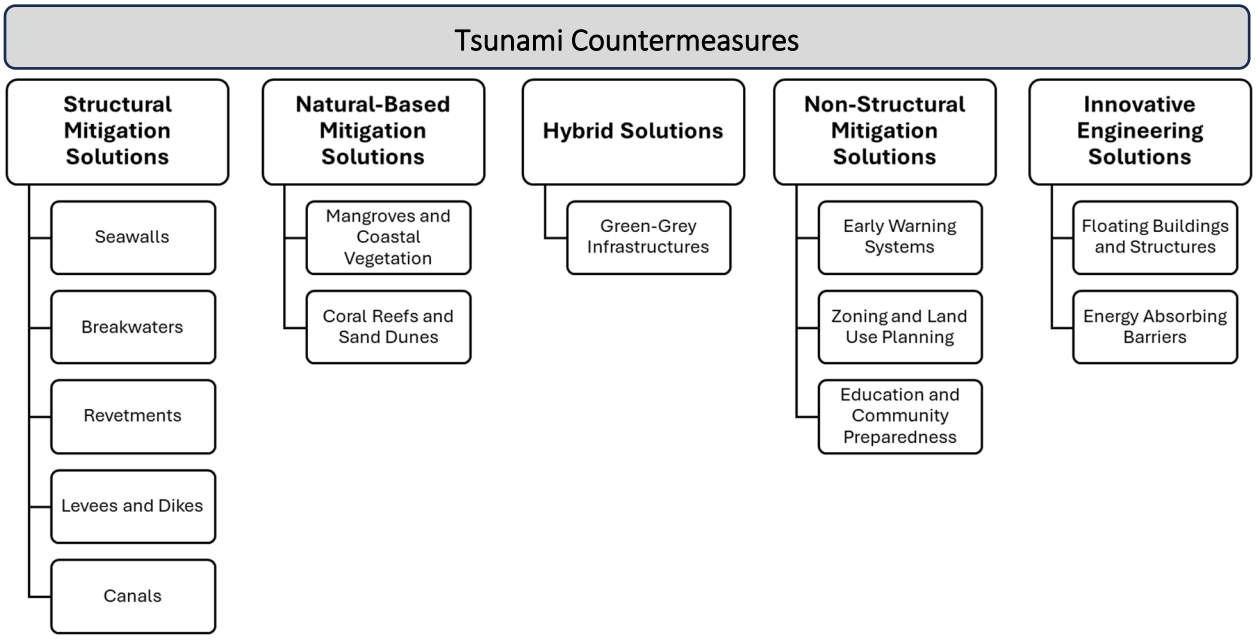

Figure 8: Tsunami countermeasures – an outline of existing options

2.3.1 Structural Measures

Structural countermeasures are engineered systems designed to attenuate tsunami-induced loads exert onto structures located near affected coastlines (Figure 9). These countermeasures are typically constructed along coastlines or in strategic inland areas to protect human life, infrastructure, and economic assets. Among the most common structural elements are seawalls, breakwaters, and canals, each with distinct hydrodynamic behaviors and performance limitations.

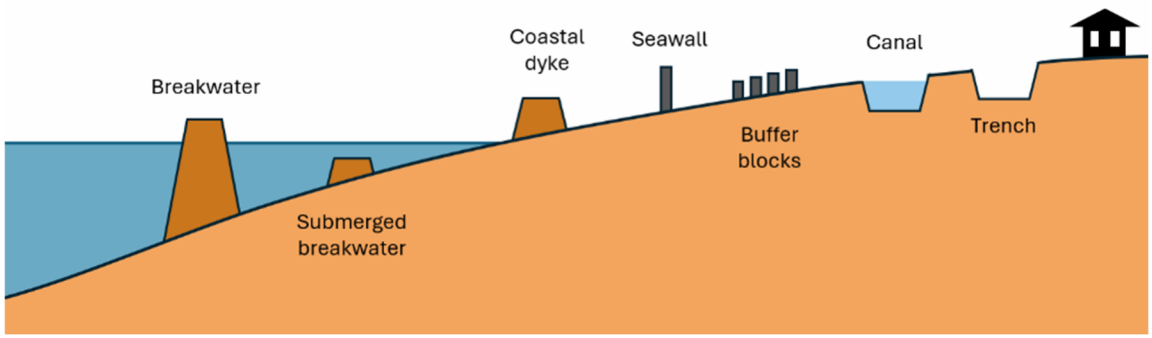

Figure 9: Typical structural coastal protection used to mitigate tsunami effects

2.3.1.1 Seawalls

Constructing seawalls in tsunami-prone coastal regions is a widely implemented strategy for reducing inundation risk. Seawalls are vertical or sloped barriers constructed along coastlines to prevent inland flooding and reduce tsunami inundation. Their primary function is to reflect or dissipate wave energy before it reaches critical infrastructure (Al-Faesly et al., 2015). While high seawalls offer effective protection against tsunamis, they can be relatively expensive to build (Triatmadja et al., 2025). Their performance, however, is highly dependent on whether overtopping occurs. In cases where overtopping is possible, seawalls may not only fail to prevent damage but also can increase destruction during extreme wave events (Reuters, 2018). Additionally, their presence can potentially reduce evacuation readiness (Nagethi et al., 2016).

2.3.1.2 Breakwaters

Among the primary structural mitigation strategies, the construction of continuous or detached breakwaters, either submerged or emerged, is widely implemented (Oetjen et al., 2022). Breakwaters are offshore structures, either floating or fixed, that act as the first line of defense by reducing incoming wave energy. In tsunami events, submerged or detached breakwaters can mitigate wave energy before they reach the shoreline. They are particularly useful in harbors and bays where port infrastructure is vulnerable. Studies has demonstrated that breakwater shape, porosity, and arrangement significantly influence tsunami dissipation. The location of the breakwater is also a critical parameter influencing its effectiveness in resisting tsunami forces (Esteban et al., 2009).

2.3.1.3 Canals

Water-filled canals, channels, or dug pools located inland or near coastal infrastructure have been introduced as innovative tsunami mitigation strategies. These features function as energy sinks by absorbing part of the tsunami bore, thereby reducing the forces exerted on structures situated behind them. Although seawalls and breakwaters are generally more effective at dissipating tsunami energy and allowing additional time for evacuation, they are often associated with significantly higher construction costs. Moreover, failure or overtopping of these structures may lead to more destructive tsunami impacts (Reuters, 2018). Post-tsunami field investigations have demonstrated that a water-filled canal parallel to the coastline can effectively dissipate the energy of incoming tsunami bores (Chock et al., 2013).

2.3.2 Non-Structural Measures

Non-structural approaches aim to reduce tsunami risk without relying on physical barriers or infrastructure. These strategies include early warning systems, hazard zoning, tsunami evacuation maps, public education, and awareness campaigns (UNISDR, 2015). Among them, urban planning plays a crucial role in restricting the development of critical infrastructure within high-risk coastal zones. Although such measures do not prevent the physical impact of tsunami waves, they are highly effective in minimizing casualties and economic losses when properly implemented (Ferreira et al., 2024). Countries like Japan exemplify comprehensive non-structural frameworks by integrating real-time alert systems, frequent evacuation drills, and robust public risk communication initiatives.

2.3.3 Hybrid Approaches

Hybrid mitigation strategies integrate both structural and non-structural elements to create multi-layered defense systems. For example, a coastal area may use seawalls in combination with elevated evacuation structures, real-time warning systems, and green infrastructure like mangroves or dunes. Some recent studies also explore combining engineered measures to balance flow reduction and overtopping control. Oshiro et al. (2015) investigated the effectiveness of canals and coastal forest barriers in reducing tsunami flow velocity and delaying wave arrival time. Rifatin et al. (2025) examined the combined effects of sea dikes and trenches as a mitigation strategy. These approaches seek to address the limitations of individual methods by leveraging the strengths of multiple systems. Future research should focus on optimizing these synergies under budgetary and spatial constraints, especially in rapidly urbanizing coastal regions.

2.4 Performance Assessment of Mitigation Measures

Coastal communities face increasing risks from tsunamis, which can result in catastrophic loss of life and severe damage to infrastructure (Nistor et al., 2009). In response, various engineered mitigation strategies have been implemented or proposed globally to reduce tsunami impacts (Yeh et al., 2009; Suppasri et al., 2013). While a wide range of structural and non-structural approaches exist, this study focuses exclusively on the structural countermeasures of seawalls, breakwaters, and water-filled canals due to their direct hydraulic interaction with tsunami bores and their prominence in both practical applications and academic research. Seawalls function as vertical or

sloped barriers that reflect and block incoming waves (Al-Faesly et al., 2015), breakwaters dissipate wave energy offshore before it reaches vulnerable shorelines (Kato et al., 2006), and water-filled canals or trenches aim to attenuate bore momentum through flow diversion and energy absorption (Arefi et al., 2025). Evaluating the performance of these systems is critical for enhancing coastal resilience and informing the development of future design guidelines. To this end, this section provides an in-depth assessment of their effectiveness based on three complementary methodologies: post-tsunami field surveys, laboratory experiments, and numerical modeling studies.

1.1. Field Observations and Surveys

Comprehensive forensic engineering field surveys were conducted by expert teams following major tsunami events (Chock, et al., 2013a, b; Saatcioglu et al., 2006; Sassa & Takagawa, 2019; Inagaki et al., 2025; Heidarzadeh et al., 2025) offering critical post-disaster data and valuable insights into tsunami impacts, structural performance, and coastal vulnerability. These surveys yield invaluable empirical data, highlighting both successes and failures, which in turn guide future design improvements and policy decisions. After each significant tsunami, researchers, engineers, and disaster experts promptly deploy to the affected coastal areas to carry out thorough field assessments. Such on-site investigations are essential because they provide direct, real-world observations of the tsunami's impact on the landscape, infrastructure, and communities (Reis et al., 2022).

Nistor and Palermo (2015) carried out detailed tsunami damage surveys shortly after three major tsunami events: the 2004 Indian Ocean tsunami (in Indonesia and Thailand), the 2010 Chile tsunami, and the 2011 Tohoku tsunami in Japan. The main goal of these surveys was to study how different structures responded to the extreme forces caused by the inland flooding from the tsunamis. Based on their field survey following the January 2024 Tsunami, Heidarzadeh et al. (2025) found three primary failure mechanisms were identified for coastal structures: overturning due to tsunami backwash, structural damage from inundation currents and wave pressure, and impacts caused by floating debris.

2.4.1.1 Post-Tsunami Damage Assessment of Seawalls

Seawalls are among the most common structural mitigation measures designed to act as physical barriers against incoming tsunami waves (Figure 10). Following the 2011 Great East

Japan Earthquake and Tsunami, extensive field surveys conducted by the Japan Meteorological Agency and research institutions documented the performance of seawalls along the northeastern coast of Honshu Island. In areas where seawalls were constructed according to updated design standards, with heights ranging from 8 to 15 meters, significant reduction in wave overtopping and inland inundation was observed (Imamura et al., 2016). These seawalls effectively shielded urban zones, preserving critical infrastructure such as power plants and transportation routes. However, some seawalls were overtopped when tsunami heights exceeded design levels, leading to catastrophic flooding. Additionally, certain seawalls suffered structural damage due to scouring and undermining at their base, indicating the need for enhanced foundation designs and scour protection (Koshimura et al., 2012).

Figure 10: (a) Seawall; and (b) Tsunami overtopping during the 2011 event in Miyako, Japan (Source: Reuters).

During a post-tsunami reconnaissance following the 2004 Sumatra event, Dalrymple and Kriebel (2005) observed increased levels of infrastructure damage directly behind openings in coastal seawalls in Phuket, Thailand. The effectiveness of seawalls is also linked to maintenance and integration with natural buffers such as coastal forests and dunes. Field data reveal that seawalls combined with vegetation cover tend to perform better due to the complementary energy dissipation by trees and shrubs (Suzuki et al., 2013).

Following their field survey after Noto Tsunami, Heidarzadeh et al. (2025) identified several locations along the Sea of Japan coast where the concrete seawall effectively prevented tsunami overtopping. This protective function was clearly evidenced by the clean and undisturbed condition of the area behind the seawall, indicating that the tsunami had not overtop the structure. They also observed cases where seawalls were overtopped by tsunami waves, showed no signs of structural damage. Despite tsunami heights reaching 3.7-3.9 m in the area, the seawall sustained

no visible damage, which the resilience is attributed to the high-quality construction and robust design of the structure. Their study highlights a failure case in which concrete seawall blocks were overturned over a 25 m stretch due to tsunami backwash, a mechanism also observed during the 2011 Tohoku tsunami (Takahashi et al., 2011). Notably, the failure occurred in an unprotected section of the seawall, whereas adjacent segments equipped with rock armor or a rockfill shoulder remained stable. This underscores the importance of reinforcing the seaward face of vertical seawalls with armor layers extending to the seawall's full height.

Based on their field survey following the 2011 Great East Japan Tsunami, Suppasri et al. (2013) identified three primary causes of seawall damage. First, the two seawalls crossed in an X shape, which caused the tsunami waves to accumulate and increase in size at the center where they intersected. Second, the foundations of the seawalls were weakened, as the soil properties near the river likely disrupted the stability of the foundations. Lastly, the seawalls were not properly maintained and were inadequately connected to each other. This allowed the tsunami to flow over the seawalls and form a high-speed water jet, with the strong current causing scouring around the foundations and further weakening the structures.

2.4.1.2 Breakwater Performance in Tsunami Events

Breakwaters, including rubble mound and submerged types, serve to reduce incoming wave energy before it reaches the shoreline (Figure 11). Following the 2004 Indian Ocean tsunami, field surveys in Aceh, Indonesia, found that coastal areas protected by breakwaters experienced substantially reduced wave heights and run-up levels compared to unprotected locations (Tanaka et al., 2011). Rubble mound breakwaters with high porosity allowed partial infiltration of tsunami waves, dissipating energy via turbulence and friction. However, in some cases, insufficient structural robustness led to breakwater displacement or partial failure under extreme loads, emphasizing the need for optimized design against hydrodynamic forces and debris impact (Harada et al., 2015).

Figure 11: Breakwater damage during tsunami event

Submerged breakwaters, being less visually obtrusive, have proven effective in dissipating wave energy by inducing wave breaking. Surveys of tsunami-affected sites with submerged reefs or artificial breakwaters indicate reductions in run-up heights by up to 30% (Chen et al., 2015). Field investigations of Nistor and Palermo (2015) following the 2011 Tohoku tsunami revealed that many breakwaters along Japan's Tohoku coast, primarily designed for storm protection, suffered severe damage or complete failure under tsunami loading. Composite breakwaters with concrete armor units showed greater resilience compared to caisson-type breakwaters, largely due to their porosity, which helped dissipate wave energy, although some armor units were also damaged. The performance of these units varied with size and weight, and current design methods for tsunamis remain underdeveloped and unverified.

The Kamaishi breakwater in, Japan, completed in 2009 at a cost of approximately ¥120 billion (around $1.5 billion), was recognized as the world's deepest breakwater. Although it was ultimately destroyed by the 2011 Great East Japan Earthquake Tsunami, it significantly reduced the tsunami's force and height by approximately 40% and delayed its inland arrival by about six minutes and provided critical additional time to evacuate to higher ground (Ishiwatari and Sagara, n.d.). Following their field survey of the 2024 Noto Peninsula Earthquake and Tsunami, Inagaki et al. (2025) emphasized the critical role of coastal protection structures in damage mitigation. They observed that areas behind breakwaters experienced minimal impact, whereas unprotected zones and structural weaknesses in hydraulic defenses were associated with significantly greater damage. They found several locations, which tsunami flooding occurred where coastal defenses were absent or had crest elevations lower than the tsunami height, emphasizing the need to address structural weak points in coastal protection systems. Tsunami waves penetrated further inland

through weak points in coastal defenses, particularly in areas lacking offshore structures like detached or port breakwaters.

Heidarzadeh et al. (2025) surveyed three locations around Toyama where no tsunami damage was observed. The area is protected by a three-layer coastal protection system consisting of a detached rubble mound breakwater about 100 m offshore, a concrete stepped revetment at the shoreline, and an earth-fill dike behind it, collectively standing approximately 2.5 m above sea level. They also reported on the Shika nuclear power plant, which sustained no damage and is protected by multiple coastal layers, including an offshore caisson breakwater, coastal vegetation, a coastal road, and a solid concrete wall, along with significant elevation above sea level.

2.4.1.3 Observations of Engineered and Natural Canals

Canals, whether natural or engineered, and whether water-filled or empty, can influence tsunami wave propagation by modifying flow patterns and velocities (Figure 12). Although less extensively studied than seawalls or breakwaters, field evidence from coastal Japan suggests that wide canals and channels can act as hydraulic buffers by diverting and attenuating tsunami wave fronts (Suzuki et al., 2013).

Figure 12: Image of tsunami propagating over a canal during the 2011 Japan Tsunami event (ASCE)

The Buckingham Canal, located near Chennai in southeast India, is a long channel about 30 meters wide and 10 meters deep that runs parallel to the coast at a distance of 1 to 2 kilometers. During the 2004 Indian Ocean tsunami, the canal helped protect some higher ground areas from damage because the tsunami first filled the canal, which acted like a buffer zone. The canal also helped return the water back to the sea within 10 to 15 minutes (Rao, 2005). Tokida and Tanimoto

(2012) demonstrated that a water-filled depression formed by tsunami flooding referred to as a "dug pool" can effectively reduce tsunami flow velocity. The Buckingham Canal played a significant role in reducing casualties, particularly among fishermen in coastal regions of Andhra Pradesh and around Chennai, India (Ramalingeswara et al., 2005). These findings highlight the potential of canals as effective tsunami countermeasures for protecting both coastal infrastructure and human lives.

In some cases, canals combined with vegetation or shallow embankments have slowed tsunami propagation, reducing peak forces exerted on downstream infrastructure (Figure 12). However, the effectiveness of such features depends heavily on canal geometry. During the 2011 Japan Tsunami, the tsunami waves swept away coastal forests, overflowed the Kita-Teizan Canal, and caused destruction far inland in Miyagi Prefecture. However, post-disaster field surveys suggest that, despite the severe conditions, the combination of vegetation and the canal may have helped to some extent in reducing the tsunami's force (Niimi et al., 2012). Historically, the design of the Kita-Teizan Canal reflected a common approach in which a coastal forest served as a windbreak, with the canal positioned behind it. This layered arrangement was likely intended to enhance natural protection along the coast (Oshiro et al., 2015).

1.2. Experimental Investigations

Laboratory experiments enable detailed study of tsunami-structure interaction under controlled and repeatable conditions. Using wave flumes, basins, and scaled physical models, researchers have explored force generation, wave reflection and transmission, overtopping, and scour effects associated with various mitigation measures. Research on tsunami loading began with the experimental work of Stoker (1957), who investigated the impact of tsunami waves on vertical walls, which his study concluded with a proposed equation for estimating tsunami-induced loads (Sarjamee et al., 2017).

2.4.1.4 Seawall Experimental Studies

Seawalls are among the most commonly implemented structural measures for tsunami protection, capable of either fully shielding coastal communities or delaying inundation to allow for evacuation (Samarasekara et al., 2017). Cross (1967) was one of the first researchers to study tsunami forces on a vertical seawall. Their experiments showed that the shape of the tsunami bore front, the forces, and the pressure matched well with what theory had predicted. This showed that

lab experiments can be a reliable way to check the accuracy of theoretical models. While seawalls are often designed to withstand tsunami inundation without overtopping, thereby protecting the structures located behind them, many experimental studies have focused solely on the forces exerted on the seawalls themselves, without considering any downstream structures. However, some recent investigations have explored scenarios involving low-height seawalls or partially protected areas, where overtopping occurs, allowing the tsunami bore to impact structures behind the seawalls.

Al-Faesly et al. (2012, 2016) conducted a series of experimental tests to evaluate the effectiveness of low-height, high-stiffness mitigation walls in reducing tsunami bore-induced impulsive forces and moments on structures. The walls were not intended to prevent inundation, but to dissipate a significant portion of the incoming bore energy and delay the impact, providing critical evacuation time. Six different wall designs including vertical, inclined, curved, and wave return walls were tested at two upstream distances from a structural model using three impoundment depths. Parameters such as wall height, angle, shape, and location were varied. Results showed that walls placed closer to the structure reduced base shear by up to 20%, though they could increase overturning moments. Curved walls proved most effective in simultaneously reducing both base shear and overturning moments, whereas inclined walls at farther distances increased impact loads.

Rahman et al. (2014) conducted an experimental study to assess the effectiveness of sea walls, both solid and perforated, in mitigating tsunami forces on coastal buildings. By varying wall height, type, and distance from a model structure, the study showed that taller sea walls (8 cm) placed closer to buildings significantly reduced impact forces, achieving up to 41% force reduction, compared to 27% for shorter walls (4 cm). Perforated walls, with 26% openings, performed nearly as effectively as solid ones (35% reduction), while offering advantages such as lower construction cost and better drainage of overtopped water, which helps reduce residual forces.

McGovern et al. (2022) studied the effects of tsunami-induced forces and overtopping on vertical seawalls to address limitations in current design codes, which often overestimate impulsive loads from bore-like waves. Using a 100-meter flume and Froude-scaled pneumatic wave generation, they tested two vertical seawall configurations under various wave scenarios. They

found that long-period tsunami waves primarily exert hydrostatic forces, typically not exceeding 1.2 times the static load. However, when short waves broke, they produced impulsive forces reaching up to 25 times the hydrostatic force. Additionally, overtopping volumes were more closely related to the duration of inundation rather than wave height, and standard wind-wave models significantly underestimated the volume of tsunami overtopping.

Zhang et al. (2023) studied how partial seawalls affect tsunami forces on coastal buildings. Using experiments in a large wave basin, they tested different wall lengths and wave types, like breaking and non-breaking waves, under runup and inundation scenarios. They found that seawalls can either protect or worsen the situation depending on their placement. When walls ended right before a structure, wave energy focused around the wall's edge, increasing force. But full coverage by the wall reduced the forces by up to 90%. Breaking waves caused short, high-force impacts, while non-breaking waves caused longer-lasting pressures. Even buildings behind the first row could get hit hard due to redirected water.

Table 1 summarizes the selected studies and highlights their findings and remarks.

Table 1: Summary of selected experimental studies on seawalls as tsunami mitigation countermeasure

Study	Scale & setup	Tsunami characteristics	Seawall geometry & configuration	Measured parameters	Key findings	Remarks
Al-Faesly et al. (2012)	Large-scale flume; dry/wet beds; bore impact	Dam-break; bore depth: 250-450 mm; velocity: 2.6-5.0 m/s	Low-height structural walls (vertical/inclined/curved); 100–150 mm height; Different locations of downstream structure	Time history of force, bore depth, moment, pressure, high-speed video	Curved wall reduced both shear and moment; inclined wall increased forces; FEMA underestimated force levels	Examined realistic tsunami impact; showed importance of wall geometry/location; evaluated design guidelines accuracy
Rahman et al. (2014)	Medium-scale flume (17.5 m); dam-break setup	Simulated tsunami-like bore; impoundment depths up to 30 cm	Solid and perforated vertical walls; 4 cm and 8 cm height; placed at varying distances	Horizontal force on building, wave height	Higher wall (8 cm) reduced force by 41% when placed close; perforated wall gave 35% reduction and better drainage	Emphasized wall height and proximity; perforated wall cost-effective with added drainage benefit
McGovern et al. (2022)	Large-scale flume (100 m)	pneumatic wave generator; Long- and short-period Froude-scaled tsunami waves; non-breaking & breaking cases	Two vertical seawalls (0.15 m & 0.25 m high); tested under variable wave conditions	Force (load cells/pressure), overtopping volume & duration	Long waves caused hydrostatic forces ≤1.2× static pressure; short breaking waves induced impulsive peaks up to 25×; overtopping driven by flow duration	Supports hydrostatic-based design with ≥1.2 safety factor for non-breaking waves; EurOtop underestimates overtopping
Zheng et al. (2023)	Large wave basin; 10×10 structure array	Solitary (breaking) and error function (non-breaking) waves; with/without currents	Partial solid seawalls (0.6 m high); varying lengths and clearance angles	Quasi-static & impulsive loads, load variation across rows	Wall end near structure increased loads by up to 1.5×; full shielding reduced forces up to 90%; breaking farther offshore reduced impact; complex inland load patterns observed	Highlights both amplification and shielding; suggests further study on perforated walls and 3D effects

2.4.1.5 Breakwater Physical Modeling

Breakwater experiments explore both submerged and rubble mound types. Rubble mound breakwaters, modeled with scaled stones or artificial porous blocks, dissipate wave energy through flow within the porous media. Breakwater porosity, slope angle, and crest freeboard significantly influence their energy dissipation capacity and stability under tsunami loads. Submerged breakwaters can help control wave breaking. Wave height reductions depend on submergence depth, demonstrating their value in wave attenuation with minimal visual impact. Failure modes such as block displacement and overturning have been studied to optimize rubble mound block sizes and armor layers.

Hanzawa and Matsumoto (2015) conducted a comprehensive physical modeling study to evaluate the effectiveness and stability of detached breakwaters made of wave-dissipating concrete blocks (Tetrapods) under tsunami wave conditions. Using a 30 m wave flume, experiments were carried out to assess tsunami wave run-up reduction, wave pressure, and the structural stability of breakwaters under solitary wave attacks. The study compared ordinary and submerged breakwater configurations under varying wave heights and water depths. Results showed that detached breakwaters significantly reduced wave run-up (by up to 90%) and wave pressures (by up to 60%), even when partially damaged. Damage to the Tetrapods was more severe at the rear slope, especially in shallow water, with landslide-type failure observed. Increasing Tetrapod mass and fixing the first rear row improved breakwater stability.

Mikami et al. (2015) investigated the effects of detached breakwaters on tsunami attacks around coastal dykes through both field observations from the 2011 Tohoku Earthquake and laboratory experiments using a 1:50 scale tsunami basin. Field data from five locations revealed that coastal dyke damage varied depending on whether the dyke was situated behind a breakwater body or an opening. Laboratory tests supported these findings, demonstrating that when the detached breakwater parameter (distance from shoreline to breakwater divided by opening length) was small, wave velocity behind the breakwater was reduced, but not behind the opening. This non-uniform velocity distribution suggests localized variations in tsunami mitigation effectiveness. The study concludes that while detached breakwaters can reduce tsunami forces locally, their design must consider opening configuration to ensure uniform protection along coastal dykes.

Muhammad and Tanaka (2019) examined the tsunami energy dissipation efficiency of a hybrid defense system composed of a sea embankment followed by a coastal forest using 1:100 scale flume experiments. The study tested both single-layer (SLM) and double-layer (DLM) vegetation models under supercritical flow conditions. Results demonstrated that the hybrid system significantly reduced tsunami energy: by up to 70% with DLMs (especially with denser submerged layers), and by up to 60% with SLMs. Hydraulic jumps played a key role in energy reduction, with their formation and location influenced by forest porosity and flow intensity. Denser forests triggered jumps further upstream, reducing velocity and improving flow resistance. This study highlights the superior performance of DLMs in tsunami mitigation.

Xu et al. (2024) explored the tsunami mitigation capacity of seawall-integrated trapezoidal breakwaters in protecting coastal bridge piers through both laboratory experiments and numerical simulations. The study used a dam-break wave flume to simulate tsunami bore impacts and evaluated the effects of seawall height, perforation, and spacing on the hydrodynamic forces experienced by bridge piers. Results showed that higher seawalls significantly reduced the forces transmitted to piers but experienced larger direct loads themselves. The pressure on the seawall was greatest at mid-height and decreased toward the crest. Moreover, an optimal spacing of 1 m between the breakwater and pier was found to maximize force attenuation. These findings underscore the balance required between protective efficiency and structural loading in designing integrated coastal defenses.

Table 2 summarizes the selected experimental studies on breakwaters as tsunami mitigation countermeasure and highlights their findings and remarks.

Table 2: Summary of selected experimental studies on breakwaters as tsunami mitigation countermeasure

Study	Scale & setup	Tsunami characteristics	Breakwater geometry & configuration	Measured parameters	Key findings	Remarks
Hanzawa & Matsumoto (2015)	30 m long, 0.5 m wide flume with slopes of 1/5, 1/20, and 1/30; wave gauges and pressure sensors	Piston wave maker; solitary waves with heights of 1–9 cm; two water depths (40 cm and 43 cm)	Detached breakwaters (ordinary: hc = 4 cm; submerged: hc = 0 cm) made of Tetrapods (58.9–125 g); Seawall at x = 13.75 m with 7 pressure gauges	Run-up height, wave pressure, breakwater damage, flow velocity field	Detached breakwaters reduced run-up height by 10–70% (ordinary) and 40–80% (damaged); wave pressure reduced to <60% and <80% for ordinary and damaged breakwaters respectively; rear slope most vulnerable; heavier units and fixed rear row improve stability	Highlights need for including damage scenarios in design; submerged breakwaters still effective
Mikami et al. (2015)	Field survey of 2011 Tohoku tsunami + 1:50 lab-scale tsunami basin (9 m × 4 m × 0.5 m)	Tsunami-like bore waves; water levels 40-80 cm; 31 test cases with variable breakwater gap and distance	Detached breakwaters with variable distance from shore and opening; tested effect on velocity behind both body and opening; stone breakwaters on 1:10 slope	Flow velocity behind breakwater body and opening	Breakwaters reduce velocity and likely tsunami impact behind the main body; no reduction behind openings; confirms field observations	Emphasizes need for optimized breakwater layout for effective protection; real-world relevance validated by 2011 Tohoku tsunami data
Muhammad & Tanaka (2019)	14 m × 0.5 m × 0.7 m flume, 1:100 scale; 7 Froude numbers (1.08–1.56); constant 1/200 bed slope	Steady supercritical flow (Fr: 1.08-1.56); designed to simulate tsunami inundation	Hybrid system: 14.5 cm embankment (1:2 slope) followed by forest models; variable porosities (78–98%)	Water depth, flow velocity, energy head, hydraulic jump type/location, ΔE (%)	Denser submerged layers induced earlier hydraulic jumps and greater resistance	Demonstrated role of hydraulic jump and porosity in flow energy reduction; relevant for hybrid structure planning in tsunami-prone coasts
Xu et al. (2024)	1:50 scale; 6 m flume	Dam-break waves; wave heights: 12-14 cm; downstream depths: 8-10 cm	Heights: 60–160 mm; perforated vs. solid designs	Horizontal forces on piers, pressure distribution, overtopping	Taller seawalls reduce pier forces but increase seawall loads; pressure peaks mid-height; optimal pier-breakwater distance = 1 m	Limited to 2D numerical validation

2.4.1.6 Experimental Evaluation of Canals

Recent laboratory investigations have focused on the use of rectangular water-filled canals positioned seaward of coastal infrastructure to reduce tsunami impact forces. These canals are typically shallow and wide that interrupt the incoming tsunami bore. The presence of such canals changes the flow field, reducing bore front velocity which leads to exerted force reduction on structures located behind the canal. Furthermore, canals can delay the arrival time of the bore, providing additional warning and reaction time for evacuation or closure of floodgates. The effectiveness of this type of tsunami mitigation measure depends on canal geometry and tsunami characteristics.

The experimental study by Nakaza et al. (2015) examined the combined effects of water-filled canals and coastal vegetation on tsunami mitigation. Their findings demonstrated that canals can significantly modify tsunami hydrodynamics by reducing front velocities by up to 25% and delaying wave arrival times. Through dam-break wave experiments, they observed that wider (50 cm) and deeper (10 cm) canals were particularly effective in dissipating tsunami energy, although they slightly increased downstream inundation depths due to flow concentration effects. Their study also showed that canals can generate isolated reflected waves upstream and temporarily trap and decelerate the tsunami front within the canal. Reduced effectiveness was observed in shallower canals (5 cm depth), primarily due to an increased likelihood of overtopping. As the tsunami bore front enters the canal, it is violently washed up and reflected by the downstream edge, remaining temporarily contained within the canal. However, in shallow canals, the bore front is less restrained and tends to overtop the downstream edge, continuing its propagation beyond the canal.

The experimental study by Rahman et al. (2016) evaluated the tsunami mitigation effectiveness of rectangular canals using a 1:100 Froude-scaled laboratory flume setup. The study compared various canal widths (25 cm and 50 cm) and depths (5 cm and 10 cm) under dam-break-induced tsunami bores with incident wave heights ranging from 2.3 cm to 5.1 cm. Results demonstrated that canals delay tsunami arrival time, reduce maximum inundation depth, flow velocity, and specific energy. Notably, the 50 cm-wide and 10 cm-deep canal reduced the bore front velocity by approximately 30% and achieved a greater delay effect than vertical seawalls of equivalent height. However, canals with lower depth (5 cm) were less effective. These findings underscore the

potential of geometrically optimized canals as effective structural mitigation measures comparable to traditional seawalls.

Watanabe et al. (2016) conducted laboratory experiments to investigate the tsunami reduction effect of Teizan Canal, inspired by observations during the 2011 Tohoku Tsunami. Using both a tsunami basin and a wave flume, the study examined how canal depth, wave height, and waveform influence overflow reduction. The tsunami basin experiments revealed that the canal significantly reduced overflow, with reduction rates varying by wave type (35.7% to 59.2%), and demonstrated that deeper canals diminished this effect. Additionally, the study highlighted the role of waveform duration in overflow dynamics, not just wave height. Wave flume experiments, employing PIV analysis, visualized fluid motion and energy loss near the canal inflow, revealing vortices and complex flow patterns. While the study provides valuable insights, the authors acknowledge limitations due to simplified canal conditions and call for further research to address real-world complexities. The findings underscore the potential of canals in tsunami mitigation but emphasize the need for more comprehensive modeling to inform practical applications.

Elsheikh et al. (2020) experimentally investigates the effects of rectangular canals on the hydrodynamics of dam-break-induced tsunami-like surges, focusing on surge height and velocity changes upstream and downstream of the canal. They tested three canal depths (0.05 m, 0.10 m, 0.15 m) and three widths (0.60 m, 1.60 m, 3.0 m) under varying impoundment depths (0.20 m, 0.30 m, 0.40 m). Results showed that upstream surge heights increased by up to 40% for narrow canals and smaller impoundments, while downstream surge heights rose by 10-50%, with minimal changes observed for a canal width-to-depth ratio of 20. Surge velocities downstream of the canal decayed by 40-60%, attributed to bed friction and momentum dissipation. The study highlights the potential of canals to mitigate tsunami impacts by reducing flow velocities, though their effectiveness depends on geometry and initial wave conditions. While no downstream structures were included to assess the exerted forces, the measurements of velocity and bore depth offer valuable insights for optimizing engineered tsunami mitigation strategies.

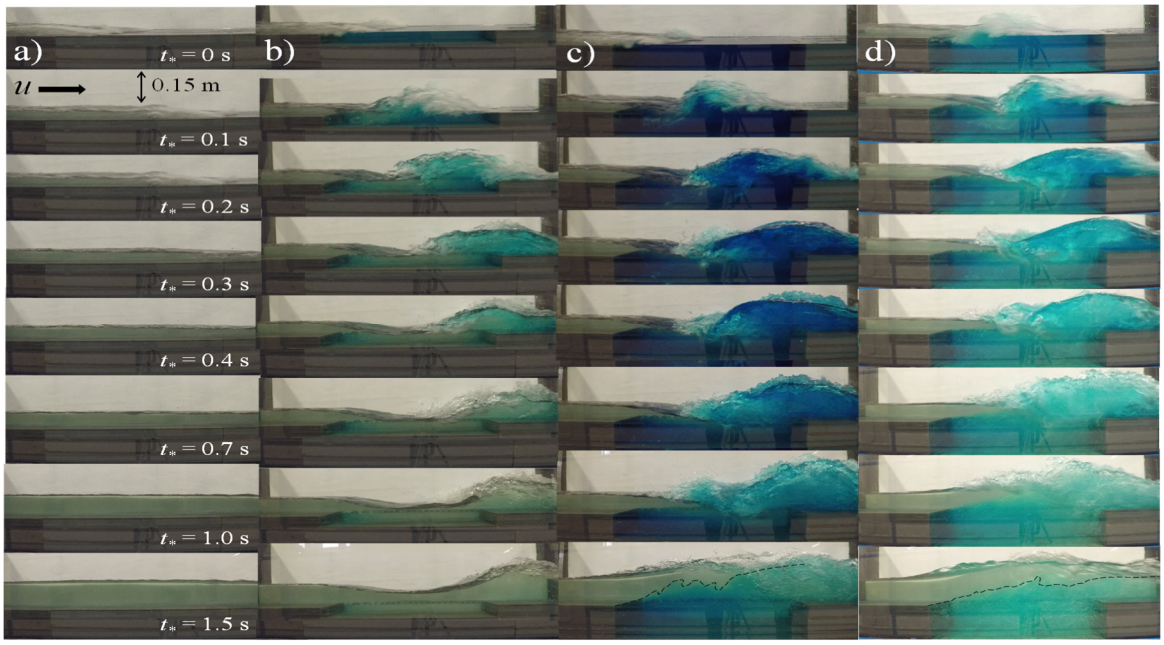

Figure 13: Effects of canal depth on tsunami bore interaction with canal (Elsheikh et al., 2022)

Arefi et al. (2025) conducted an experimental study to assess the effectiveness of rectangular water-filled canals in mitigating tsunami-like bore forces exerted on a structural column. Unlike previous studies, which focused solely on flow characteristics or upstream wave behavior, this study uniquely placed a structural column downstream of the canal and directly measured the horizontal force exerted on it. Using a Froude-scaled (1:10) flume with dam-break generated bores and varying canal geometries, the study recorded time histories of bore depth and impact force on the column. Results showed that wider and deeper canals significantly reduced the bore front velocity and decreased the peak horizontal force by more than 25%. Despite some limitations related to flume size, the findings demonstrated that water-filled canals can effectively dissipate tsunami bore energy and reduce forces on nearshore infrastructure, making them a promising and economical structural mitigation solution.

Table 3 summarized selected experimental studies and their key findings and remarks.

Table 3: Summary of selected experimental studies on canals as tsunami mitigation countermeasure

Study	Scale & Setup	Tsunami Characteristics	Canal Geometry & Configuration	Measured parameters	Key Findings	Remarks
Nakaza et al. (2015)	Scale 1:100; 10 m long and 60 cm wide flume	Dam-break	Rectangular canal	Time history of bore depth and flow velocity along the flume	Wider and deeper canals reduced front velocity up to 25% and delayed wave arrival; shallow canals overtopped easily; flow concentration slightly increased inundation	Different tests for canal depth and width, and water depth inside the canal; a series of tests with combination of canal and vegetation
Rahman et al. (2016)	Froude scale 1:100; 10 m-long flume	Dam-break induced bore depth of 2.3–5.1 cm	Rectangular canal; widths = 25 & 50 cm, depths = 5 & 10 cm; with/without embankments	Time history of bore depth and flow velocity along the flume	Wider (50 cm) and deeper (10 cm) canals reduced flow velocity by ~30% and delayed wave arrival more than seawalls; 5 cm-deep canals were less effective.	Demonstrated canals can match or outperform seawalls in energy dissipation.
Watanabe et al. (2016)	1:50 wave flume	Waveforms based on 2011 Tohoku event; 3 wave types; variable duration and height	Canal depths: 0, 2, and 4 cm	Overflow volume via collection tank; PIV-based flow visualization (vortex formation, energy loss); wave height measurements	Overflow reduced up to 59%; deeper canals caused more overflow; waveform shape and duration had greater influence than peak height	Demonstrated real-world relevance using Tohoku tsunami data; vortex and energy loss observed at canal inflow using high-speed PIV
Elsheikh et al. (2022a, b)	15.56 m long, 0.38 m wide, and 0.60 m deep glass-walled flume	Dam-break wave with impoundment depth of 40 cm	Rectangular canals; widths = 0.6, 1.6, 3.0 m; depth = 0.15 m	Time histories of bore depth and velocity; calculated non-dimensional discharge, momentum flux; high-speed video analysis of bore flow and interactions	Medium and wide canals significantly reduced maximum non-dimensional discharge (up to 67%), peak non-dimensional momentum flux (up to 80%), and peak bore impulse (up to 89%) compared to no-canal cases	Canal effectiveness increases with width; wide canals generate turbulence and air entrainment that enhance energy dissipation
Arefi et al. (2025)	Froude scale 1:10	Dam break with water impoundment depth of 20-40 cm	Rectangular water-filled canal with depth of 5-15 cm and width of 60-300 cm	Time history of bore depth and horizontal force on column; high-speed video analysis of bore flow and interactions	Wider and deeper canals reduced bore front velocity and peak horizontal force on a downstream column by >25%; unlike previous studies, this study directly measured tsunami forces on a structure placed behind the canal.	Demonstrated effectiveness of water-filled canals in reducing tsunami-induced forces on nearshore structures.

2.4.2 Numerical Modeling Studies

Numerical simulations are essential for capturing the complex and nonlinear interactions between tsunami waves and mitigation structures. Advanced computational tools allow parametric studies that can incorporate realistic bathymetry, complex geometries, and transient wave conditions.

2.4.2.1 Performance of Seawalls through Numerical Simulation

Numerical studies have simulated seawalls with varying heights, slopes, and material properties to investigate flow impact and overtopping. The higher seawalls reduce wave overtopping but increase reflected wave energy, potentially intensifying local scour (Pinto et al., 2025).

Hsiao and Lin (2010) investigated tsunami-like solitary wave interactions with impermeable trapezoidal seawalls on a 1:20 sloping beach using both laboratory experiments and the COBRAS numerical model (a RANS-based solver with k–ε turbulence closure). Three wave-structure interaction types were observed, ranging from direct bore impacts to overtopping and collapse behind the seawall. The study found that dynamic wave forces peaked during run-up and overtopping stages, especially under high wave nonlinearity and low freeboard conditions. The COBRAS model closely matched experimental results, demonstrating its capability in capturing free-surface dynamics, turbulence, and pressure evolution in coastal defenses subjected to extreme wave action.

Sarjamee et al. (2017) used Large Eddy Simulation (LES) in OpenFOAM to assess how small-scale mitigation walls affect tsunami-induced forces on coastal structures. Their study compared LES with traditional RANS turbulence models and found that LES more accurately captured impulsive bore forces and run-up behaviors. Through validated dam-break bore simulations, they tested the effects of curved and inclined low-height walls placed upstream of a square column. A curved wall located three times the column diameter upstream reduced hydrodynamic forces by approximately 30%, while the same wall at one diameter upstream increased impact forces due to flow accumulation. Inclined walls performed poorly, intensifying forces through a launching mechanism.

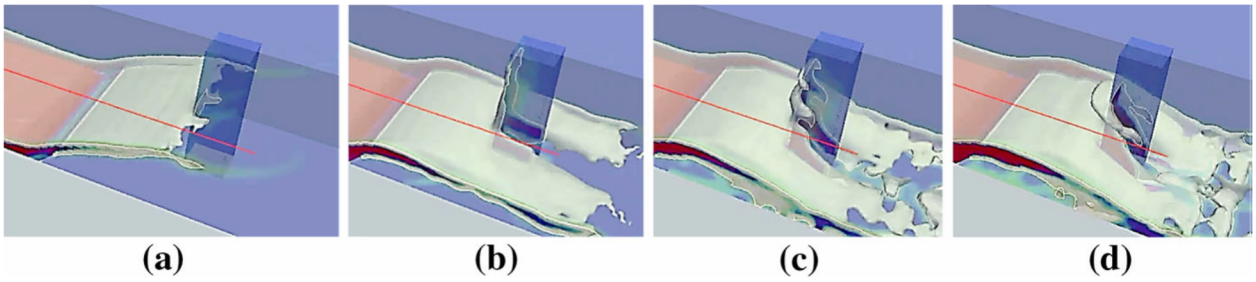

Figure 14: (a) The incoming flow first hits the column, (b) The bore climbs up the surface of the column, (c) The water that has climbed up begins to fall back toward the incoming flow, (d) The raised water fully collapses onto the incoming flow (Sarjamee et al., 2017).

Huang et al. (2022) assessed the performance of seawalls in mitigating tsunami impacts using the nonhydrostatic wave model NHWAVE, focusing on more realistic tsunami-like waves derived from the 2011 Japan tsunami. The study demonstrated that tsunami-like waves have significantly greater energy, overtopping volume, and reflection potential compared to solitary waves. Through a series of numerical experiments, the authors examined how variables such as wave height, water depth, seawall side slope, and beach slope influence wave runup, overtopping, and reflection. Results showed that tsunami-like waves cause more severe hydrodynamic loads, leading to greater potential for damage and secondary hazards, particularly if wave reflection is not properly accounted for.

Triatmadja et al. (2025) investigated the performance of tsunami seawalls of varying heights using Smoothed Particle Hydrodynamics (SPH) simulations via the DualSPHysics model. Tsunami waves were generated through a dam-break mechanism in a flume and assessed the effectiveness of seawalls with height-to-water-depth ratios (H_w/H_o) of 0.33, 0.50, and 0.67. Results showed that seawalls with $H_w/H_o \geq 0.50$ effectively reduced tsunami wave velocities by 72–100%, delayed overtopping, and dissipated wave energy through turbulence. In contrast, low walls ($H_w/H_o = 0.33$) occasionally increased downstream velocities post-overtopping due to energy concentration, potentially intensifying inland damage. The study concludes that seawalls must be carefully designed with a minimum height ratio of 0.50 to balance performance, safety, and cost, particularly in resource-limited but tsunami-prone regions (Figure 15).

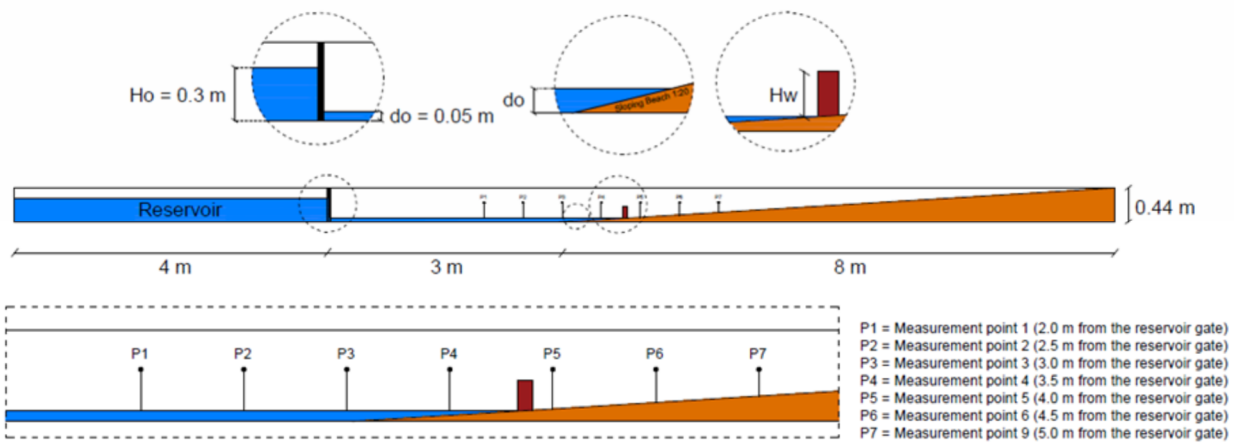

Figure 15: Schematic of numerical setup (Triatmadja et al., 2025)

Table 4: Summary of selected numerical studies on seawalls as tsunami mitigation countermeasure

Study	Numerical Model	Dimension	Tsunami generation method	Seawall Geometry	Evaluated Parameters	Main Findings	Validation	Limitations
Hsiao & Lin (2010)	COBRAS (RANS with k–ε turbulence model)	2D	Solitary wave generator in lab flume; varied wave types	1:20 sloped beach with trapezoidal impermeable seawall	Free surface elevation, dynamic pressure, vortex behavior	Lower freeboard and higher nonlinearity increased forces; vortex and air entrapment reduced pressure behind wall	Numerical results closely matched lab data (wave profiles and pressures)	2D model only; no downstream structures modeled; Air-water interactions simplified; limited to idealized solitary waves
Sarjamee et al. (2017)	OpenFOAM	3D	Dam-break bore (based on Al-Faesly et al. 2012 experiments)	Rectangular flume with square column (D = 0.305 m); mitigation walls (15 cm)	Impulsive force, run-up height, pressure-time histories	Curved wall reduced force by ~30%; LES captured turbulence better than RANS	Validated against lab-scale bore impact experiments (Al-Faesly et al. 2012)	No structural deformation modeled; only tested two wall shapes; no overtopping debris or sediment transport included
Huang et al. (2022)	NHWAVE (Nonhydrostatic Wave Model)	2D	Parameterized tsunami-like waveform based on 2011 Japan tsunami	Sloped beach with trapezoidal seawall (varied slope angles)	Wave energy, overtopping volume, reflection coefficient, runup height	Realistic tsunami-like waves exhibit higher energy (4.65×), greater overtopping, and reflection than solitary waves; seawall side slope and beach slope significantly affect runup and overtopping	Model validated against analytical and existing numerical results; based on 2011 event waveform	No experimental validation; limited to 2D simulations; structural forces on seawall not computed directly
Triatmadja et al. (2025)	DualSPHysics (SPH method)	2D	Dam-break system in a scaled flume (15 m × 0.3 m × 0.44 m)	Flat flume bed with vertical seawalls at varied Hw/Ho ratios (0.00–0.67)	Flow velocity, wave run-up, propagation speed, overtopping behavior	Seawalls with Hw/Ho ≥ 0.50 reduced velocities by 72–100%; low walls (Hw/Ho = 0.33) may increase downstream flow post-overtopping	Validated with lab-scale flume experiments using 0.003 m particles	2D simulations; limited real-world complexity; no structural failure modeling; no downstream structures modeled

2.4.2.2 Evaluating Breakwater Effectiveness Using Numerical Modeling

In numerical simulations of breakwaters and their role in tsunami energy dissipation, rubble mound porosity is shown to significantly reduce transmitted wave energy. Additionally, submerged breakwaters must be carefully designed with an optimized crest submergence depth to maximize wave breaking and enhance energy attenuation.

Takagi and Bricker (2014) assessed the performance of general-purpose breakwaters in Ishinomaki City during the 2011 Great East Japan Tsunami, focusing on their role in reducing tsunami inundation and building damage. Using GIS building data and 2D shallow water numerical simulations, the study compared a residential area without breakwaters, where 87% of buildings were destroyed, to a neighboring industrial zone shielded by breakwaters, which saw only 25% damage. However, the modeling showed that breakwaters did not significantly reduce water levels or flow velocities due to wide openings that allowed tsunami energy to rapidly flood the port. Simulations using higher Manning's roughness values ($n = 0.30$) matched observed inundation more accurately than traditional values ($n = 0.06$), emphasizing the role of surface complexity and debris. The study concludes that general breakwaters, unless modified with closures or elevated crests, offer limited tsunami protection.

Wei and Dalrymple (2016) numerically assessed the effectiveness of breakwaters and service road bridges in mitigating tsunami-induced forces on coastal bridge superstructures using the Smoothed Particle Hydrodynamics (SPH) model GPUSPH. Validated against laboratory experiments, the model evaluated both horizontal and vertical force reduction under various configurations. Rubble mound and caisson breakwaters reduced tsunami forces by up to 58% when placed at an optimal distance, approximately 8 times the water depth or 13 times the tsunami height, upstream of the bridge. However, breakwaters themselves were vulnerable to failure due to high hydrodynamic loads and seabed scouring, posing additional risks from debris. Comparatively, parallel service bridges offered 36–50% force reduction but often failed under extreme conditions. The SPH model accurately captured initial impact forces but had limitations in simulating high-frequency responses due to its single-phase fluid assumption. This study underscores the need to balance structural durability and mitigation performance in tsunami-prone bridge design.

Xue et al. (2022) proposed a novel tri-semicircle submerged breakwater to protect coastal bridges from extreme wave events. Using OpenFOAM-based numerical simulations, the study compared this modular design to conventional trapezoidal breakwaters in terms of wave force reduction on T-girder bridge decks. Horizontal force reductions ranged from 31.4% to 71.6%, and vertical force reductions from 26% to 38.3%, far exceeding those of trapezoidal breakwaters. The force mitigation was attributed to enhanced flow separation and eddy dissipation, which minimized overtopping and velocity near the bridge.

Wu et al. (2025) proposed and evaluated a hybrid tsunami mitigation system combining a semicircular breakwater with an L-shaped fairing to reduce hydrodynamic forces on T-girder coastal bridges. Using two-dimensional RANS simulations with the k–ε turbulence model, the study tested the performance of the system under various wave heights and breakwater-bridge spacings. Results revealed that the combined system significantly reduced both horizontal (up to 55%) and vertical (up to 34.2%) tsunami-induced forces, outperforming conventional breakwater types and standalone fairings. The force reduction improved with increased spacing between the breakwater and the girder.

Table 5: Summary of selected numerical studies on breakwater as tsunami mitigation countermeasure

Study	Numerical Model	Dimension	Tsunami generation method	Breakwater Geometry	Evaluated Parameters	Main Findings	Validation	Limitations
Takagi & Bricker (2014)	2D shallow water equations	2D	2011 Great East Japan Tsunami (field data calibrated)	Urban floodplain of Ishinomaki City, with and without port breakwaters	Inundation height, flow velocity, drag force, building damage ratio	Breakwaters did not significantly reduce inundation due to wide openings; simulated full enclosure greatly improved performance; land use and drag forces explained damage variation	Calibrated using satellite and field survey data (Tohoku Joint Survey)	Based on 2D model; tsunami bore physics and 3D effects not captured; structural behavior not explicitly modeled
Wei & Dalrymple (2016)	GPUSPH (Smoothed Particle Hydrodynamics)	3D	Solitary-like tsunami wave in wave tank	Bridge with and without upstream breakwater or service road	Horizontal and vertical forces on bridge deck	Breakwaters reduced forces by up to 58% at optimal distance	Validated against lab data	Single-phase fluid only; high-frequency force components underestimated; debris and air effects excluded
Xue et al. (2022)	OpenFOAM	2D	Solitary waves simulating extreme storm surge or tsunami	Tri-semicircle submerged breakwater + T-girder bridge	Horizontal and vertical wave forces, velocity field, force	Horizontal force reduction up to 71.6%; vertical up to 38.3%	Compared with validated trapezoidal breakwater simulations	2D only; no structural fatigue or cost evaluation; ecological impacts and 3D turbulence left for future study
Wu et al. (2025)	ANSYS Fluent	2D	Inflow wave conditions; solitary-like tsunami bores	T-girder bridge with semicircular breakwater and L-shaped fairing in front	Horizontal and vertical peak forces, influence of wave height and breakwater spacing	Combined system reduced horizontal forces by up to 55% and vertical forces by 34.2%; optimal breakwater-bridge distance ~5 m; performance holds across 3–4.8 m wave heights	Numerical results validated by improved empirical formulas	2D only; lacks 3D flow effects and experimental validation

2.4.2.3 Numerical Investigation of Water-Filled Canal Performance under Tsunami Loads

Recent numerical modeling studies have focused on the performance of water-filled canals as tsunami mitigation elements. Studies show that canals act as hydraulic dampers, dispersing wave energy via complex flow patterns.

Dao et al (2013a, b) conducted a numerical study to assess the effectiveness of the Kita-Teizan Canal, a shore-parallel canal along the Sendai Coast, in mitigating tsunami impacts during the 2011 Great East Japan Earthquake and Tsunami. Given the limitations of shallow water equations in capturing wave breaking and nearshore turbulence, a two-dimensional RANS-based model of NEWFLUME developed by Lin and Liu (1998) was employed. Although the study did not consider any downstream structures to directly evaluate the canal's influence on tsunami forces acting on them, the analysis of tsunami energy and depth-averaged velocity indicated that the canal reduced tsunami energy and delayed the wave's arrival time compared to a scenario without the canal. The canal was particularly effective during small tsunami events, with offshore wave heights of 3 to 4 meters, reducing the potential damage to residential infrastructure by approximately 3 to 4 percent.

Rahman et al. (2017) performed both experimental and numerical modeling to assess the effectiveness of perpendicular water-filled canals as tsunami mitigation measures. They used the improved Moving Particle Semi-Implicit (MPS) method to simulate dam-break type bores representing tsunami-like waves. They considered several canal configurations with varying widths (25–50 cm) and depths (5–10 cm) and validated the numerical results with flume experiments. Their results showed that canals alone can delay tsunami arrival time, reduce bore velocity by up to 48%, and partially reflect wave energy, although inundation depth was not significantly reduced. The numerical simulations captured the splash, reflection, and energy dissipation phenomena observed in the experiments with reasonable accuracy. Furthermore, when a canal was combined with a dune, the combined countermeasure significantly reduced both inundation depth and flow velocity, highlighting the importance of integrated strategies.

Hashimoto et al. (2018a, b) performed studies to evaluate the tsunami mitigation effects of existing and proposed canals along the Sendai Bay coast in Miyagi Prefecture, Japan. They focused on the Teizan and Kitakami Canals, using a 2D finite difference shallow water model to simulate

the 2011 Tohoku tsunami. The canals were found to reduce tsunami arrival time, flow velocity, and inundation depth, and to effectively drain tsunami backflow, especially in the Iwanuma and Yamoto areas. Different configurations such as canal widening and levee heightening were examined, with the combination proving most effective in reducing flooding extent and energy. They explored the feasibility of constructing a new canal in the Watari and Yamamoto areas, south of the Abukuma River where no canals currently exist. The proposed canal (36 m wide, 3.7 m high) was evaluated under the same tsunami scenario using a similar 2D model. Results showed that the new canal significantly delayed tsunami arrival (by up to 196 seconds), and reduced inundation depth (up to 1 m), run-up speed, flow velocity, and flooded area/volume (by 1.46 km^2 and 1.4 million m^3, respectively). Their studies support the use of shore-parallel canals as effective components in multi-layered tsunami defense systems, though they are limited by the two-dimensional nature of the analysis and assumptions of structural integrity.

Elsheikh et al. (2022a, b) conducted a detailed numerical and experimental investigation into the mitigation performance of rectangular water-filled canals subjected to tsunami-like turbulent bores generated by a dam-break setup. Their study explored the influence of canal depth and orientation on bore hydrodynamics, including specific momentum, energy dissipation, and vortex dynamics. Three impoundment depths (0.2, 0.3, and 0.4 m) and three canal depths (0.05, 0.10, and 0.15 m) were analyzed using OpenFOAM-based 3D multi-phase modeling. Turbulence was modeled using the k-ε family, with the standard model showing the best agreement. Their results showed that deeper canals significantly reduced the maximum specific momentum and mean flow energy by enhancing turbulence and air entrainment. As canal depth increased, energy dissipation became more effective, and the bore jet stream became shorter and less intense. Vortex eyes formed near the upstream edge of the canal, with their downstream movement and dissipation depending on canal depth. Orientation also played a role, while all canal angles reduced momentum downstream, a 45° orientation caused the highest localized energy and momentum but led to greater dissipation further downstream due to increased turbulence.

Arefi et al. (2025) conducted a numerical investigation using FLOW-3D to evaluate the effectiveness of rectangular water-filled canals in mitigating tsunami-like bore forces on a downstream column. Among different turbulence modelling approaches, Large Eddy Simulation (LES) was selected as it provided the best match to the experimental data. The model was

calibrated using flume experiments and further extended to full-scale simulations to eliminate scaling effects and better represent real tsunami dynamics. Various canal depths (0.5-4.5 m) and widths (10-40 m) were tested. Their results demonstrated that the presence of the canal significantly reduced the initial impact force, with up to 40% reduction for a 4.5 m-deep and 40 m-wide canal. Their study found that canal width had a greater influence on force reduction than depth, although a threshold was observed beyond which further increases in either dimension yielded minimal additional benefit. The bore front velocity was notably reduced after canal passage, with a substantial change in flow regime and turbulence characteristics contributing to energy dissipation (Figure 16).

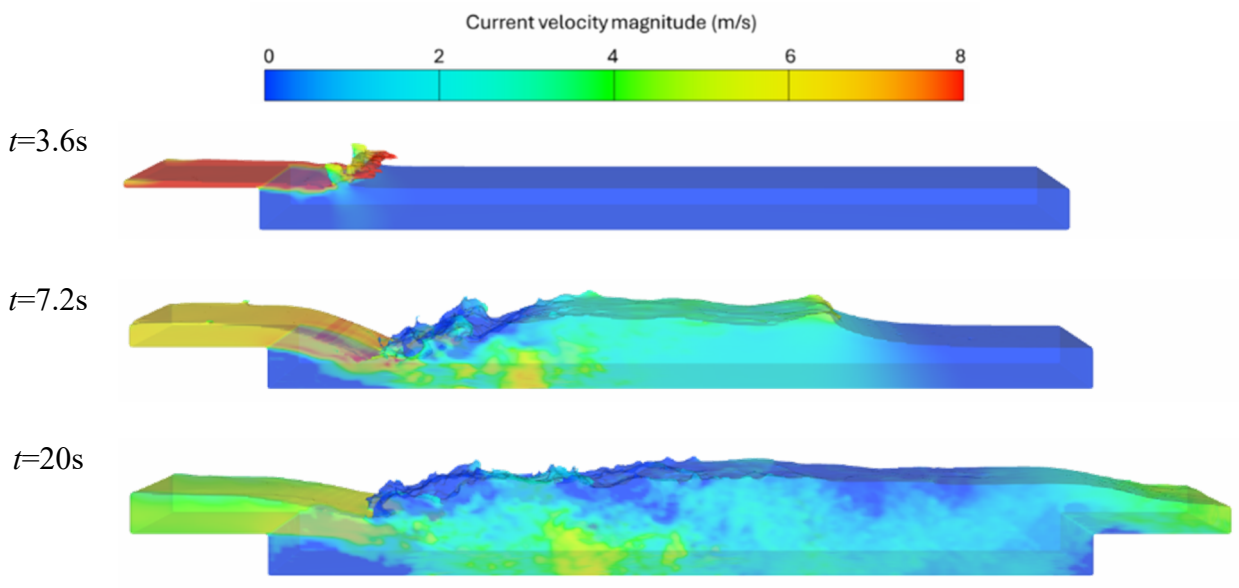

Figure 16: Interaction of tsunami bore with water-filled canal (Arefi et al., 2025)

Table 6: Summary of selected numerical studies on canals as tsunami mitigation countermeasure

Study	Numerical Model	Dimension	Tsunami generation method	Canal Geometry	Evaluated Parameters	Main Findings	Validation	Limitations
Dao et al. (2013a, b)	NEWFLUME	2D	Solitary wave	Shore-parallel, fixed width	Energy, depth-averaged velocity	Canal reduces tsunami energy and delays arrival time	Field conditions in Sendai Coast	No downstream structure; limited to small tsunami cases; 2D only
Rahman et al. (2017)	Improved MPS	2D	Dam break	Perpendicular canal, widths 25-50 cm, depths 5-10 cm	Wave height, velocity, inundation depth	Canals reduce wave velocity and delay arrival; combining canal with dune improves depth and velocity mitigation	Flume experiments	Simplified lab scale; no structural loading or large-scale urban modeling considered
Hashimoto et al. (2018a, b)	In-house 2D model (finite difference)	2D	Real 2011 tsunami fault model	Teizan & Kitakami canals, realistic cross-sections	Arrival time, water level, flow velocity, inundation extent, backflow	Canals delayed tsunami, reduced flow speed and flooding, drained return flow; widening + levee best	Compared with observed traces	No 3D effects considered; no structural force data
Elsheikh et al. (2022a, b)	OpenFOAM	3D	Dam break	Rectangular, constant width (0.6 m), depths 0.05-0.15 m, angles 0°-60°	Specific momentum, energy, vorticity, velocity profiles	Deeper and angled canals enhance energy dissipation; standard k-ε model accurate; 45° angle induces higher localized momentum	Experimental flume data	Limited canal widths; did not study structural impact forces or real topography
Arefi et al. (2025)	FLOW-3D	3D	Dam break	Rectangular, varying depth (0.5-4.5 m) & width (10-40 m)	Bore depth, force on column, velocity profiles, pressure	LES was found to be better, Canal reduced bore force by up to 40%; width more influential than depth; threshold beyond which no added benefit observed	Lab-scale calibration and full-scale validation	Limited to only dry bed; no complex urban features or real topography; canal orientation not examined

2.5 Discussion

This section provides a comprehensive study of existing research on structural tsunami mitigation measures, with a particular focus on their effectiveness in reducing tsunami energy and mitigating impacts on downstream coastal infrastructure. Unlike many previous studies that primarily examine the structural resistance or failure of individual mitigation structures, this review emphasizes their functional role in modifying tsunami flow characteristics and reducing impacts on protected areas. Consequently, only a carefully selected subset of studies was included, prioritizing those that investigated impact mitigation rather than structural strength alone.

Seawalls and breakwaters are widely recognized as established coastal protection measures. When appropriately designed and maintained, they can reduce tsunami energy, delay inland inundation, and protect critical coastal assets. However, their performance is highly dependent on factors such as geometry, construction quality, local bathymetry, and tsunami characteristics. While these structures are generally effective for more frequent, moderate events (Level 1 tsunamis), numerous studies indicate that their performance deteriorates during rare but extreme events (Level 2 tsunamis). Failure mechanisms such as overtopping, scour, and structural instability frequently dominate under such conditions, limiting their reliability as stand-alone protection systems.

Water-filled canals represent a comparatively recent and less-explored structural countermeasure. Available laboratory and numerical studies suggest that canals can dissipate tsunami energy by reducing bore front velocity and attenuating hydrodynamic forces acting on downstream structures. Their effectiveness appears particularly promising when canals are strategically integrated within coastal layouts or combined with natural features such as vegetated buffers. Nevertheless, the broader implementation of canals is constrained by the absence of standardized design guidelines, limited field validation, and a lack of large-scale performance data from real tsunami events.

From a methodological perspective, both laboratory experiments and numerical simulations play essential and complementary roles in advancing understanding of tsunami-structure interactions. Physical experiments enable controlled investigation of complex hydrodynamic processes such as bore formation, overtopping, and turbulence in the vicinity of mitigation

structures. Experimental results consistently demonstrate the strong influence of structure geometry, relative freeboard, and local bathymetry on flow transformation and downstream impacts.

Numerical modeling offers greater flexibility for exploring a wide range of tsunami scenarios and structural configurations that are difficult or impractical to reproduce experimentally. Advances in three-dimensional CFD modeling, turbulence models, and free-surface tracking have significantly improved predictions of bore dynamics, pressure distribution, and overtopping behavior. Despite these advances, numerical simulations remain sensitive to mesh resolution, turbulence modeling choices, and boundary condition specification. The lack of high-quality field data and standardized benchmark experiments continues to pose a major challenge for robust model validation.

Across both experimental and numerical studies, consistent trends emerge regarding the performance of structural mitigation measures. Seawalls and breakwaters can effectively modify inundation patterns and reduce incident wave energy under moderate conditions, but their effectiveness diminishes rapidly during extreme events. Water-filled canals, while supported by promising evidence, require further investigation to clarify scale effects, transient flow interactions, and performance when combined with other structural or nature-based systems.

Several key research gaps were identified through this review. Field validation of experimental and numerical results remains limited, reducing confidence in real-world applicability. The influence of mitigation measures on downstream infrastructure is often overlooked in both design and modeling efforts. Optimization studies addressing canal and barrier dimensions, placement, and configuration under varying tsunami conditions are scarce. Additionally, geomorphological processes such as sediment transport, scour, and debris impact are frequently simplified or neglected, despite their importance in determining structural performance and failure mechanisms.

2.6 Conclusions

This review examined the current state of experimental, numerical, and field-based research on structural tsunami mitigation measures, with particular emphasis on seawalls, breakwaters, and water-filled canals. By focusing on studies that evaluate impact mitigation rather than structural

resistance alone, the review provides a consolidated perspective on how these measures influence tsunami energy dissipation and downstream structural loading.

The findings confirm that seawalls and breakwaters remain important components of coastal defense systems, particularly for reducing impacts from frequent, moderate tsunami events. However, their performance is highly site- and event-dependent, and they are vulnerable to overtopping, scour, and instability during extreme tsunamis. As such, reliance on these structures as single-line defenses may be insufficient for long-term coastal resilience.

Water-filled canals emerge as a promising but underutilized mitigation strategy. Existing laboratory and numerical studies demonstrate their potential to reduce bore velocity and attenuate forces on downstream structures, especially when integrated into broader coastal protection systems. Nonetheless, their practical implementation is currently limited by insufficient field validation, the lack of standardized design methodologies, and minimal real-world performance data.

The review highlights the necessity of stronger integration between experimental and numerical approaches, supported by systematic validation using field observations and benchmark datasets. Future research should prioritize high-fidelity CFD modeling combined with large-scale laboratory experiments to better capture three-dimensional turbulence, transient flow behavior, and structure-induced flow transformations. Greater emphasis should also be placed on system-level performance, including the interaction between multiple mitigation measures and their combined effects on downstream infrastructure.

Ultimately, no single countermeasure can fully eliminate tsunami risk. Integrated, multi-layered mitigation strategies—such as combining seawalls with canals, vegetated buffers, and elevated evacuation infrastructure—offer more resilient and adaptable solutions. Addressing the identified research gaps will improve predictive capabilities, reduce uncertainty in design, and support the development of effective, scalable, and context-specific tsunami mitigation strategies for vulnerable coastal regions.

Chapter 3. Physical Modelling Experiments[2]

Abstract

Following several extreme tsunami events, such as the 2004 Indian Ocean Tsunami and the 2011 Tohoku Tsunami, which devastated coastal infrastructure in countries around the Indian Ocean and the Pacific Ocean shores, respectively, there has been an increased research effort to investigate tsunami-induced forces exerted on structures located near the coastline. Many researchers have investigated the mechanisms and characteristics of tsunami forces exerted on structures, and proposed mitigation countermeasures to reduce the impacts of tsunamis and subsequently minimize destruction. Forensic engineering post-tsunami field investigations have revealed that water-filled canals can reduce the inflow tsunami bore energy and act as an effective mitigation solution. However, studies on the effects of canals as mitigation countermeasures have been few and limited in scope, thus necessitating further research. This study presents a comprehensive experimental program conducted to investigate the effects of rectangular water-filled canal on mitigating tsunami horizontal force exerted onto a square structural column using a scale of 1:10. A rapid-release vertical gate was used to generate a tsunami-like hydraulic bore which propagated over a horizontal, dry, and smooth bed, further crossing over a rectangular water-filled canal, and subsequently impacting a vertical column. The time history of the bore depth at various locations along the flume, as well as the time history of horizontal force exerted onto the column were recorded. Several parameters were found to affect the degree of force reduction, some of which were the water impoundment depth behind the gate which sets the characteristics of the bore, the canal width, and its depth. The obtained results indicate that the presence of a water-filled canal can significantly reduce the bore front velocity, and consequently, the maximum impact horizontal force exerted onto the column by more than 25%. These findings

[2] Arefi, R., Nistor, I., Mohammadian, A., & Elsheikh, N. (2025). Effects of a rectangular water-filled canal on bore induced horizontal force exerted on a nearshore structure. *Natural Hazards*. https://doi.org/10.1007/s11069-025-07709-y

suggest that water-filled canals, as a potential solution, could effectively mitigate the impact of tsunami bores' energy, reduce structural damage, and potentially save lives.

Highlights:

- Water-filled canals reduced the tsunami impact force on a column by over 25%.
- Bore front velocity decreased significantly in the presence of the canal.
- Canal width and depth influenced the effectiveness of the force reduction.
- Time history of the bore depth and associated impact force exerted onto a column were analyzed through an experimental program.
- Water-filled canals showed potential as a possible tsunami mitigation measure.

Keywords: Tsunami-like bore, dam-break method, tsunami mitigation measures, rectangular water-filled canal, force-on-column, experimental tests.

3.1 Introduction

Tsunamis (originated from Japanese tsu= harbour, nami= wave) are a series of significantly long waves which can generated in oceans or large lakes, and which are long and occasionally extreme waves which impact coastlines (Röbke and Vött, 2017). Tsunamis can result from various mechanisms, such as submarine earthquakes, aerial or submerged landslides, and volcanic eruptions (Dias et al., 2014). The energy of these events is transmitted to the water body and that leads to the generation of a series of massive, long-period waves with periods of the order of minutes to hours (Larsen et al., 2017).

Although tsunamis are relatively rare phenomena, they are among the deadliest natural hazards (Goltz and Yamori, 2020), causing significant destruction of structures near affected coastlines and resulting in significant number of fatalities worldwide (Nistor et al., 2009). Figure 17, maps the locations of tsunami-generating sources between 2000 and 2025, based on data from the NOAA NCEI/WDS Global Historical Tsunami Database. It illustrates the global distribution of

tsunami sources, including events triggered by submarine earthquakes, landslides, and volcanic eruptions, but excludes meteorological tsunami events.

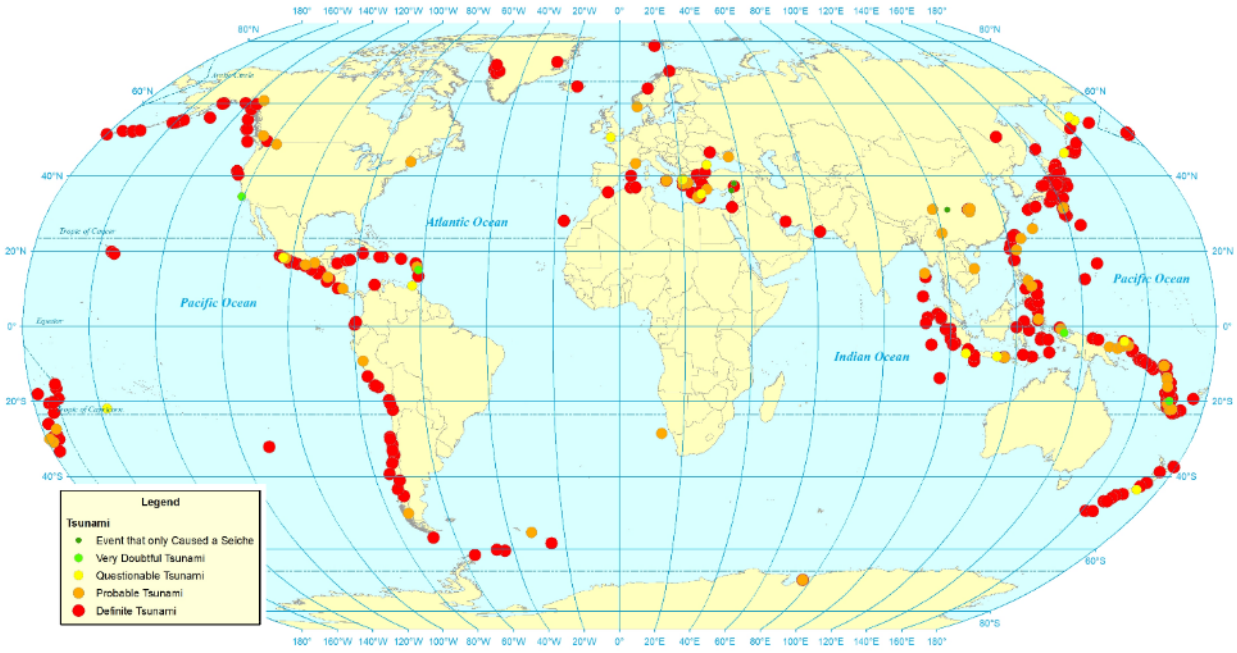

Figure 17: Locations of tsunami-generating sources between 2000 and 2025, based on data from the NOAA NCEI/WDS Global Historical Tsunami Database. This map includes tsunamis generated by submarine earthquakes, landslides, and volcanic eruptions.

Structural damage to coastal infrastructure caused by tsunami inundation is due to several factors, including hydrostatic forces and hydrodynamic forces. Other contributing factors include impact from floating debris, fire spread through floating debris and flammable liquids, and soil erosion and associated slope or foundation failures (FEMA, 2019). Recent tsunami events, including the 2004 Indian Ocean Tsunami, the 2011 Tohoku Tsunami, the 2018 Sulawesi Tsunami in Indonesia, and the 2024 Noto Tsunami in Japan, have underscored the critical need for developing effective measures to mitigate such disaster impacts, safeguard infrastructure, and reduce the costs of rebuilding coastal communities (Inagaki et al. 2024). Various design provisions and planning/zoning measures have been introduced to reduce the tsunami-induced effects on coastal infrastructure (Oetjen et al., 2022). Researchers have studied the effects of natural features and man-made construction to reduce the energy of tsunami inundation of which sea walls (Matuo, 1934; Rahman et al., 2014; Huang et al., 2022), breakwaters (Burcharth and Hughes, 2003; Hanzawa and Matsumoto, 2015; Mikami et al., 2015), canals (Dao et al., 2013a, b; Rahman et al.,

2017; Elsheikh et al., 2022a, b), and coastal forests (Kathiresan and Rajendran, 2005; Nateghi et al., 2016) are among such features/solutions.

Among various man-made structures aimed at reducing the energy of tsunami inundation, constructing a canal parallel to the coastline has been hypothesized as a potential mitigation measure. While the primary function of canals has traditionally been for drainage, irrigation, or urban infrastructure, post-tsunami forensic field investigations following the 2011 Tohoku Tsunami (Chock et al., 2013) revealed that some shore-parallel canals incidentally helped reduce tsunami forces and inland inundation. Based on these observations, the present study explores the potential of canals as a useful tsunami mitigation measure. Our experimental results, together with field evidence, suggest that when appropriately designed or modified, such canals can function similarly to conventional coastal defense structures such as seawalls or breakwaters in reducing tsunami impact forces.

While seawalls and breakwaters may generally be more effective than canals in reducing tsunami energy and providing additional time for evacuation, it should be noted that they incur high costs. For example, following the 2011 Tohoku Tsunami in Japan, approximately 395 km of seawalls were subsequently built at a cost of 1.35 trillion yen (USD 12.74 billion). Moreover, their failure or overtopping can exacerbate tsunami impacts (Reuters, 2018). Post-tsunami field surveys have shown that a water-filled canal parallel to the coastline can dissipate the energy of the incoming tsunami inundation (Chock et al., 2013). During the 2004 Indian Ocean Tsunami, the Buckingham Canal, located along the Chennai coastline, measuring 30 meters wide and 10 meters deep, played a crucial role in reducing the energy of the tsunami bore and saved the lives of many fishermen (Rao et al., 2005; Ramalingeswara et al., 2005). Several studies have shown that such canals have the potential to significantly reduce the tsunami inundation energy (Dao et al., 2013a, b; Usman et al., 2014; Rahman et al., 2017; Elsheikh et al., 2022a, b). Figure 18 shows the Kita-Teizan Canal in Japan which is parallel to the coastline and the overland bore propagation during the 2011 Tohoku Tsunami. Field investigations revealed that the presence of a water-filled canal influenced tsunami inundation by reducing the tsunami bore velocity and consequently the damage to infrastructure located landward of the canal (Adityawan and Tanaka, 2016).

Figure 18: Japan 2011 Tsunami inundation propagating over the Kita-Teizan Canal (ASCE, 2022)

By comparing Google Earth satellite images before and after the 2011 Tohoku Tsunami, and as illustrated in Figure 19 and Figure 20, it was shown that while the buildings located seaward of the Kita-Teizan canal were completely destroyed by the tsunami (in the area marked with red dashed line), while those located landward of the canal were less affected by the tsunami-induced loading due to the presence of the water-filled canal which acted as a mitigating measure. Although the most appropriate comparison would involve two nearby regions, one with the presence of a canal and the other one without it, such a direct comparison was not available in that region. To address this, areas near the canal in Kita-Teizan, Japan, were carefully examined. In this region, several buildings with similar structural characteristics (based on visual analysis of satellite images) were located. In addition, buildings situated close to the canal were selected to minimize the influence of varying topographies, bed roughness, and other site-specific factors.

(a)

(b)

Figure 19: Images of the Kita-Teizan Canal's effects on reducing tsunami flooding effects on structures: (a) prior, and (b) after 2011 Tohoku Tsunami (38° 7'43.62"N, 140°55'46.37"E) (source: Google Earth)

Figure 20: Effects on reducing tsunami flooding effects on structures: (a) prior, and (b) after the 2011 Tohoku Tsunami (38° 4'24.42"N, 140°55'16.52"E) (source: Google Earth)

Despite existing guidelines and standards proposed for designing structures to withstand tsunami effects such as FEMA-P646 (2019) and ASCE7-16 (2022), respectively, there is a need for additional studies to develop new and effective tsunami mitigation measures. This study focuses on an experimental program aimed at assessing the impact of water-filled canals on mitigating the tsunami bore force exerted on the model of a structure. This involved generating a tsunami-like bore and subsequently measuring the time history of the force exerted by the bore on a square column as the bore passed over a rectangular water-filled canal and impacted the structure,

as well as the time history of bore depth at various locations during the propagation of the tsunami-like bore before and after the canal.

3.1.1 Literature review and research needs

Several experimental and numerical studies investigated the impact of tsunamis on vertical seawalls that block the entire width of the flume (Esteban et al., 2015; Huang et al., 2022). Additionally, there has been research related to low-rise structures that allow overtopping (Rahman et al., 2014; McGovern et al., 2023) as well as studies which address tsunami-induced forces on pipelines (Ghodoosipour et al., 2019; Zhao et al., 2019). However, studies focusing on the impact of tsunami bores on vertical structures that allow flow to pass around the structures are limited.

Previous studies have shown that the blockage ratio (column width relative to channel width) significantly influences bore-induced forces. Arnason et al. (2009) and Chock et al. (2013) reported that increasing the blockage ratio increases the drag and impact forces due to enhanced flow obstruction and wave-structure interaction. Conversely, small blockage ratios (below 5-10%) result in lower force coefficients, which are more aligned with Morison-type equation loading estimation. Moreover, a circular column generally produces less flow separation and lower drag than a square column of equal projected width, resulting in slightly lower horizontal forces. Square or rectangular columns experience up to 10–20% higher drag coefficients than circular columns under similar wave or tsunami flow conditions (Yeh et al., 2014; Hayatdavoodi et al., 2014). The difference becomes more pronounced in impulsive bore impacts, where flow stagnation occurs on the flat faces of the column.

In a comprehensive investigation, Nistor et al. (2009), Palermo et al. (2009), and Nouri et al. (2010) studied the force components on structures induced by turbulent bores as representative of tsunami bores by conducting an experimental program. Their objectives were to better understand the bore-structure interaction and to improve the existing design guidelines at the time for the design of buildings located near coastlines in tsunami-prone areas. A rapidly opening swing gate was used to generate tsunami-like bores and the time histories of pressures and forces exerted on all sides of columns with different cross-sections (square or diamond, and circular) and walls were recorded using pressure transducers and a six degrees of freedom dynamometer, respectively. They also measured the bore depth and flow velocity along the flume and around the structures and stated that when turbulent bores impact the structures, surge, run-up, and drag forces are generated,

with drag being dominant at shallower depths while the surge, and run-up are dominating at increasing depths.

Bremm et al. (2015) performed a series of experimental tests to study the interaction of a rapidly transient flow with different periods and amplitudes using a single rectangular structure mounted on a 1:40 sloping beach. They measured the time history of the force exerted on the structure and studied the flow pattern around the structure in a series of physical experiments. Their studies showed that drag force coefficients change during flow-structure interactions, making it essential to use the time-history instead of constant values to accurately compute drag forces in transient flow scenarios.

Shafiei et al. (2016) carried out physical modeling to study the force exerted on an inland square prism. They measured the vertical pressure distribution and studied the effects of prism orientation. They measured the pressure at five different levels by placing differential pressure sensors inside a 300 mm ×300 mm ×600 mm square column. According to their study, bore flow consistently applied a positive pressure on the structure irrespective of the column orientation, and the bore velocity had a greater impact on tsunami pressure than bore depth.

There are different approaches to decrease the destructive effects of tsunami events. Oetjan et al. (2022) categorized them as prevention, spatial planning, and management. A considerable body of research has investigated the influence of both nature-based solutions, such as coastal and mangrove forests (Kathiresan and Rajendran, 2005; Teh et al., 2009; Tanaka et al., 2018) as well as man-made structures, such as breakwaters, coastal seawalls, and onshore dikes (Al-Faesly et al., 2012; Hanzawa and Matsumoto, 2015; Samarasekara et al., 2017) on tsunami-like bore hydrodynamics. However, only a limited number of studies have addressed water-filled canals as potential mitigation measures against tsunamis. In the following sections, some studies that have investigated the effect of canals on tsunami-like bore hydrodynamics are presented.

Dao et al. (2013a, b) examined the effectiveness of shore-parallel canals in reducing the tsunami energy. They employed a numerical model based on the Navier-Stokes equations and simulated the coastal inundation during the 2011 Tohoku Tsunami. They investigated how these factors influenced tsunami energy reduction by varying the width and depth of the canal. Their findings revealed that the Kita-Teizan Canal significantly decreased the tsunami energy, with wider canals leading to greater energy dissipation. They mentioned that for small tsunamis with

offshore heights of 3 to 4 m, the presence of the canal can reduce tsunami damage to coastal infrastructure by approximately 3 to 4%. Their findings illustrate that the velocity of tsunami-like bores diminishes in the presence of water-filled canals due to turbulent behavior when the bore enters the canal, and that the canal plays a crucial role in attenuating the bore velocity.

Usman et al. (2014) studied the effectiveness of modifying the onshore topography to reduce the tsunami bore energy. They explored various modifications, including the use of embankments parallel to the coastline, hollow topography, and vegetated areas. Their numerical modeling results showed that digging a canal can reduce the bore depth and velocity.

Watanabe et al. (2016) conducted laboratory experiments to investigate the impact of a rectangular canal on bores generated by various impoundment water depths in reducing overflow bore velocity and dissipating energy from tsunami-like bores. Their research revealed that the presence of a mitigation canal resulted in a decreased overland flow velocity and an increased bore depth in front of the canal, indicating effective energy absorption by the canal. Additionally, they observed that the quantity of the overflow in a flume with a partially filled canal was smaller than that in a flume without a canal, with the damping rate varying based on factors such as water level and waveform. Their findings emphasized the importance of canal design and water depth in controlling overflow quantity and mitigating tsunami-induced inundation.

Rahman et al. (2017) performed a series of laboratory experiments to assess the effectiveness of different dimensions of rectangular canals in mitigating the tsunami's impact on coastal areas. They found that the most significant reduction in bore velocity occurred when the bore passed over the deepest and widest canal. The experiments, which focused on a limited range of canal aspect ratios, consistently showed a delay in tsunami arrival time and velocity reduction across different canal configurations. Their study concluded that while canals could partially absorb tsunami wave energy, they also caused reflected waves, leading to varied inundation depths compared with scenarios without canals. Their experiments involved altering canal geometry to observe the effects on tsunami flow, with wider and deeper canals demonstrating greater impact reduction.

Elsheikh et al. (2020, 2022a, b) investigated the impact of rectangular canals on turbulent surge hydrodynamics both before and after the canal. They conducted a series of experimental and numerical tests using dam-break simulations, in which a rapidly opening vertical gate was removed to simulate a tsunami-like bore. They validated their 3D numerical modeling with their

experimental tests which were performed in a glass-walled tilting flume that was 15.56 m long, 0.38 m wide, and 0.60 m deep. They considered different canal depths (5, 10, and 15 cm), widths (60, 100, and 150 cm), and upstream impoundment water depths (20, 30, and 40 cm). By measuring the time history of the surge heights and bore velocities at various locations before and after the canal, they assessed the effect of the water-filled canal on tsunami energy attenuation. Their analysis indicated that wider canals were more effective at reducing the momentum of tsunami bores, while deeper canals absorbed more energy as the bore passed through. Their experimental and numerical results demonstrated that the existence of the canal led to an increase in the maximum bore depth landward of the canal, while the maximum velocity of the tsunami-like bore decreased as it passed over the water-filled canal.

Table 7 presents a selection of studies that investigated tsunami bore interactions with structures or considered countermeasure structures to reduce the tsunami inundation energy. Various types of tsunami generators have been employed, including vertical quick-release gates (Rahman et al., 2017; Elsheikh et al., 2022), chamber-type generators (Watanabe et al., 2016), and swinging or sluice gates (Al-Faesly et al., 2012; Nouri et al., 2010; Shafiei et al., 2016). Among these, water canals have received significant attention as a structural mitigation strategy. Their dimensions varied notably from narrow channels 25 cm wide (Rahman et al., 2017) to broader canals up to 300 cm in width (Elsheikh et al., 2022) with different depths and impoundment water levels tested. Bore velocities in these experiments ranged from approximately 1.5 to 4.9 m/s, while bore depths reached up to 0.47 m, depending on the setup. Mitigation walls, such as those tested by Al-Faesly et al. (2012), showed comparable bore flow conditions, but with more emphasis on structural interactions. Notably, the structural types also varied from simple square and circular columns to more complex configurations, reflecting the diversity in design and objectives across studies. Although not all experimental parameters are analyzed in detail here, they are included in Table 7 to ensure transparency and to assist future researchers in replicating or building upon these findings.

As previously mentioned, several studies have investigated the effects of canals as mitigation solutions; however, these investigations remain limited in scope and important aspects have not yet been fully addressed. Few studies have examined the interaction of tsunami-like bores with structures in the presence of a water-filled canal, and detailed force measurements of such

structures remain scarce. Furthermore, the existing codes and manuals that establish construction regulations for infrastructure exposed to tsunamis do not incorporate the potential mitigating effects of canals. The present study aims to address these limitations through a series of experimental tests focusing on the influence of a rectangular water-filled canal on the interaction between tsunami-like bores and coastal structures.

Table 7. Summary of selected studies investigating tsunami-like bore interactions with structures and countermeasure strategies for energy reduction

Reference	Type of tsunami generator	Countermeasure type	Countermeasure dimensions (cm)	Structure dimensions and type	Impoundment water depth (cm)	Bore velocity (m/s)	Bore depth (m)
Rahman et al. (2017)	Vertical quick release gate	Water canal	Width: 25, 50 Depth: 5, 10	-	10 15 20 25	1.5-2.2	0.023-0.048
Watanabe et al. (2016)	Chamber type	Water canal	Width: 30 Depth: 5	-	55 79 80	N.A.*	0.026-0.041
Elsheikh et al. (2022)	Vertical quick release gate	Water canal	Width: 60, 160, 300 Depth: 5, 10, 15	-	20 30 40	2.1-2.6	0.11-0.21
Al-Faesly et al. (2012)	Swinging gate	Mitigation wall	Height: 10, 15	30.5 cm square 30.5 cm circular	55 85 115	2.5-4.9	0.26-0.47
Nouri et al. (2010)	Swinging gate	-	-	20 cm square 32 cm circular	50 75 85 100	2.31-4.63	0.21-N.A.
Shafiei et al. (2016)	Rapid sluice gate	-	-	30 cm square	40 50 60	1.98-2.45	0.14-0.21
Bremm et al. (2015)	Volume-driven wave maker	-	-	10 cm square	N.A.	N.A.	0.06-0.13

*N.A.: Not presented any results

3.1.2 Objectives and novelty

This experimental study aims to comprehensively investigate the potential of a rectangular water-filled canal to mitigate tsunami-like bore forces on coastal structures. An experimental program was developed to examine how various input parameters affect tsunami energy attenuation. The findings are intended to support engineers in designing coastal infrastructure that accounts for tsunami-induced loading. The main objectives of the study were:

i) To investigate the influence of bore characteristics, canal dimensions, and the location of a square column on the horizontal force exerted by tsunami-like bores.

ii) To record the time-history of bore depth at key locations: before the canal, after the canal, and in front of the column.

iii) To measure and analyze the time-history of the horizontal force acting on a rigid square column, with a focus on how the presence of a mitigation canal alters the force characteristics.

iv) To investigate bore propagation, canal interaction, and bore-structure interaction using video analysis.

v) To quantify the reduction of bore-induced forces resulting from the presence of rectangular water-filled canals.

3.2 Experimental set-up

A comprehensive experimental program was conducted at the Water Resources Engineering Laboratory of the University of Ottawa, Canada, to investigate the impact of the presence of a rectangular water-filled canal and its features on the attenuation rate of the horizontal force exerted on a model column induced by a fast-propagating tsunami-like bore. The flume used in this experimental program was 15.60 m long, 0.38 m wide, and 0.60 m deep with glass sidewalls, which allowed the monitoring of bore propagation and its interaction with the canal and the column.

Figure 21 shows the experimental setup and the locations of the different measuring instrumentation. A 15 cm horizontal and smooth false bed was constructed by placing specially designed PVC boxes along the flume bed, filled with water, and strongly fixed to the bottom and side walls using silicon to prevent their displacement due to buoyancy and the uplift force of the tsunami-like bore. Different configurations of canals with depths of 5, 10, and 15 cm (measured from the top of the false floor) and widths of 60, 160, and 300 cm were designed and installed using three rows of PVC boxes with height of 5 cm and lengths of 60, 100, and 70 cm, which were filled with sand and installed on top of the flume bed. A 1:6 slope bed was designed and installed upstream of the gate to minimize local turbulence at the front of the horizontal false bed. Although the model canal depths tested in the laboratory were 5 cm, 10 cm, and 15 cm, applying the 1:10 Froude scale yields prototype canal depths of 0.5 m, 1.0 m, and 1.5 m, respectively. These prototype depths fall within the lower range observed in some existing shore-parallel canals in

tsunami-prone regions, e.g., sections of the Kita-Teizan Canal in Japan (2 m) and the Buckingham Canal in India (0.9 m). Due to the physical limitations of the laboratory flume and the constraints of the canal construction method, it was not possible to test deeper canal configurations.

The Reynolds number (Re) primarily affects the quasi-steady force on the column by controlling flow separation, while the Weber number (We) influences hydrodynamic forces through surface tension effects. According to the characteristics of bore and experimental set up, Re≈3.2–4.0×10^4 and We≈1.3–1.6×10^3 and by considering Froude scale of 1:10, $Re_{prototype}$≈1.0–1.3×10^6, $We_{prototype}$≈4.0–5.0×10^4. Although both Reynolds and Weber numbers are larger at prototype scale, the model tests are conducted at sufficiently high Re (>10^4) where drag coefficients and flow separation are known to be relatively insensitive to further increases in Re (quasi-inertia-dominated regime). Similarly, the Weber number is also sufficiently large (>10^3) that the surface tension effects are negligible in the model. Therefore, although the exact dynamic similarity for Re and We is not achieved, the hydrodynamic forces measured in the experiments are expected to be representative of the prototype conditions.

A rapidly opening vertical gate which was manufactured from plexiglass was installed at x=0 (7.8 m from the upstream end of the reservoir) and retaining water in an impoundment reservoir. Tsunami-like bores were generated using a rapidly uplifting gate. The generated bore propagated along the flume, crossed over the canal, and finally after hitting the column, dropped through a vertical drain at the end of the flume, directing the flow to the underground laboratory reservoir. In this study, impoundment depths were 20, 30, and 40 cm, resulting in volumes of 0.805, 1.208, and 1.611 m^3, respectively. Because the upstream reservoir was not rectangular, to calculate the aspect ratio of the reservoir length to water impoundment depth (L/d_0), an equivalent length was calculated as L=10.6 m. In these cases, the equivalent aspect ratios of the reservoir L/d_0 for reservoir depths (d_0) of 20, 30, and 40 cm were calculated to be 53, 35.3, and 26.6, respectively, which are significantly larger than the recommendations of Lauber and Hager (1998) for generating an ideal tsunami-like bore.

Four ultrasonic sensors were installed at specific locations to measure the depth of the bore as it propagated along the flume and towards the column. The location of these ultrasonic wave gauges was modified for each test, based on the dimension of the canal and the location of the column in order to allow proper comparison of bore parameters between tests. It is worth mentioning that

US1 was positioned 90 cm upstream of the gate (x=-90 cm) to determine the gate opening time as discussed in the next section. Two of the ultrasonic sensors were placed 30 cm behind and in front of the canal. A fourth one was installed 30 cm in front of the column, at a distance where run-up and water splash did not interfere with sensor's measurements. Additionally, a six-degrees of freedom load cell capable of measuring the time history of the horizontal force exerted on the column was rigidly attached at top of the column. Furthermore, five cameras were used to record bore propagation, gate opening, and bore interaction with the canal and column.

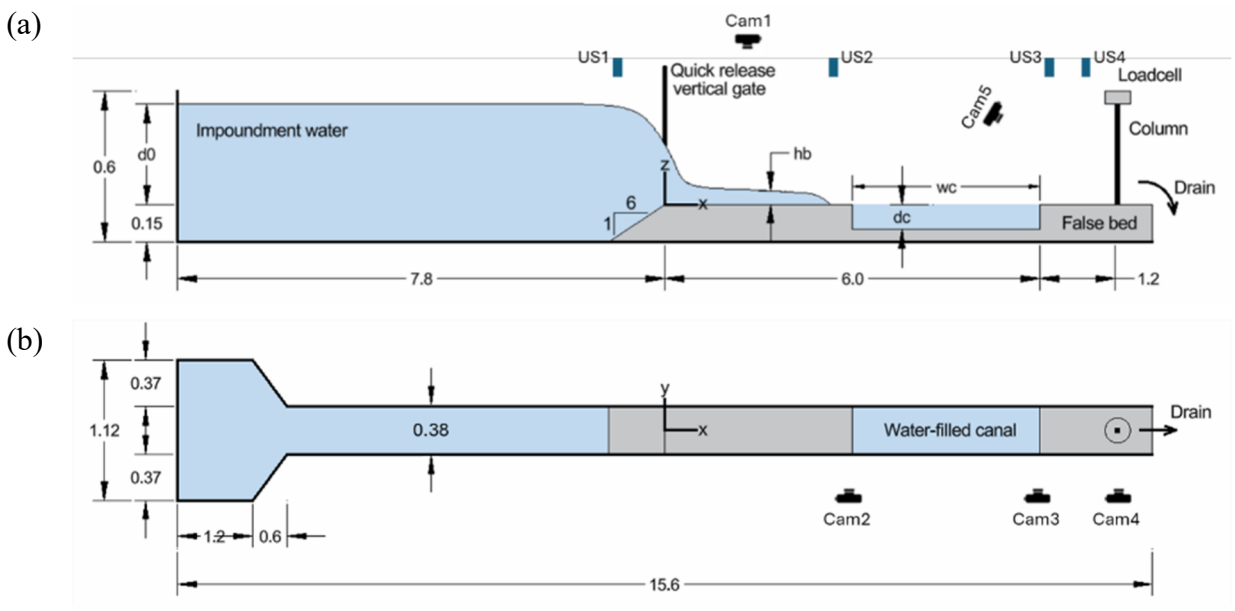

Figure 21. Schematic of the experimental setup (a) side and (b) plan view (not at scale, all dimensions in cm)

Froude scaling was used to convert the experimental measurements to prototype quantities. ASCE 7-22 (2022) states that the minimum scale factor for the physical modeling of structural components, such as columns in a tsunami, should not be less than 1:10. As shown in Table 8, the 2004 Indian Ocean and 2011 Tohoku Japan tsunamis exhibit a wide range of flow depths and velocities. In the present study, the measured bore depths and flow velocities for the three scenarios were approximately 10, 12, and 18 cm and 1.7, 2.0, and 2.3 m/s, respectively. By applying a 1:10 scale factor, the experiments represent a realistic moderate tsunami-like bore, as further explained in the following sections. The authors recognize the limits of their test program, as the effect of smaller and slower, for instance, bore heights and velocities were not investigated.

Table 8. Selected reported tsunami flow parameters

Event	Reported flow depth (m)	Reported flow velocity (m/s)	Reference
2004 Indian Ocean Tsunami	4-7	3-8	Dias et al., 2006; Matsutomi et al., 2006; Rossetto et al., 2007
2011 Japan Tohoku Tsunami	6-8	8-13	Fraser et al., 2012; Suppasri et al., 2012; Hayashi and Koshimura, 2013; Jaffe et al., 2012

In this study, the column had a square cross section with a side of 4 cm, while the canal width and depth were varied during tests from 60 to 300 cm and from 5 to 15 cm, respectively. Using a Froude geometrical scale of 1:10, the prototype size represented a square column with a 40 cm side (which is comparable to the size of a column typically used in multi-storey buildings) and a canal with a depth of 0.5 to 1.5 m and a width of 6 to 30 m. Each experimental test lasted approximately 40 seconds, which corresponds to about 125 seconds on the prototype scale based on a Froude scale of 1:10. While the duration of the modeled tsunami inundation cycle may be less than that of a real tsunami, this is of secondary relevance to this study as the maximum impact force is exerted during the first seconds of the tsunami impact.

3.2.1 Wave generation mechanism

Various methods for generating tsunami-like bores have been reported in the literature, including wave makers to generate solitary waves, dam-break bores by removing a quick-release gate, long-period waves, piston motion, and landslide generators (Wüthrich et al., 2018a). In this study, the quick release of water impounded behind a vertically lifting gate was used to generate a dam-break bore, relying on existing analogies between tsunami-like bores and waves generated by dam breaks (Chanson, 2006). This approach was chosen to model the tsunami-like bore propagation and its impact on a column located downstream of the canal. In recent years, the dam-break method has been demonstrated to be one of the most suitable techniques for generating tsunami-like hydraulic bores (Wüthrich et al., 2018b) and has been widely utilized by researchers, both experimentally and numerically (Asadollahi et al., 2019a, b; Ghodoosipour et al., 2019). While a tsunami-like bore cannot be strictly classified as a dam-break wave, there are numerous

similarities between these two types of waves, and consequently, tsunami-like bores are often generated by removing a quick-release gate (Aureli et al., 2023).

An ideal dam break occurs when the following criterion, proposed by Lauber and Hager (1998), is met, which fulfills the definition of the dam sudden removal:

$$T_0 = t_0 \sqrt{\frac{g}{d_0}} < \sqrt{2} \qquad 1$$

where T_0 is the dimensionless gate opening time, t_0 is the gate opening time, g is the gravitational acceleration (m/s^2), and d_0 is the depth of the impounded water. If the time required for the gate to open does not meet this criterion, meaning it is not short enough, then it can affect the formation and propagation of the dam-breaking wave, and consequently, the force exerted on the column. In this study, the dimensionless opening time was calculated using video analysis of images captured with a high-speed camera installed in front of the gate (Cam1) and was found to be less than 0.6, thus ensuring the formation of a realistic tsunami-like bore. Comparison of repeated tests showed that this small variability has a negligible influence on the generated bore characteristics

3.2.2 Instrumentation

To record the time history of bore depth along the flume, non-intrusive ultrasonic distance sensors (model MASSA, M-5000/220, Massachusetts, USA) with a sampling frequency of 200 Hz were deployed. The sensors provide non-contact measurements with a detection range of 100 mm to 1 m, and their accuracy is 0.1% of the total range to be measured, assuming a homogeneous environment. The locations of the ultrasonic sensors are shown in Figure 21. In the subsequent sections, the ultrasonic sensors were numbered according to their location; for example, US270 corresponds to the sensor placed at x=270 cm. The non-intrusive ultrasonic sensors were installed at the centerline of the flume, and to avoid any interference between adjacent ultrasonic sensors, a minimal distance of 1 m between them was considered.

A 6-axis load cell (model 6A154 Interface) was attached atop the column to monitor the time history of the horizontal force exerted by the tsunami-like bore on the column (Figure 22). The capacity of the load cell in x-direction was 100 N with a sampling frequency of 1 kHz and an accuracy of approximately 1%. The transduced calibration matrix was provided by the

manufacturer to convert the electric signals to the forces exerted on the load cell. A 0.5 mm gap was maintained between the column and the false bed to avoid any contact during the impact of the bore on the column. The gap was filled with lubricant (regular Vaseline, petroleum jelly) to prevent flow penetration and subsequent force distortion. Connecting all ultrasonic sensors (US) and the load cell to a HBM acquisition system allowed the synchronization of the time histories of the bore depths and the horizontal force exerted onto the column.

Five GoPro Hero5 video cameras were employed to monitor the propagation of the bore along the flume, as well as its features before and after entering the canal (Cam2 and Cam3), and the flow around the column (Cam4, and Cam5). In addition, a camera (Cam1) was placed atop the flume in front of the gate to record the movement of the bore front and to check the gate-opening time.

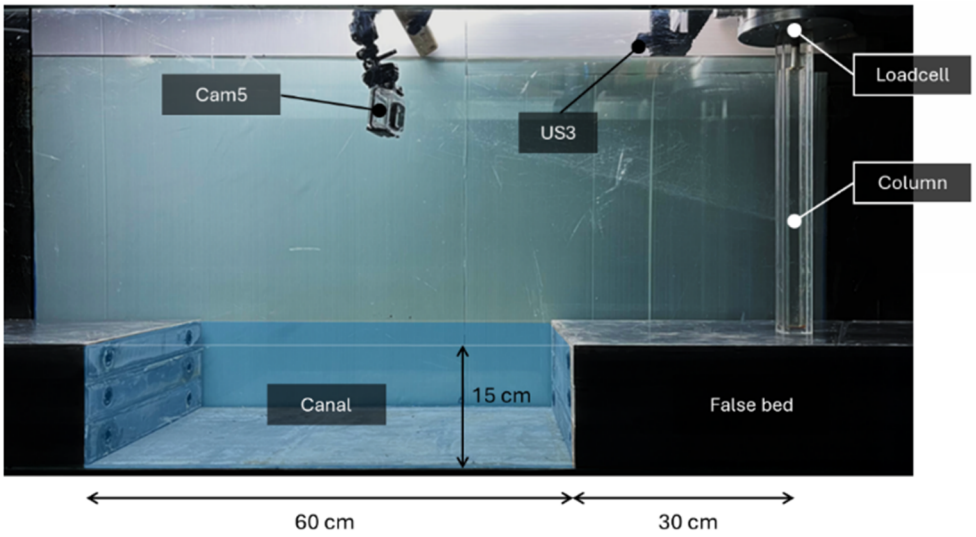

Figure 22. Laboratory experimental setup for a canal with a width of 60 cm and a depth of 15 cm

3.2.3 Experimental program

Table 9 presents the experimental tests conducted in this study and their specific variables. The tests were categorized into four different groups with different combinations of canal and column presence. Parameters such as canal width (w_c), canal depth (d_c), and position of the canal and column with respect to the system of coordinates were selected among the different parameters that affect the performance of the canal in mitigating the horizontal force exerted onto the column. The test designation was based on the water impoundment depth (d_0), canal depth (d_c), and the location of the water canal and column. For example, test number D40-C300360-d10-S420

represents a test with an impoundment depth, d_0=40 cm, in which a mitigation canal is located at x=300 cm to x=360 cm, with a width, w_c=60 cm, and depth, d_c=10 cm, and the column was installed at x=420 cm.

While the experimental flume setup for the last group of tests with considering both canal and column could, in principle, accommodate a broader range of canal and column configurations, the scope of the present study was intentionally limited to scenarios deemed most representative of severe tsunami bore impacts. Preliminary tests indicated that column position relative to the canal had minimal influence on the maximum horizontal force, and therefore a fixed column location was adopted for consistency. Moreover, canal depth and impoundment water level were selected to represent the largest practical values achievable in the facility, which correspond to more extreme prototype conditions.

Table 9. Experimental test program

Group	Test No.	Test designation	d_0 (cm)	w_c (cm)	d_c (cm)	Position of upstream edge of the canal (cm)	Column position from the gate (cm)
No canal No column	1	D20	20	-	-	-	-
	2	D30	30	-	-	-	-
	3	D40	40	-	-	-	-
No canal With column	4	D20-S420	20	-	-	-	420
	5	D30-S420	30	-	-	-	420
	6	D40-S420	40	-	-	-	420
	7	D20-S520	20	-	-	-	520
	8	D30-S520	30	-	-	-	520
	9	D40-S520	40	-	-	-	520
	10	D20-S660	20	-	-	-	660
	11	D30-S660	30	-	-	-	660
	12	D40-S660	40	-	-	-	660
With canal No column	13	D40-C300360-d05	40	60	5	300	-
	14	D40-C300360-d10	40	60	10	300	-
	15	D40-C300360-d15	40	60	15	300	-
With canal With column	16	D40-C300360-d05-S420	40	60	5	300	420
	17	D40-C300360-d10-S420	40	60	10	300	420
	18	D40-C300360-d15-S420	40	60	15	300	420
	19	D40-C300360-d15-S660	40	60	15	300	660
	20	D40-C300460-d15-S660	40	160	15	300	660
	21	D40-C300600-d15-S660	40	300	15	300	660

3.2.4 Coordinate system and time synchronization

As shown in Figure 21, the origin of the system of coordinates (x=y=z=0) is at location of the gate which situated 7.8 m downstream from the intake end wall of the reservoir. Furthermore, the origin of the time of synchronization of all instruments was selected as the moment of the gate opening, which was determined by analyzing the water surface level of the reservoir behind the gate using an ultrasonic sensor located 90 cm behind the gate. As shown in Figure 23, the instant of the gate opening (t_0) was determined by detecting the water level drop instant in the impounding reservoir (t_d) and considering incipient instant of the formation of the negative wave moving upstream in the reservoir. It should be noted that the dropping point is related to the time required

for the negative wave to propagate from the gate location (x=0) towards the ultrasonic sensor location ($\Delta x = x_{gate} - x_{US1}$), which was calculated as $\Delta t = \frac{\Delta x}{C}$ (Lauber and Hagger, 1998). Moreover, all video cameras were synchronized using the GoPro Quik app (GoPro, Inc., 2025), and the instant of gate opening, which was captured by the Cam1 located in front of the gate, was set as the origin of the time for all video cameras.

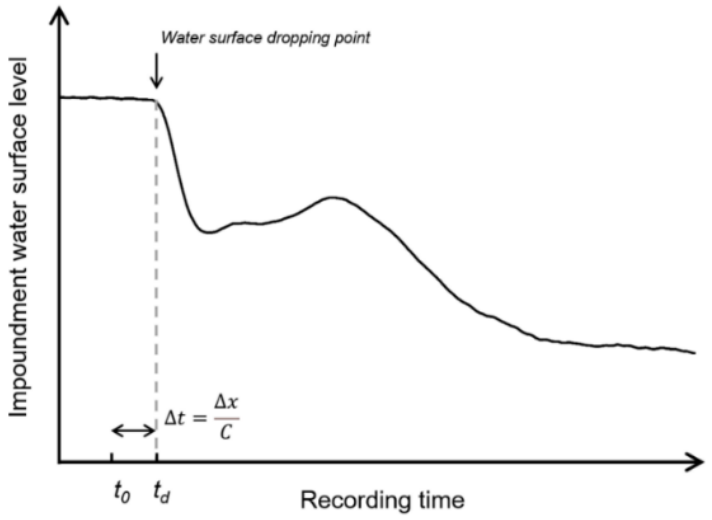

Figure 23. Determination of gate opening time by analyzing the water surface level behind the gate

3.2.5 Repeatability of results

All tests were repeated three times under the same conditions to verify the repeatability of the force measurements and the water surface level variations. Figure 24 and Figure 25 depict the time-histories of the measured horizontal force exerted on the column located at x=660 cm and the water surface levels at x=630 cm for two different tests, D40-C300600-d15-S660 and D40-S660, with and without the presence of the canal, respectively. As illustrated in these figures, the maximum difference in the measured force between the results of the repeated tests is associated with the initial impact of the tsunami-like bore on the column. While no average values were computed, all three repetitions showed similar bore shapes and force behavior. Although some differences were observed between the maximum and minimum force curves in the test with the canal, applying denoising techniques minimized these differences, resulting in negligible discrepancies at the peak force.

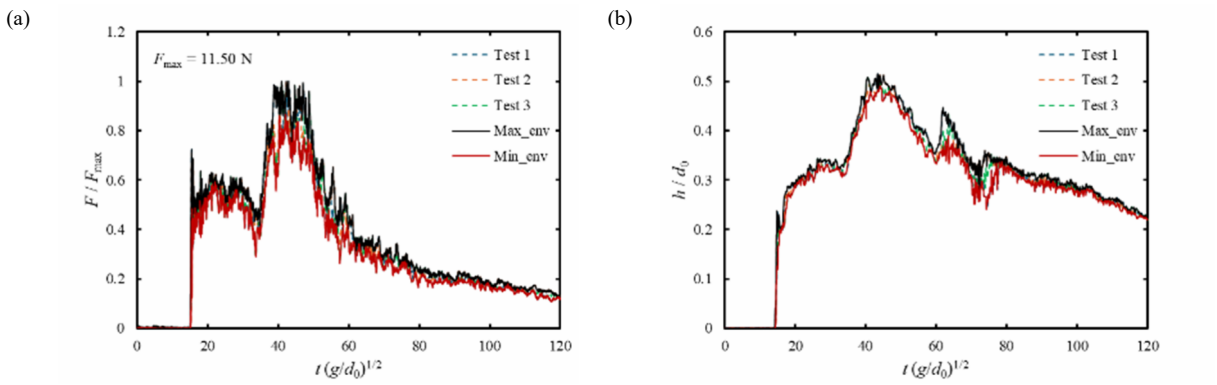

Figure 24. Repeatability of (a) the force exerted on the column (F) and (b) bore depth (h) at x = 630 cm for the test D40-C300600-d15-S660.

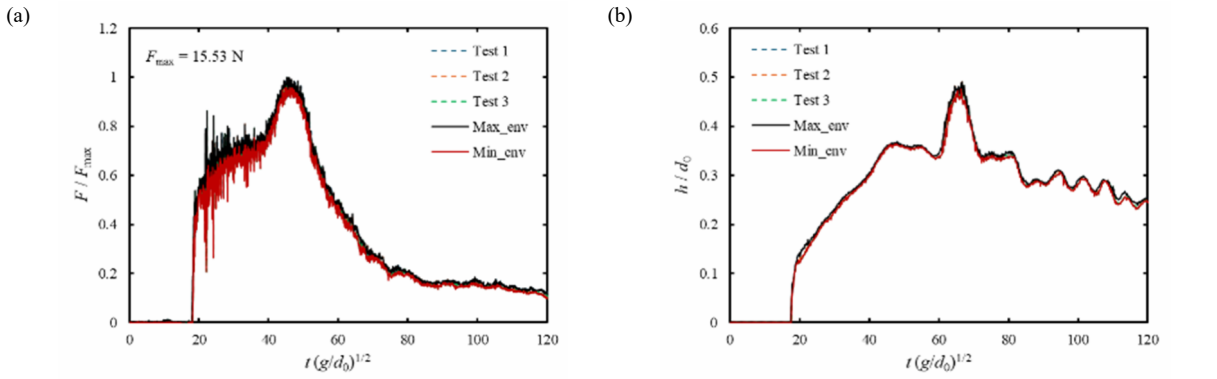

Figure 25. Repeatability of (a) the force exerted on the column (F) and (b) bore depth (h) at x = 630 cm for the test D40-S660.

3.2.6 Data recordings: signal preparation

Denoising time-series data is essential for obtaining accurate and reliable experimental results. This filtering process is crucial because it preserves the integrity of the signal, ensuring that important features are retained while unwanted noise is eliminated. In this study, a Butterworth low-pass digital filter was used to remove noise from the recorded time series of bore depth and the horizontal force exerted on the column, which were captured by the ultrasonic sensors and the load cell, respectively. The challenge was to determine the correct values of the coefficients of the filtration parameters. If the signal is overly smoothed, some peaks and variations are probably lost. Conversely, if the signal is not sufficiently smoothed, there is still excessive noise. A hammer test was conducted, which showed that the natural frequency of the column in wet conditions was 24 Hz. A comparison of the filtered data with various cut-off frequencies revealed that using a cut-

off frequency of 30 Hz yielded satisfactory filtered signals. Consequently, this denoising approach was applied to all time-series data. Figure 26 illustrates the comparison of filtered data with raw data for the time series of the non-dimensional bore depth and the horizontal force measurements for test D40-S520, demonstrating the effectiveness of the filtering process in enhancing the data quality.

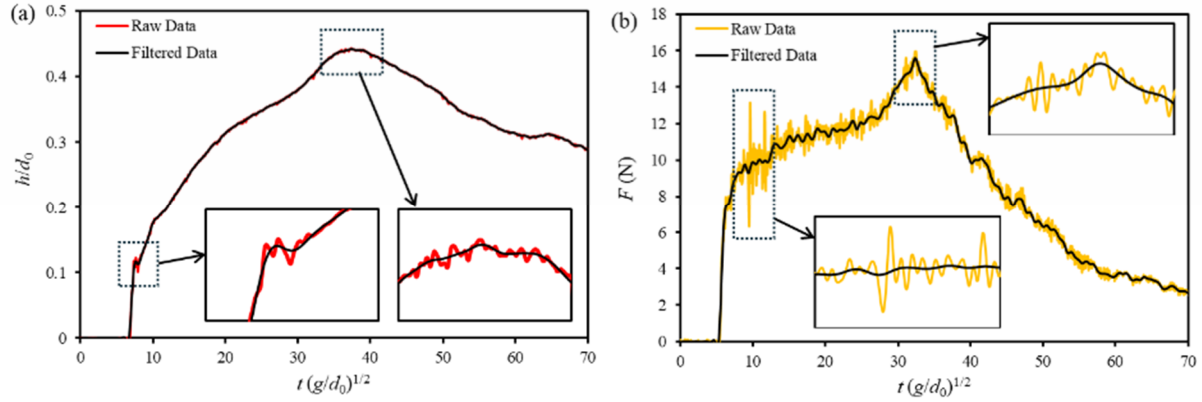

Figure 26. Effect of denoising on the time history of (a) non-dimensional bore depth, and (b) horizontal force measurements

3.3 Results

3.3.1 Bore depth and velocity

To study the effects of tsunami-like bores on structures, it is essential to generate a fully developed bore and analyze its depth and velocity. Using the dam-break method to generate a tsunami-like bore, the water impoundment depth behind the gate is the most important factor governing the bore depth and bore velocity along the flume. As depicted in Figure 27, increasing the water impoundment depth increased the bore depth. This figure shows the time history of bore depth at location x=270 cm in tests of D20, D30, and D40 (corresponding to increasing impoundment depths), where bore propagation was measured in the case of a flat, dry, and smooth bed and in the absence of the canal and the column. As the bore propagated along the flume, the bore depth initially increased to reach its maximum and then began to gradually decrease as the volume of water in the upstream reservoir decreased. The arrival time, represented by the first positive value of the bore depth in the time series, is directly a function of the water depth behind the gate, which determines also the bore front velocity. A higher water impoundment depth has a

higher bore velocity, and consequently, a shorter arrival time to a given location downstream the flume.

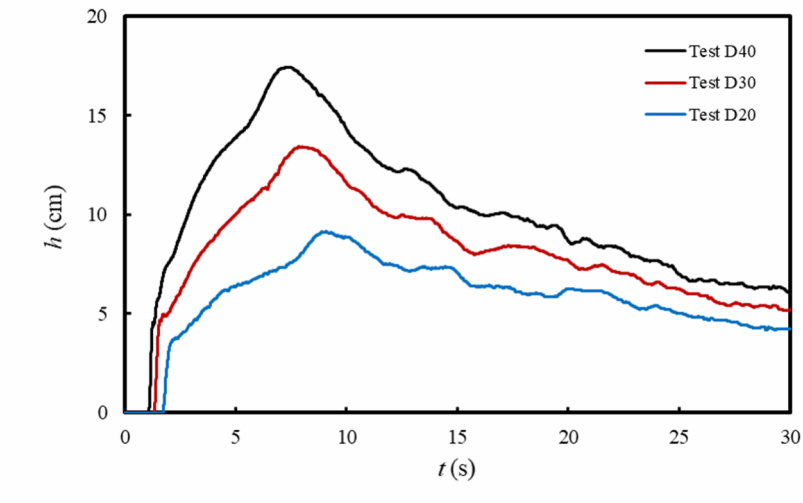

Figure 27. Time histories of the bore depth at location x=270 cm generated by different water impoundment depths of 20, 30, and 40 cm in the absence of the canal and of the column

Figure 28(a) illustrates the time history of bore depth at different locations along the flume in a non-dimensional form during the test D40. A noticeable reduction in the peak bore depth was observed at sensor locations farther downstream from the gate. This attenuation in bore height indicates the dissipation of flow energy as the bore propagates downstream, which is attributed to the viscous and diffusive behavior of the flow (Wüthrich et al., 2018a). It is important to note that no denoising filter was applied to the curves in this figure, as only raw data were utilized. To facilitate a better comparison of these curves, the bore arrival time was used for the horizontal axis. In this study, t^*=0 represents the moment when the bore arrives at the ultrasonic sensor's location. In this figure, each curve corresponds to a measurement location which US270 located at x=270 cm, making it the nearest sensor to the gate, and in contrast, US630 positioned at x=630 cm, which was the farthest sensor from the gate. As shown in Figure 28(b), by non-dimensionalizing the bore depth time series, dividing the bore depth by the maximum bore depth, it can be observed that the curves at different locations are similar. This similarity indicates that the flow is fully developed along the flume. The propagation of the tsunami-like bore on a horizontal, smooth, and dry bed does not lead to a turbulent flow with a high rate of air entrainment, which explains the low fluctuations in bore depth variations.

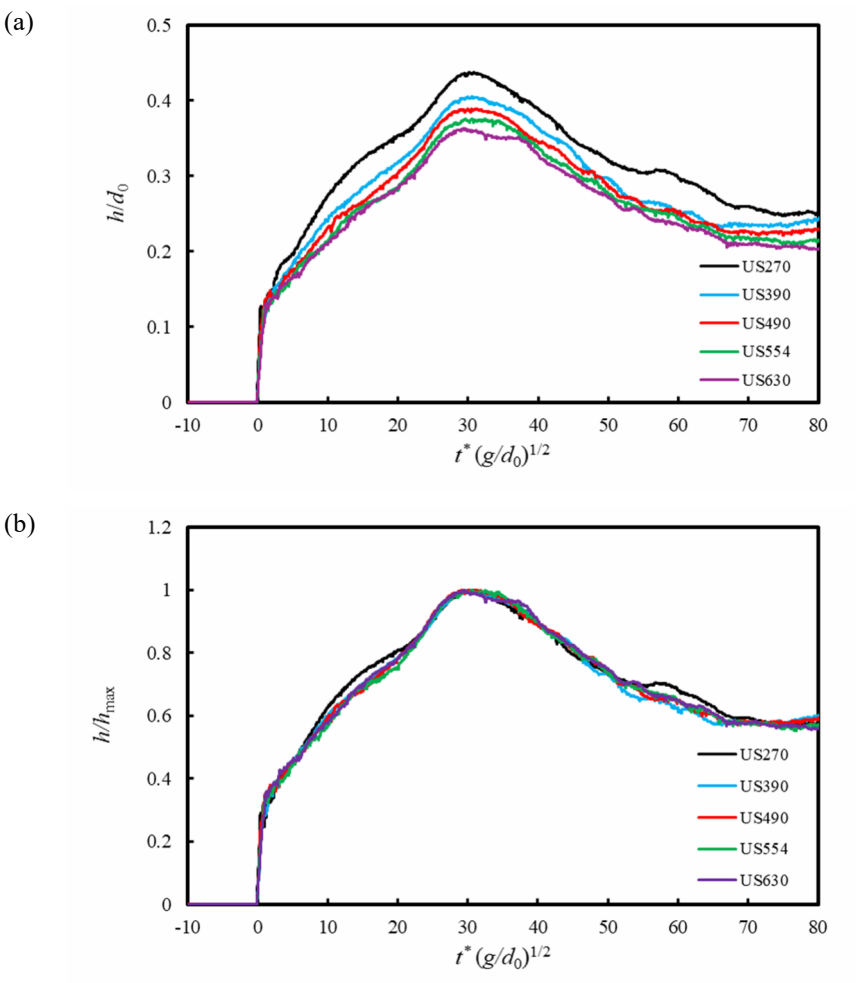

Figure 28. Bore depth variations at different locations for test D40 at two different non-dimensional form of (a) h/d_0, and (b) h/h_{max}

Figure 29 illustrates the values of the maximum bore depth at all locations and water impoundment depths. These results are from tests D20, D30, and D40, in which no canal or column was present, and the bore propagated unobstructed over the horizontal dry bed.

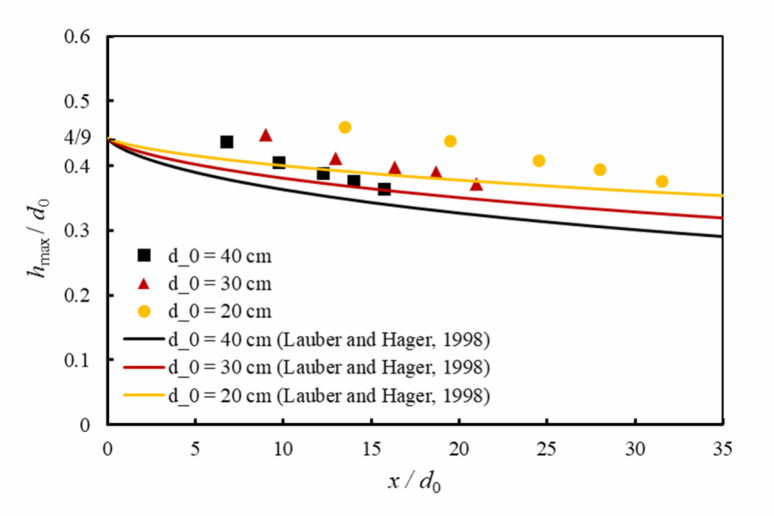

Figure 29. Maximum bore height at different locations for tests D20, D30, and D40 (without canal and column) compared with theoretical values

In this figure, the non-dimensional parameter of the maximum bore height is compared with the theoretical value proposed by Lauber and Hagger (1998) as follows:

$$\frac{h_{max}}{d_0} = \frac{4}{9}\left(1 + \frac{(x/d_0)^{2/3}}{L/d_0}\right)^{-5/4} \qquad 2$$

where h_{max} is the maximum bore depth, d_0 is water impoundment depth, x is the distance from the gate, and L denotes the reservoir length. As mentioned before, in this study, the impounded volumes of water behind the gate for three different water impoundments of 20, 30, and 40 cm were 0.805, 1.208, and 1.611 m^3 respectively and the equivalent reservoir length was L=10.6 m. Consequently, the equivalent aspect ratio of reservoir length to the water depth (L/d_0) were 53, 35.3, and 26.6. It should be noted that one of the reasons for the difference between theoretical values and measured data may be related to the non-rectangular shape of the upstream section of the reservoir behind the impoundment gate. The non-uniform reservoir shape may have potentially influence the flow regime by increasing discharge when the negative wave, generated after the gate opening, reaches the reservoir's widened section. While this widening is not expected to significantly affect the maximum horizontal force observed 8–10 seconds after gate opening, it may influence the analysis of maximum bore depth when comparing experimental results to theoretical predictions.

Ritter (1892) introduced a theoretical parabolic profile for the longitudinal water bore depth as follows:

$$\frac{h}{d_0} = \frac{1}{9}\left(2 - \frac{x}{t\sqrt{gd_0}}\right)^2 \qquad 3$$

As shown in Figure 30, by comparing the theoretical equation with the experimental data extracted at different locations of the ultrasonic wave gauges, good agreement was observed. The discrepancies observed at the very tip region of bores ($\frac{x}{t\sqrt{gd_0}} > 1.1$) are related to the fact that Ritter's formula does not account for the bore friction with the bed.

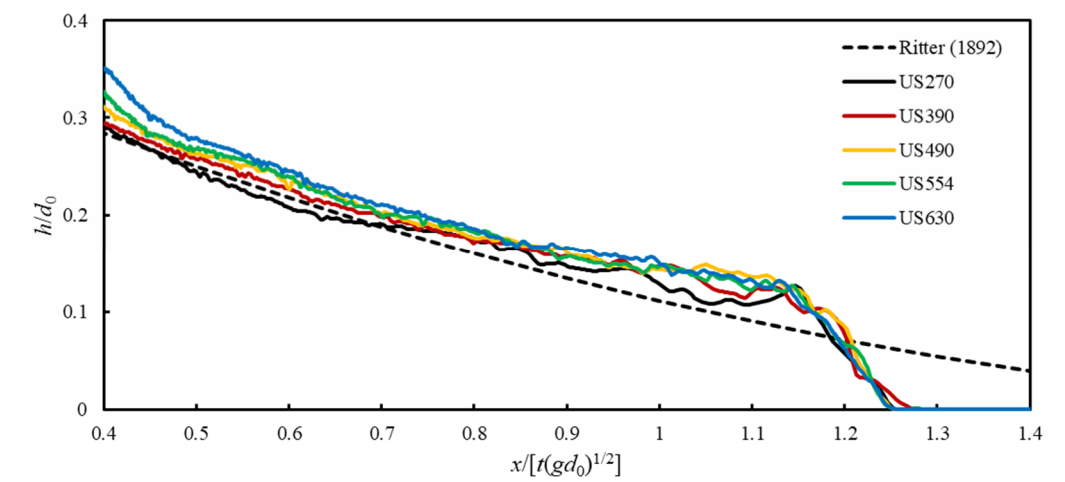

Figure 30. Bore depth variation for different locations along the flume longitudinal axis (test D40)

In this study, the bore front velocity, *U*, was calculated using two different methods. First, by analyzing the videos captured by Cam1, which was installed on top of the flume, looking downward, the position of the bore front and of the floating-colored plastic beads released at different time steps were extracted. These colored plastic beads were placed in the reservoir and behind the gate and traveled with the bore starting from the opening of the gate. The average bore front velocity was calculated by dividing the distance traveled by the bore front or the colored beads along the flume by the corresponding time:

$$U = \frac{\Delta x}{\Delta t} \qquad 4$$

where Δx represents the distance traveled by the bore front or colored plastic beads and Δt represents the time difference between the captured photos. Figure 31 illustrates the locations of the bore front and colored balls at different time steps at the front of the gate for test D40.

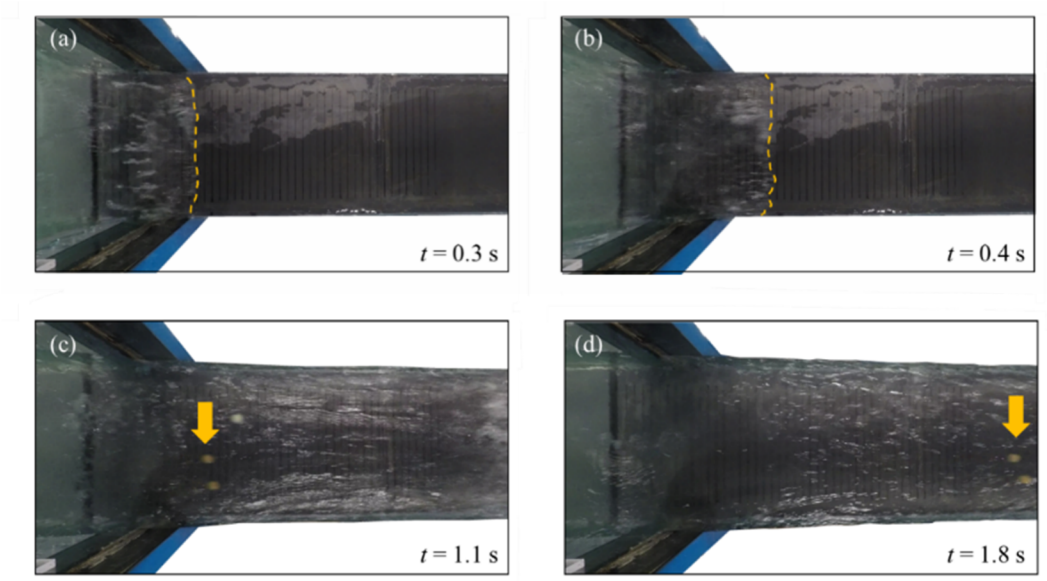

Figure 31. Determination of bore velocity by analyzing videos captured by Cam1; (a) bore front location at t=0.3 s, (b) bore front location at t=0.4 s, (c) bead location at t=1.1 s, and (d) bead location at t=1.8s

With the second method, the average bore front velocity was calculated by analyzing the time history of the bore depth. The bore arrival time to US gauge locations was defined as the moment when the recorded bore depth became greater than 0.01 m (Figure 32). Using the same equation, the average velocity was calculated by dividing the distance between two adjacent US gauges by the difference between the arrival times at their respective locations.

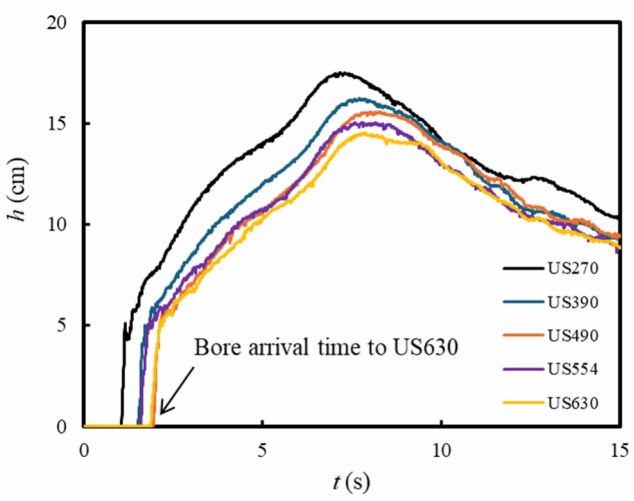

Figure 32. Bore depth time-history at different locations, and determination of bore arrival time to US630 for test D40

The bore velocity is correlated with the depth of the water impoundment, a relationship frequently established in the literature, and is expressed as:

$$U = \alpha\sqrt{g d_0} \qquad 5$$

where U is the bore front velocity, α is a constant whose value was proposed by various researchers with estimates ranging from 0.66 (Matsutomi and Okamoto, 2010) to 1.83 (Murty, 1977), g is the gravitational acceleration, and d_0 is the water impoundment depth. These values were mostly developed based on physical models tested at the laboratory scale. Figure 33 shows the comparison between the average bore front velocity calculated in this study and the ranges delimited by the values presented in FEMA (2001) (upper boundary) and CCH (2000) (lower boundary), which encompass all other references in the literature (Wüthrich et al., 2018a). The error bars correspond to the various values of bore front velocity calculated by different methods for different tests. In the present study, a coefficient α=1.2 was shown to exhibit the best correlation with the data extracted from the experimental results.

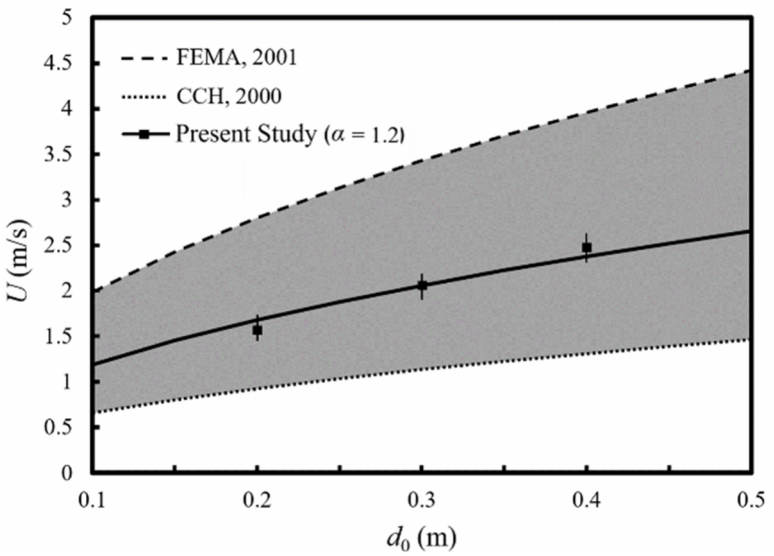

Figure 33. Bore front velocity (U) for different water impoundment depths (d_0). (The error bars are related to the various velocities were calculated, while the gray area encompasses different α values proposed by previous researchers, bounded by the FEMA and CCH values provisions)

Figure 34 shows the propagation of the tsunami-like bore along the flume recorded at different locations of the US gauges. As described in Table 9, these tests were performed in the absence of a canal and without the presence of a column. The location of the US gauges is indicated by the vertical axis on the right-hand side. The origin of the left vertical axis corresponds to the US270 measurements, and the values show the bore depth measured using this US gauge. The time histories of bore depth for the other US wave gauges were drawn based on the distance from each other. The red dotted lines show the bore celerity, which is calculated based on the bore front arrival time at the location of each US gauges. The bore front velocities were calculated to be 1.57, 2.06, and 2.48 m/s for water impoundment depths of 20, 30, and 40 cm, respectively.

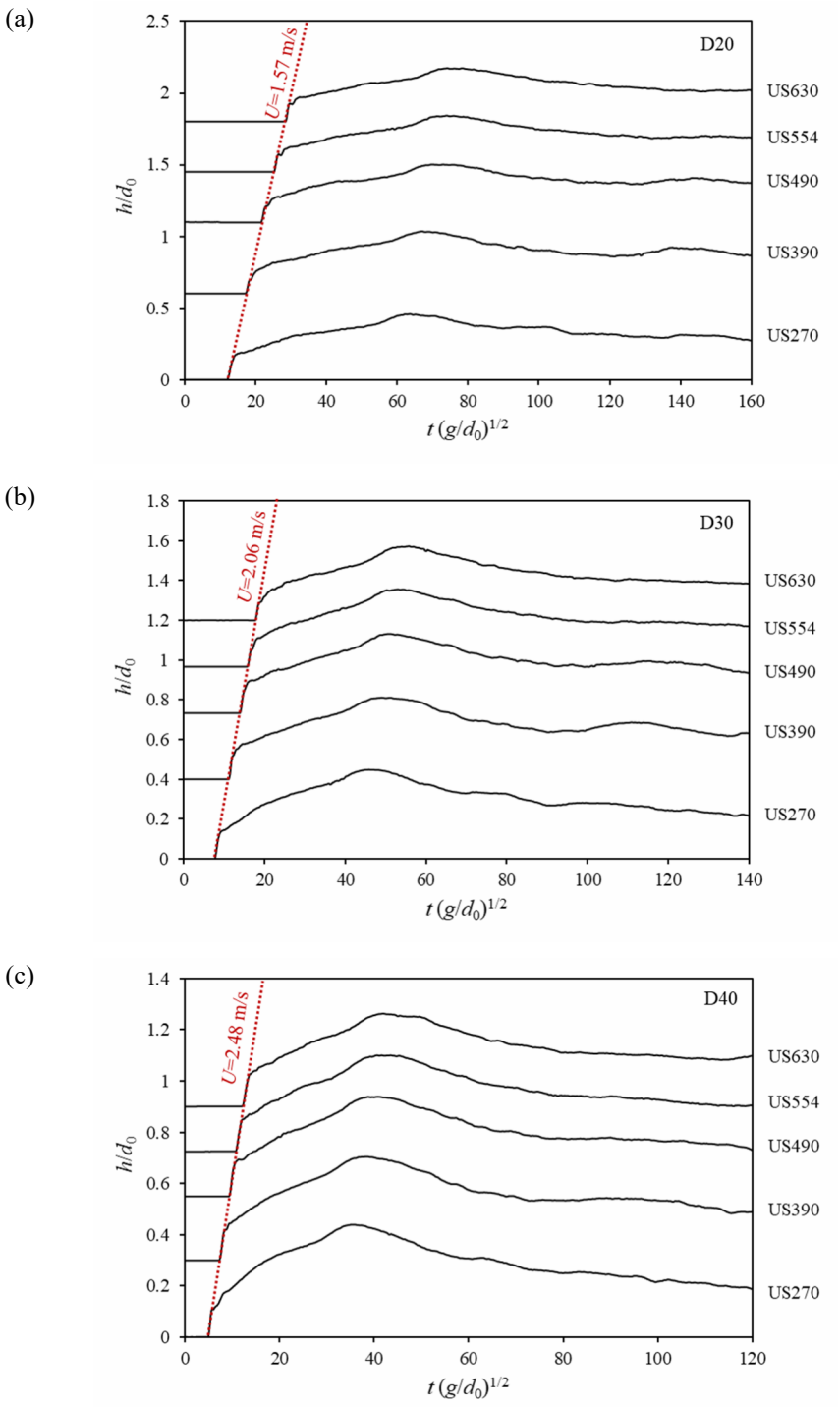

Figure 34. Time series of bore depth for different water impounded depths (d_0) for tests (a) D20, (b) D30, and (c) D40; the red lines show the bore front velocity

By calculating the bore front velocity, it was possible to sketch the bore front profile based on the time history of bore depth. To accomplish this, the bore arrival time at each ultrasonic sensor's location was first calculated, and the time series of the bore depth was plotted based on the distance

that the bore propagated downstream. As shown in Figure 35, this method is similar to capturing a side-view photograph of the bore moving downstream with velocity U (left panel) or measuring a fixed bore depth with an ultrasonic sensor moving upstream with velocity U (right panel).

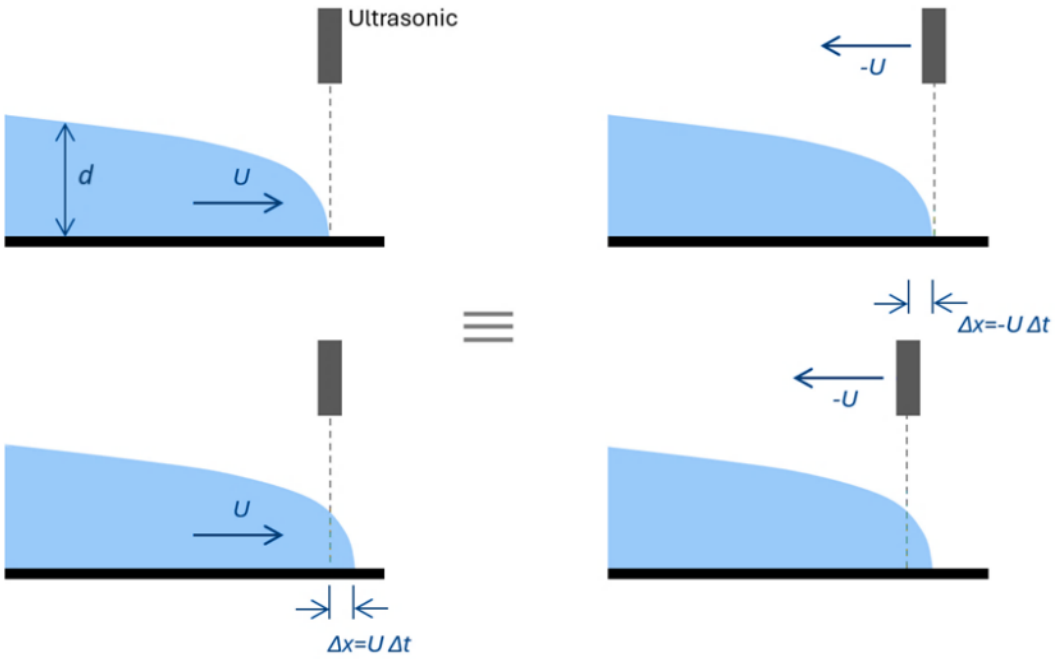

Figure 35. Bore front profile capturing using ultrasonic wave gauge measurements

Considering the sampling frequency of the ultrasonics, where measurements were taken every Δt, and based on the bore velocity (U), the ultrasonic wave gauges recorded the bore depth with a resolution of $\Delta x = U \times \Delta t$. To analyze the bore front profile, the time history of bore depth at different ultrasonic locations was depicted. As illustrated in Figure 36, the bore front profiles for tests D20, D30, and D40 at different ultrasonic wave gauges' locations show good agreement with the analytical solution proposed by Chanson (2009). In these figures, x_s denotes the location of the ultrasonic wave gauge.

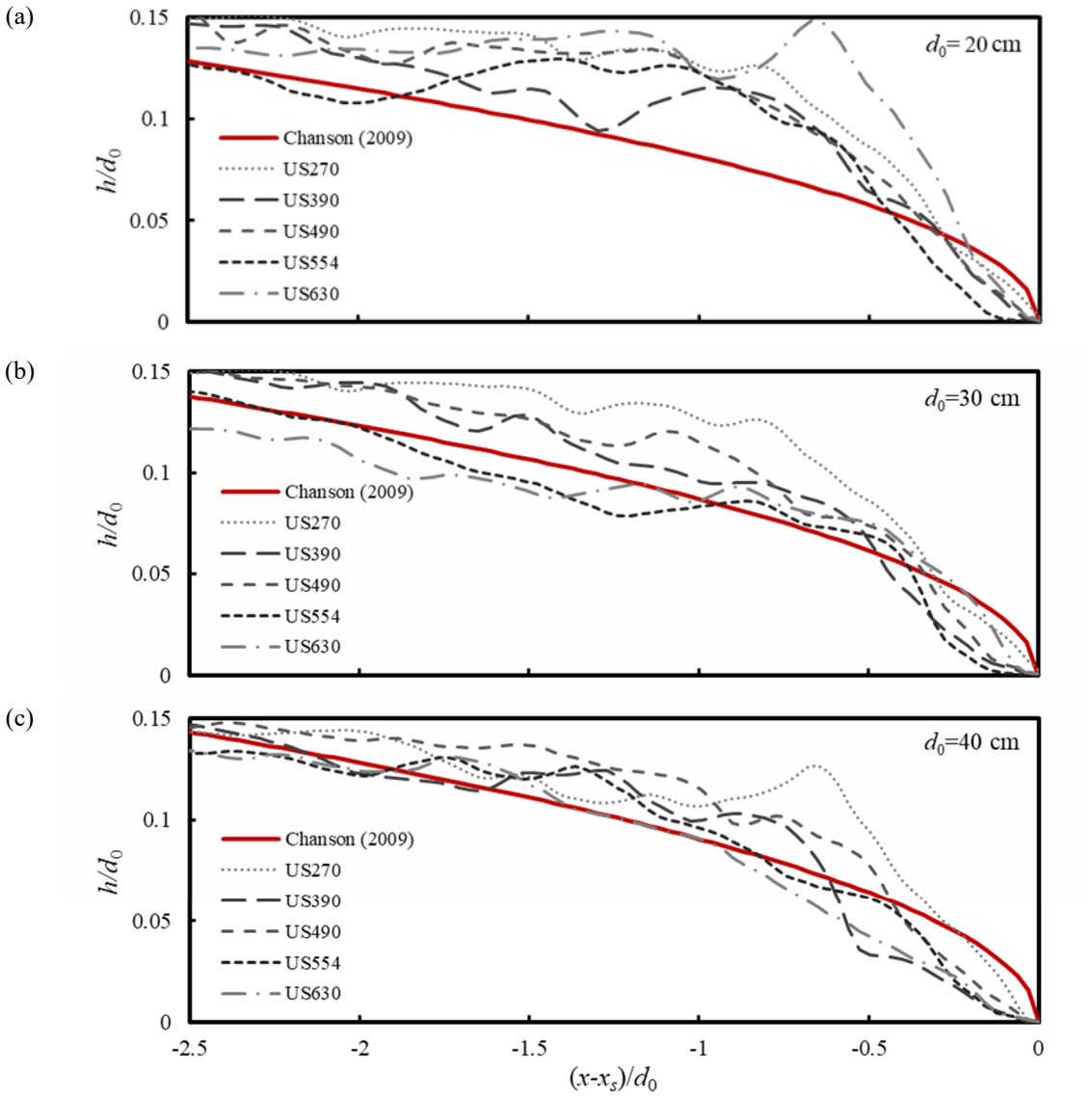

Figure 36. Bore front profile at different locations of ultrasonic wave gauges for tests (a) D20, (b) D30, and (c) D40

3.3.2 Horizontal Force on column

Figure 37 displays photographs of the impact of tsunami-like bore on the column from the side view, downstream, and upstream perspectives for the test D40-S660.

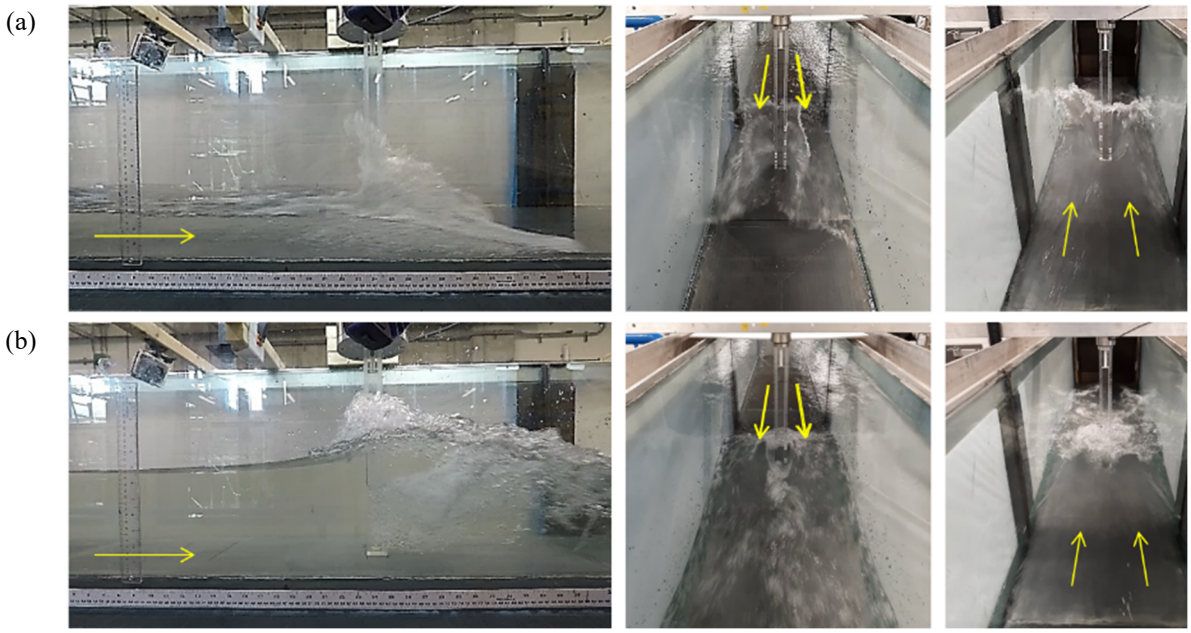

Figure 37. Impact of the bore onto the column at (a) the initial bore impact on the column at t=3.6 s, and (b) the time of maximum force exerted on the column at t=8.2 s for test D40-S660 from side view (left panel), downstream (middle panel), and upstream perspective (right panel), the arrows show the flow direction

The presence of the column caused the bore to initially splash and then run-up significantly in front of it, resulting in significant air entrainment and associated turbulence in this region. On the opposite side of the front face (behind the column), the column acted as a flow divider, causing the water flow to separate and form a wake. Figure 37(a) and (b) corresponds to the moments when the bore front reached the column, and the maximum force was exerted on the column respectively. By analyzing the videos capturing the interaction of bore and the column, It was observed that the splash and air entrainment are maximal when the bore impacts the front edge of the column and diminishes over time, as the bore depth and its velocity increased. Air entrainment, turbulence, and column vibration were among the most influential factors contributing to noise in force measurements. Figure 38 presents the raw data of the force exerted on the column. As shown in Figure 38, the fluctuations in the magnitude of the force were visible at the initial impact of the bore, between $(t\text{-}t_a)(g/d_0)^{1/2}$ = 5 to 15, and decreased over time, especially after the moment of maximum force. In this figure, the grey dashed lines indicate the times at which the photos in Figure 37 were taken.

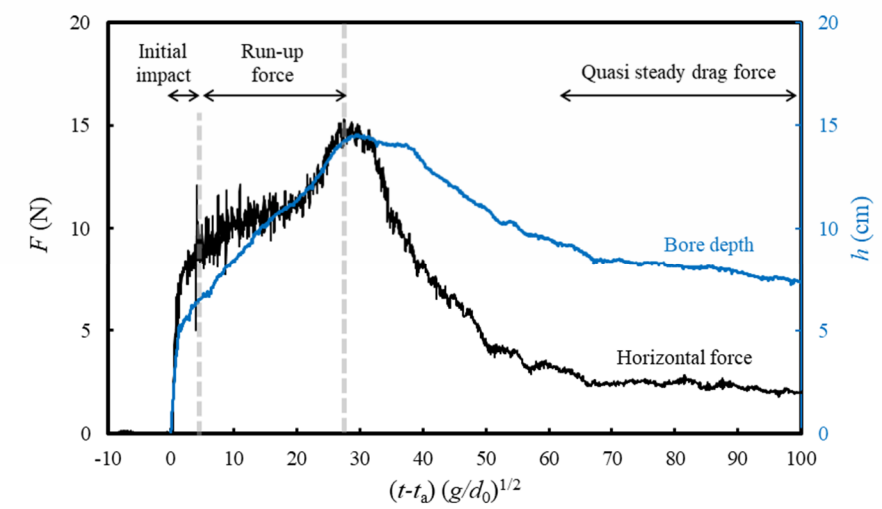

Figure 38. Time history of bore depth at x=630 cm in the absence of canal and column (test D40), and the time history of the horizontal force exerted on column (test D40-S660); the left and right dashed lines indicate the capture times of photos a and b shown in Figure 37, respectively.

The time history of the horizontal force exerted on the column placed at x=660 cm and the time history of the bore depth in the absence of the column are presented in Figure 38. These time-histories were recorded for the tests with bores generated by an impoundment depth, d_0=40 cm. As shown in this figure, the horizontal force increased with the rising water surface level in front of the column, reaching its maximum when the bore depth is the deepest, and as the bore depth decreased, the magnitude of the horizontal force also decreased. A reflected wave generated by the column was observed at this moment, which impacted flow velocity and, subsequently, the magnitude of the horizontal force.

The impoundment depth was proportional to the horizontal force exerted on the column. As illustrated in Figure 39, an increase in the impoundment depth directly led to an increase in the magnitude of the horizontal force exerted onto the column. To facilitate a comparison of the curves related to different impoundment depths, the origin of the horizontal axis was set as zero which corresponds to the arrival time of the bore at the column. The horizontal force exerted on the column by the bore was directly influenced by both the bore depth and bore velocity.

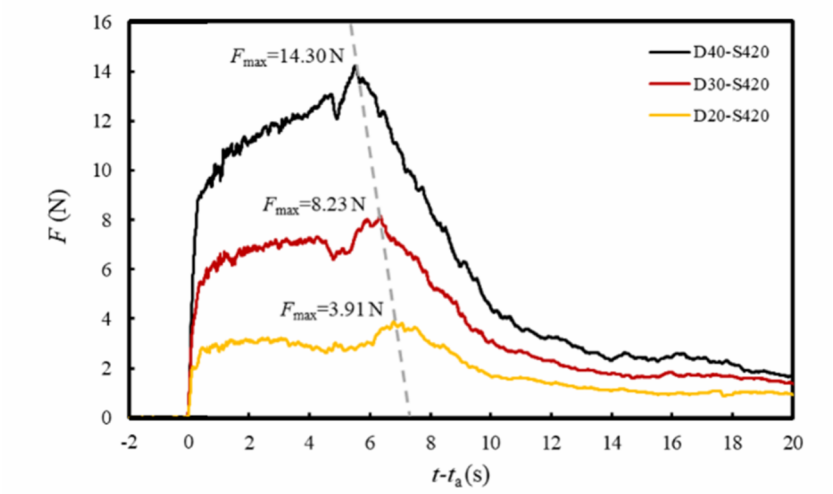

Figure 39. The effect of impoundment depth (d_0) on magnitude of the horizontal force exerted on the column; the peaks of the curves lie along the grey dashed line

On the other hand, t_p, which represents the interval between the initial impact of the bore onto the column and time corresponding to the maximum force exerted on the column, directly depends on the magnitude of the impoundment depth and, subsequently, on the bore velocity. This time was 5.3, 6, and 6.8 seconds for water impoundment depths of 40, 30, and 20 cm, respectively, as shown in Figure 39. Increasing the water impoundment depth, which led to an increase in the bore depth and velocity, decreases this time interval. The average bore velocities were 1.57, 2.06, and 2.48 m/s for water impoundment depths of 20, 30, and 40 cm, respectively. By considering a linear curve between the bore velocity and interval time, the following equation was fitted to the extracted data with a correlation coefficient of approximately 1:

$$t_p = 9.39 - 1.65U \qquad 6$$

To study the effect of the distance between the column and gate on the force, the column was placed at different locations, and the time history of the force exerted on the column was compared between the presence and the absence of a canal. As illustrated in Figure 40, the distance between the column and the gate did not significantly affect the force exerted on the column. This is because the experiments were conducted on flat, dry, and smooth beds.

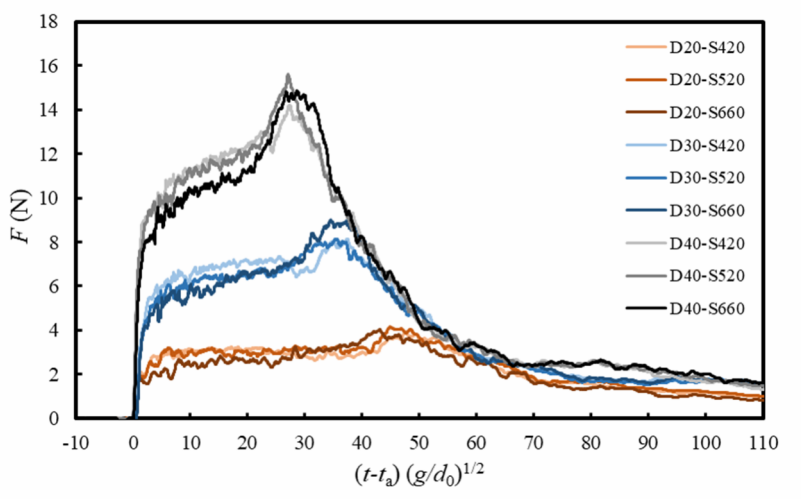

Figure 40. Effect of the column's position on the horizontal force time history

The presence of the column caused bore reflection, which temporarily increased the water level in front of the column. To monitor water level time history, one of the ultrasonic wave gauges was placed 30 cm upstream of the column. It should be noted that due to the high splashes in front of the column, it was not possible to place the sensor closer to the column. As depicted in Figure 41(a), a 4 cm square column placed at x=520 cm caused wave reflection, increasing the water surface level in front of the column. Depending on the column's location and the impoundment depth, the presence of the column increased the maximum water surface level by 35–50% at 30 cm in front of the column. It should be noted that this increase in water surface level was much greater adjacent to the column, as shown in Figure 37.

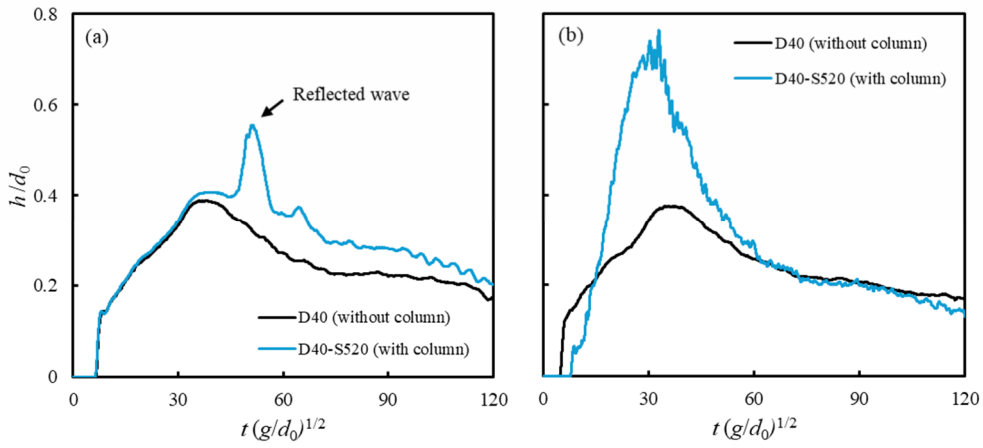

Figure 41. The effects of column on water surface level time-history at (a) 30 cm front of the column at x=390 cm, (b) 30 cm downstream of the column at x=454 cm

Figure 41(b) shows the water level time-history 30 cm behind the column edge. Flow separation and wake formation behind the column caused a highly turbulent regime, with high fluctuations in the time series of the water surface levels. As shown in this figure, in the test in which the column was present, the arrival of the water 30 cm behind the column (blue line) along the centerline of the flume, where the ultrasonic sensor was installed, was delayed compared to the test without the column (black line). This delay was caused by flow separation at the initial impact of the bore with the column, which directed the flow toward the flume sidewalls, leaving the area immediately behind the column without water. The side-diverted flows around the column further reunited toward the centerline, behind the column, leading to an increase in the water level in this area. The impact of the flow against the sidewalls of the flume and its subsequent return to the centerline intensified the increase in the water level at the middle of the flume, behind the column (Figure 42).

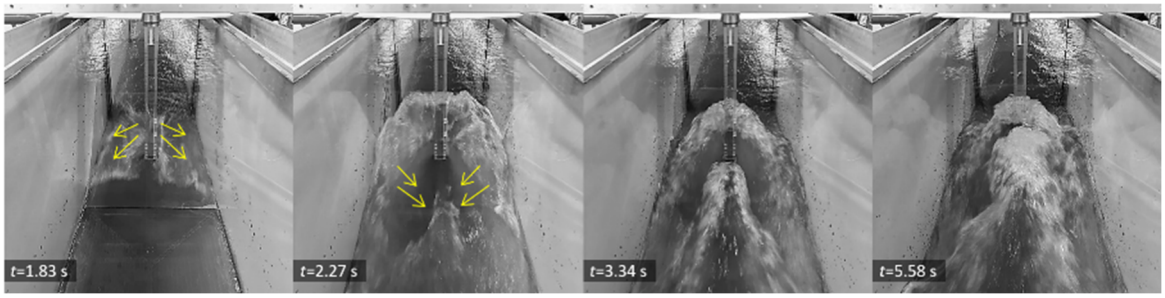

Figure 42. Flow separation and wake formation behind the column at different time steps (test D40-S520)

Although in the flume experiments, the reflected wave propagated upstream for a long distance due to the narrow flume width, in a real, open-sea environment, such reflected waves would be expected to dissipate more rapidly. However, the reflected waves increased the water surface level upstream the column, which inherently affected the horizontal force exerted on it. Figure 43 illustrates the propagation and initial impact of the bore on the column as well as the formation of reflected waves. It is noteworthy that during the first stages of the bore propagation - time steps (t-t_a<7 s) - the reflected wave could not propagate upstream due to the supercritical flow condition of the bore. However, as the water surface level increased in front of the column and the flow velocity decreased, the reflected wave propagated upstream.

Figure 43. Bore impact on column and wave reflection causes water level rise at front of column (test D40-S520)

3.3.3 Effects of water-filled canal

Water-filled canals as mitigation countermeasures may be able to influence bore hydrodynamics and, subsequently, reduced the horizontal force exerted onto structures. Previous studies (Elsheikh et al., 2022; Rahman et al., 2017) have reported that the interaction of the bore with the water-filled canal causes significant turbulence and the subsequent dissipation of energy. Additionally, these studies have shown that a reflected wave is generated at the first impact of the bore with the water inside the canal. Figure 44 illustrates the time history of bore depth measured at 30 cm upstream and 30 cm downstream a 60 cm wide canal with different depths of 5, 10, and 15 cm.

As shown in Figure 44(a), the presence of the water-filled canal led to the formation of a reflected wave, the magnitude of which depended on the canal depth. An increase in canal depth corresponds to a higher reflection coefficient. Analysis of the time history of the bore depth behind the canal revealed that the presence of the canal caused turbulence and air entrainment, as demonstrated by the fluctuations in the bore depth shown in Figure 44(b). The initial impact of the bore on the water inside the canal displaces a significant volume of water, causing the water surface

level downstream of the canal to suddenly rise. The experimental results indicate that as the canal depth increases, the volume of displaced water also increases, leading to a more pronounced rise in downstream water levels at the initial instant of bore impingement. This behavior suggests that deeper canals can modify the downstream hydrodynamics compared to shallower canals or the case without the canal.

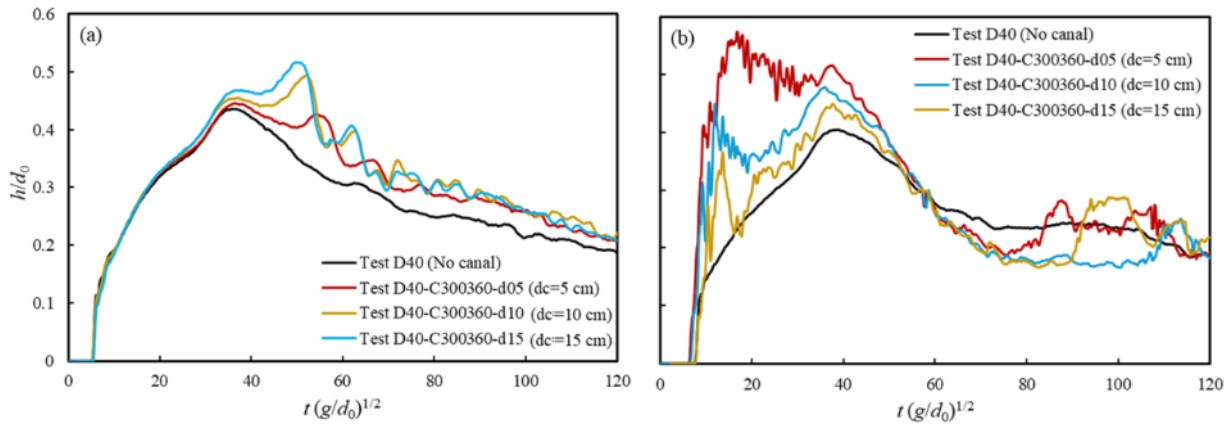

Figure 44: Bore depth time-history at (a) 30 cm before and (b) 30 cm after canal with 60 cm width and different water depths

In addition to reducing tsunami energy, increasing available evacuation time is another reason for the development of mitigation countermeasures (Rahman et al., 2017). By increasing the evacuation time, people may be able to evacuate safely, ultimately saving their lives. By comparing the bore arrival time at the location of ultrasonic wave gauges for different tests with and without the presence of the canal, it is shown that the presence of canal did lead to a delay in the bore front arrival time (Figure 45), and that the wider canals led to a higher delay in arrival time.

Canals with widths of 60, 160, and 300 cm resulted in delays of 0.31, 0.36, and 0.38 s respectively. Although this delay is not substantial enough to effectively extend the evacuation time in real tsunami events the same way that seawalls do, for instance, the presence of canal reduces bore front velocity. In the present study, canals with 60, 160, and 300 cm width resulted in an average velocity reduction of 18, 20, and 21%, respectively.

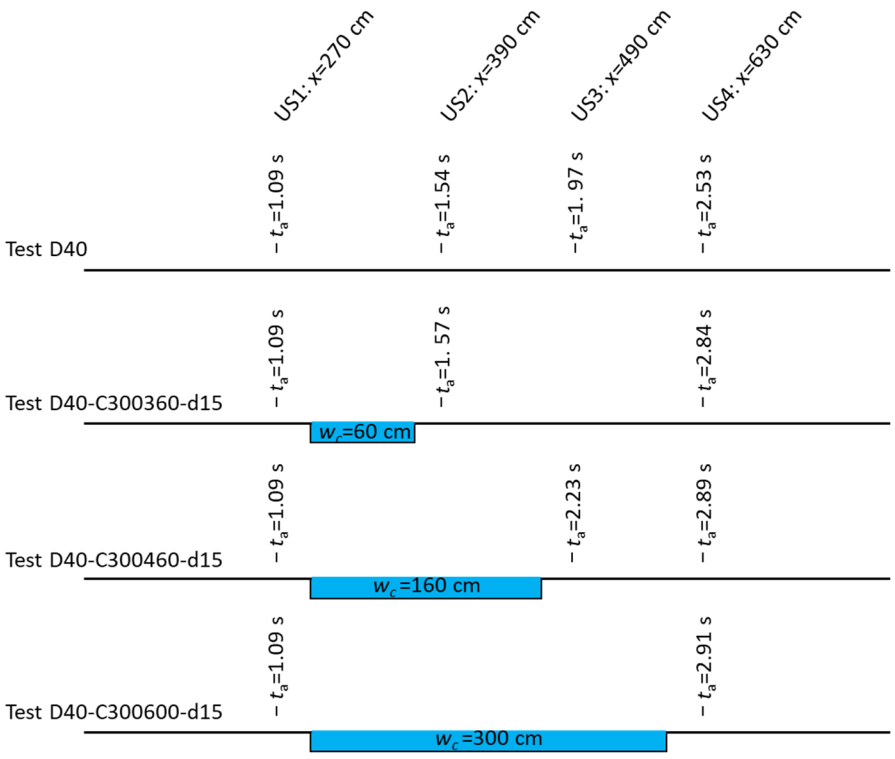

Figure 45: Bore arrival time (t_a) to ultrasonic wave gauges' locations for different tests

As previously mentioned, the primary purpose of placing mitigation structures in the path of tsunami inundation is to reduce its energy and, consequently, decrease the force exerted on inland infrastructure. Figure 46 shows the time history of the bore depth at a location 30 cm before and 30 cm after the canal's location for various combinations of canal and column placements. In these tests, a 60 cm wide and 15 cm deep canal was placed between x=300 cm and x=360 cm, while the column was installed at x=420 cm. The interaction of the bore with the canal resulted in a certain volume of water from the canal being displaced downstream the canal. This discharge is the reason for the higher water level at $10<t(g/d_0)^{1/2} < 50$, as depicted in Figure 46(b), when the canal was present (blue and yellow lines), compared with the water level without the canal (black and red lines). As depicted in Figure 46(b), the presence of the column also resulted in noticeable reflection occurring at approximately $t(g/d_0)^{1/2} = 50$ which led to a higher bore depth (indicated by the yellow and red lines).

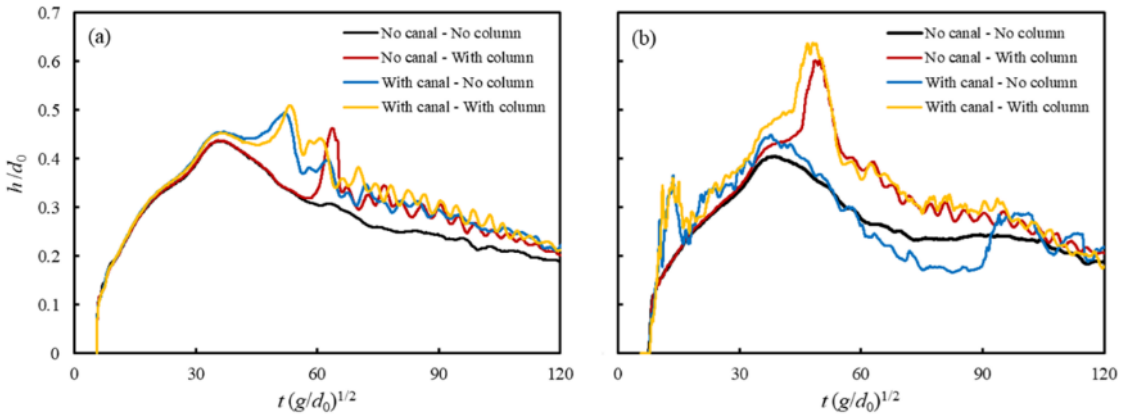

Figure 46: Time history of bore depth at (a) 30 cm before canal (x=270 cm), and (b) 30 cm after canal (x=390 cm) with different combinations of the canal and column existence (for all tests: d_0=40 cm, w_c=60 cm)

Figure 47 shows the time history of water level at 30 cm front of the column, as well as the time history of the horizontal force exerted on a 4 cm square column for various canal widths of 60, 160, and 300 cm.

(a) (b)

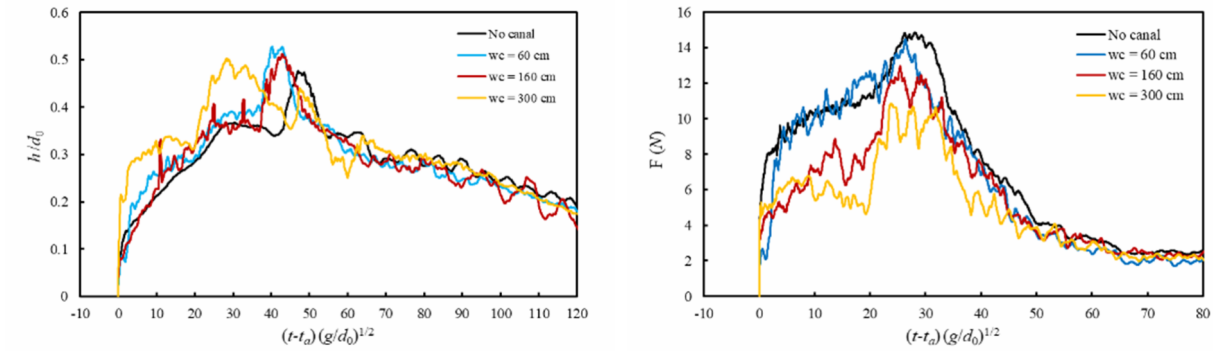

Figure 47: Influence of the canal width on the (a) Time history of bore depth at 30 cm in front of the column, and (b) time history of force exerted onto the column, for canals with different widths (in all tests: d_0=40 cm, d_c=15 cm, upstream edge of canals was located at x=300 cm, and the column was placed at x=660 cm)

In all the tests shown in this figure, the impoundment water depth (d_0) and canal depth (d_c) were kept constant at 40 and 15 cm, respectively, and the column position remained the same (x=660 cm), ensuring that the bore traveled the same distance from the gate. As illustrated in this figure, the bore depth increased to a maximum value and then began to decrease. Reflected waves created multiple subsequent peaks with smaller magnitudes, and their locations depended on the canal width. Due to the supercritical flow regime, reflected waves could not travel upstream following the initial bore impact on the column. As the water level increases and the bore velocity

decreased, the Froude number also decreased, modifying the flow regime and allowing the reflected wave to propagate upstream. The formation of these reflected waves indicates that the flow regime changes more quickly in wider canals because the increased canal width causes more energy dissipation and reduces the current velocity. As depicted in this figure, while the impact of a 60 cm wide canal was not very significant on the force exerted on the column, the 160 cm and 300 cm wide canals significantly reduced the initial impact and run-up forces. In particular, the 300 cm wide canal resulted in a 25% reduction of the maximum force magnitude, decreasing from 15.2 N to 11.4 N (Figure 48).

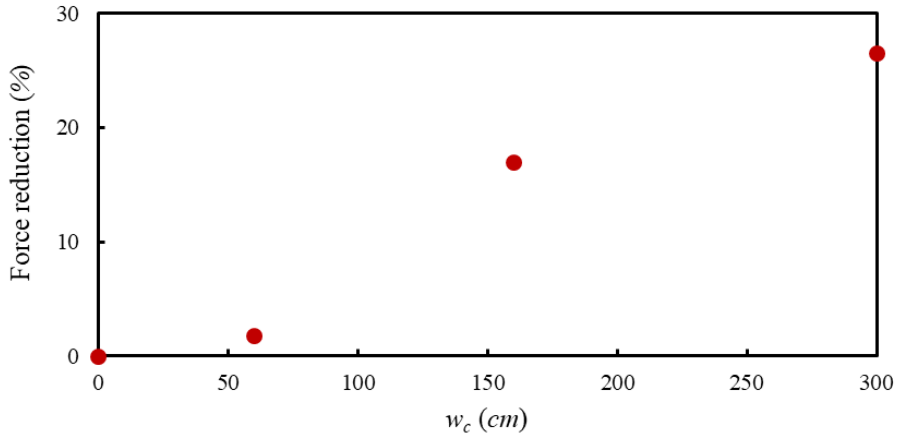

Figure 48: Horizontal force reduction as a function of the canal width

3.4 Discussion

This experimental study demonstrated the effects of a rectangular water-filled canal on the bore hydrodynamics, as a potential mitigation measure for reducing the tsunami-like bore energy exerted on a column. A comprehensive test program was conducted to investigate the time history of a tsunami-like bore generated through a dam-break mechanism, measured at various locations along the experimental flume. The time history of the horizontal force exerted onto a column attached to a 6-degrees of freedom load cell was investigated to assess the effect of the hydraulic bore on the horizontal force. Additionally, photos captured from multiple perspectives with respect to the canal and column locations during bore propagation and subsequent impact provided further insights into the phenomenon. A comparison of bore depth variations at different locations along

the flume revealed a consistent pattern when nondimensionalized, indicating a fully developed flow throughout the flume. Two methods were used to calculate the bore front velocity, and both yielded similar results. The velocities calculated were within the range predicted by Froude similitude, with a constant coefficient (α) of 1.2 used to calculate them, showing t strategy he highest correlation with the experimental data. This coefficient falls within the range established by previous researchers (Matsutomi and Okamoto, 2010; Murty, 1977), suggesting confirming that the physical modeling approach captured key bore dynamics accurately. Similarities were also observed between experimental and analytical data for the front tip of the bore, further validating the experimental methodology.

Using a Froude scaling ratio of 1:10, the bore depths and velocities were adjusted to those observed in real tsunamis. At this scale, the dimensions of the canal were 6, 16, and 30 m wide, with depths of 0.5, 1, and 1.5 m. For comparison, the coastal structure was represented by a 4 cm column, equivalent to a 40 cm wide column in real-world dimensions, similar to a typical column found in low-rise buildings. The results suggest that such scaled canal dimensions could feasibly be implemented in practice for tsunami force reduction. The presence of the water-filled canal in the flume changed the bore flow dynamics and reduced the bore-front velocity. Some of the volume of water inside the canal was pushed out by the bore, resulting in higher water levels downstream of the canal and in front of the column, especially in the initial stages of the bore propagation. This indicates that the canal temporarily stores and redistributes bore energy, which reduces the momentum of the incoming flow. Additionally, the induced turbulence and air entrainment act as energy dissipation mechanisms, similar to hydraulic jumps observed in other coastal flow studies. Decreasing the bore velocity delayed the bore arrival times to locations downstream of the canal. Although the delay was not substantial enough to significantly extend evacuation time, it demonstrates a measurable reduction in flow momentum, which is beneficial for structural force mitigation.

The presence of a canal also reduced the force exerted onto a column placed downstream of the canal, particularly in the case of the wider and deeper canals. The 300 cm wide and 15 cm deep canal reduced the maximum horizontal force by more than 25%, demonstrating the canal's effectiveness in energy dissipation and subsequent force reduction on coastal infrastructure. This reduction aligns with the performance of other structural countermeasures, such as seawalls or

submerged breakwaters, but canals offer a simpler and more economical approach that avoids the risk of catastrophic failure if overtopped. These findings suggest that canals, as a potential countermeasure, can help reduce tsunami impacts on nearshore inland structures, though both their practical implementation and economic feasibility require further evaluation. Although the scale of this experimental program met the minimum scale for physical modeling of columns in a tsunami prescribed by the ASCE7-22 standard, the authors recognize certain limitations of their experiments. Among these, the relatively small width and depth of the flume did not allow for the use of deeper tsunami-like bores or the use of tests with a larger scale. Future studies should include larger facilities, additional structural geometries, and numerical modeling to complement these physical results and assess the performance of canals under a broader range of tsunami conditions.

Although the present study focused on the maximum horizontal force exerted on the column, it is recognized that the hydrodynamic impulse ($I=\int F(t)\,dt$), which accounts for both the magnitude and duration of the force, is another important measure of structural loading. Because of potential variations in the sensor response time and data acquisition sampling rate, impulse-based metrics are sometimes considered more physically representative of tsunami-induced loads (Chanson, 2006; Arnason et al., 2009). While impulse calculations were not included in the present analysis, the recorded force-time histories could enable such an assessment in future work. Given the observed reduction in bore velocity and energy dissipation caused by the canal, it is postulated that the canal would also lower the total impulse on the downstream structures.

It is acknowledged that the present experimental does not cover all possible combinations of canal geometry, impoundment depth, and column positioning. The physical testing was constrained by setup complexity, significant preparation time for canal modification.

3.5 Conclusions

This study provides insights into the dynamics of tsunami-like bores and their interactions with a nearshore structure, focusing on the effects of rectangular water-filled canals placed parallel to the shoreline and in front of a structural model of a column. The experiments were conducted with the following four categories.

No canal or column: These experiments analyzed tsunami-like bore generation and propagation along the flume without a canal and column. The time history of bore depth along the flume demonstrated the generation and propagation of a stable and fully developed flow over a smooth and dry bed, which is consistent with previous studies (Murty, 1977; Matsutomi and Okamoto, 2010; Wutrich et al., 2018a, b). The time histories of the bore depth and its front tip characteristics agreed well with theoretical predictions (Ritter, 1892; Lauber and Hagger, 1998). These experiments were conducted using upstream impoundment depths of 20, 30, and 40 cm, and showed that both the bore depth and its velocity directly depend on the impoundment depth which an increase in the impoundment depth led to greater maximum bore depths and associated velocities.

Water-filled canal only: Analysis of the bore depth time-history in conjunction with the analysis of the side-view video recordings of the bore propagation demonstrated that the interaction between the advancing bore and the water-filled canal resulted in significant water displacement immediately downstream of the canal, involving significant turbulence and air entrainment, which effectively reduced bore energy. Additionally, the presence of the canal reduced the velocity of the bore front, resulting in a delayed arrival time downstream of the canal. However, this delay was insufficient to significantly increase the evacuation time.

Column only: In this series of tests, the time history of water level in front of the column, time histories of horizontal force exerted on the column, and photographs from different angles of view were analyzed. The presence of the columns significantly modified bore dynamics, increasing turbulence and the horizontal force. The time interval (t_p) between the initial bore-column interaction and the peak horizontal force was directly affected by the impoundment depth (and subsequent bore velocity) and was shown to decrease with a higher impoundment depth. When only the location of the column relative to the gate was increased for the same bore, minimal impact on the horizontal force exerted on the column was recorded. However, this was due to the limited length of the flume; most probably, a significant increase of this distance would inherently lead to a decrease of the horizontal force, depending on the bore characteristics and the bed roughness of the flume.

Canal and column: To explore the impact of the water-filled canal on reducing tsunami bore energy and subsequent horizontal force exerted onto a downstream column, various canal

dimensions with depths of 5, 10, and 15 cm and widths of 60, 160, and 300 cm were considered. These findings indicate that water-filled canals can efficiently dissipate the incoming bore energy, diminish its velocity, and markedly decrease the horizontal force exerted on structures located across the canal. Wider and deeper canals proved to be more effective, with the broadest and deepest canal in this study, reducing peak forces by approximately 25%, underscoring their effectiveness in energy dissipation and reducing the force exerted on structures located in the tsunami inundation zone.

These findings enhance the understanding of tsunami bore dynamics and inform the design of coastal countermeasures. Future research should explore the impacts of bore interaction with various coastal structures and the potential for further optimization of mitigation strategies, such as canals, by focusing more on the hydrodynamics of bore propagation and its impact on coastal infrastructure.

Chapter 4. Numerical modeling[3]

Abstract

Although tsunamis are unpredictable natural events, their impact on coastal areas can be mitigated through the implementation of effective countermeasures. Both engineered and nature-based strategies have been employed to dissipate tsunami energy to protect infrastructure near affected coastlines and safeguard human life. Among these countermeasures, water-filled canals have proven to be effective in reducing tsunami energy, as demonstrated through field investigations, experimental studies, and numerical analyses. The interaction of tsunami bores with water-filled canals and their subsequent impact on structures is a complex phenomenon that requires a detailed investigation. Understanding the flow hydrodynamics around the canal and structure, pressure distribution, and force-time history on structures is essential for optimizing such mitigation strategies. In this study, a series of calibrated numerical simulations were conducted using a prototype-scale model to investigate the effectiveness of various dimensions of water-filled canal to reduce the horizontal force exerted on a downstream column. FLOW-3D was selected as the modeling tool due to its robustness and demonstrated capability to simulate complex fluid-structure interactions. The reduction factor for a specific tsunami bore characteristic depends on the geometry of the canal. In this study, for a tsunami-like bore generated by a 4 m-deep dam-break flow, the reduction factor reached up to approximately 40% for a canal with a depth of 4.5 m and a width of 40 m. The results showed that the presence of the canal had a much greater effect on reducing the tsunami-like bore-induced force on the column during the initial impact. The results also indicate that there is a threshold for both canal width and depth, beyond which further increases do not significantly enhance force reduction on the column. Moreover, the effect of canal width on increasing the reduction factor is considerably greater than that of canal depth. These

[3] Arefi, R., Mohammadian, A., & Nistor, I., (2026). Numerical Analysis of Bore-Induced Forces on Structures: Evaluating the Mitigation Potential of a Water-Filled Canal.

findings suggest that, in designing a canal as a tsunami mitigation countermeasure, both the absolute dimensions and the ratio of width to depth should be carefully considered.

Highlights:

- Investigated the effectiveness of rectangular water-filled canals in mitigating tsunami-like bore forces on columns.
- Calibrated FLOW-3D numerical simulations were used alongside experimental data for validation.
- Developed real-scale models to eliminate scaling effects and better represent tsunami dynamics.
- Found that canal width had a greater impact than depth, achieving up to 40% force reduction.
- Provides practical design insights for future coastal protection using water-filled canals.

Keywords: Tsunami-like bore, tsunami mitigation countermeasures, water-filled canal, horizontal force, numerical modeling, FLOW-3D

4.1 Introduction

Tsunamis are complex natural phenomena that are typically generated when a large volume of water suddenly moves, creating a long wave. These waves can travel across the entire ocean at high speeds, grow in height as they approach shallow coastal waters, and may eventually break into several bores, often causing catastrophic damage to infrastructure, ecosystems, and communities (Bryant, 2014). Tsunamis, though rare, represent a profound hazard to coastal zones, often resulting in widespread devastation and significant loss of life (Nistor et al., 2009).

As tsunamis occur rarely, it is difficult to perform field experiments. Therefore, most studies on how tsunamis propagate and interact with structures located in coastal areas have relied on laboratory experiments and numerical simulations (Wei et al., 2015). While significant

advancements have been made in understanding and modeling tsunamis, challenges remain in predicting their occurrence and mitigating their effects, particularly in densely populated coastal regions. Understanding these dynamics is crucial for enhancing disaster resilience and response strategies (Synolakis & Bernard, 2006).

Field surveys of recent tsunami events, such as the 2004 Indian Ocean Tsunami (Heidarzadeh et al., 2020), 2011 Tohoku Tsunami (Chock et al., 2013), 2018 Indonesia Tsunami (Syamsidik et al., 2019), and 2024 Noto Tsunami (Inagaki et al., 2025), have highlighted the urgent need for effective disaster mitigation strategies to protect coastal communities and infrastructure. The implementation of comprehensive risk-reduction measures can significantly reduce the impact of tsunamis, as evidenced by various methodologies and technologies developed in recent research. To mitigate tsunami-induced effects on infrastructure, various design provisions and planning measures have been developed that focus on both natural and man-made solutions (Suppasri et al., 2013; Oetjen et al., 2022).

Hard engineering solutions, such as sea walls, breakwaters, and offshore barriers, provide physical protection by deflecting or dissipating the force of incoming tsunami waves. However, they are often expensive to construct and maintain (Synolakis & Bernard, 2006). In contrast, soft engineering approaches such as mangrove plantations, dune restoration, and wetland rehabilitation enhance coastal resilience through natural processes, offering sustainable and cost-effective defense while benefiting local ecosystems, although they typically provide less robust protection during extreme events and require time to establish (Alongi, 2008). Among these, water-filled canals have emerged as a particularly effective solution for reducing tsunami energy. Their effectiveness has been validated through field investigations, experimental studies, and numerical modeling, highlighting their potential as reliable mitigation measures for coastal protection strategies (Rahman et al., 2017; Elsheikh et al., 2020).

Canals aligned parallel to coastlines have been shown to effectively dissipate tsunami energy, thereby reducing the impact of coastal inundation. A prominent example is the Buckingham Canal, located along the Chennai coastline, which measures approximately 30 m wide and 10 m deep. During the 2004 Indian Ocean tsunami, it significantly reduced the energy of the incoming bore and played a vital role in saving lives (Peng et al., 2024; Grant & Cooker, 2023). The Buckingham Canal's role during the 2004 tsunami exemplifies the life-saving potential of these measures (Peng

et al., 2024). Similarly, field investigations of the 49 km Kita-Teizan Canal revealed its effectiveness in mitigating damage during the 2011 Japan tsunami by reducing bore velocity and the resulting forces on downstream infrastructure (Cheng et al., 2023). While these findings underline the critical role of water-filled canals in tsunami impact mitigation, their effectiveness is highly dependent on factors, such as canal design, location, and local geographic conditions. This emphasizes the need for further research on the interaction of tsunami bores with water-filled canals and the dynamics of force transmission to structures located downstream. Understanding these interactions will aid in optimizing canal designs to maximize energy dissipation and enhance infrastructure protection.

Water-filled canals can significantly mitigate tsunami energy and reduce the force exerted on downstream structures by reducing the tsunami inundation velocity (Rahman et al., 2016). The interaction of tsunami waves with canals creates turbulence, which dissipates energy and reduces the impact on downstream structures.

Although experimental tests offer valuable insights into tsunami-induced hydrodynamics, they often have notable limitations that necessitate the use of numerical modeling. Laboratory experiments typically rely on scaled-down physical models. In addition, physical modeling is both costly and resource-intensive, often requiring extensive setup, instrumentation, and specialized facilities. Given these constraints, numerical modeling offers a practical and efficient alternative. This allows for high-resolution analysis of fluid dynamics over complex geometries and extended domains. In this study, FLOW-3D was employed for its capability to simulate transient free-surface flows and fluid-structure interactions which make it well suited for this study. The numerical model was calibrated using experimental data. To capture the detailed interactions between the tsunami bore, the canal, and the structure, the simulations were conducted at real scale. Various dimensions of the water-filled canal were considered to investigate their effects on reducing the force exerted on a column located behind the canal. Key parameters examined include flow depth along the tsunami path, velocity patterns around the canal and column, and the time history of the force acting on the column. These analyses aim to provide a better understanding of the canal's effectiveness as a tsunami mitigation countermeasure.

4.1.1 Objectives and novelty

This study aims to investigate the effectiveness of water-filled canals as a mitigation strategy for reducing tsunami-induced forces on structures located in coastal areas. While previous research has explored various countermeasures, the role of water-filled canals has not been fully evaluated in terms of their hydrodynamic behavior and energy dissipation performance under tsunami-like bore impacts. To address this gap, a series of calibrated numerical simulations was conducted using FLOW-3D software. These simulations were designed at the prototype scale to analyze how different canal configurations influence wave transformation, flow patterns, and the resulting forces exerted on downstream structures.

The primary objectives of this study were as follows:

i) To investigate the effectiveness of a rectangular water-filled canal in reducing tsunami bore forces on a column.

ii) To use calibrated numerical modeling for a deeper understanding of the interactions between tsunami-like bores, water-filled canals, and structures.

iii) To apply real-scale numerical simulations to eliminate scaling effects and obtain a more realistic representation of tsunami behavior.

iv) To conduct a detailed assessment of how canal geometry (width and depth) influences force reduction, turbulence, and flow dynamics.

4.2 Experimental Setup

To calibrate the numerical modeling, a series of experimental tests were performed at the Water Resources Engineering Laboratory of the University of Ottawa, Canada, using a tilting flume with 15.60 m in length, 0.38 m in width, and 0.60 m in depth. Figure 49 illustrates the side and plan views of the experimental setup.

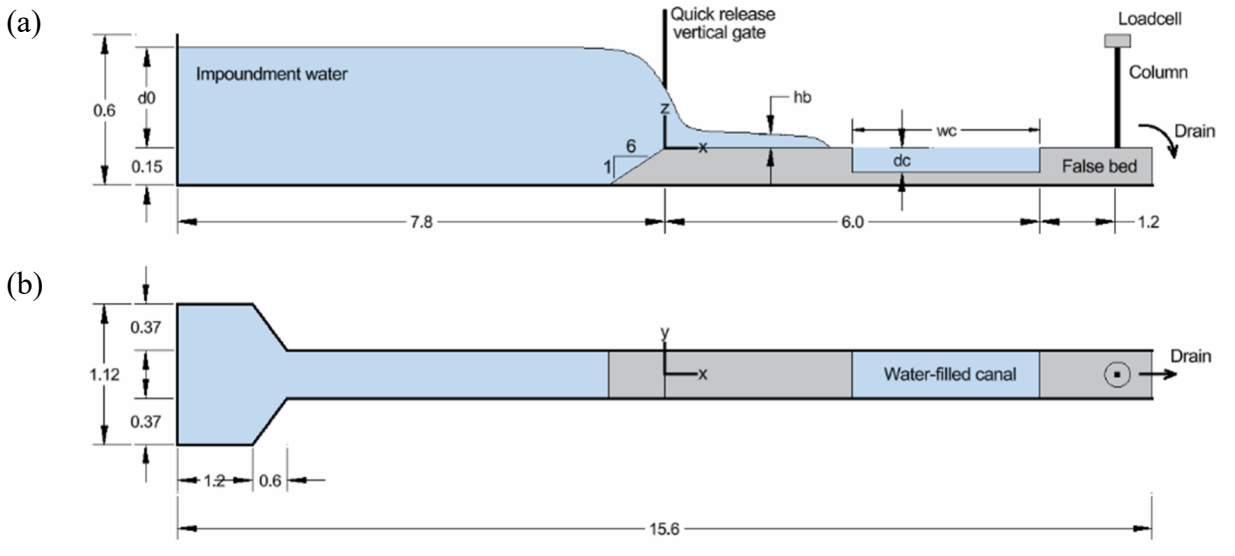

Figure 49. Schematic of the experimental setup (a) side, and (b) plan view (all dimensions in m)

Various canal configurations were tested, featuring depths of 5, 10, and 15 cm and widths of 60, 160, and 300 cm, by replacing the boxes installed on the bed of the flume. A 1:6 sloped bed was installed upstream of the gate to mitigate the local turbulence at the front of the false bed. A 4 cm square column was positioned at the end of the flume.

Tsunami-like bores were generated by rapidly lifting the gate was positioned at 7.8 m upstream end of the reservoir (x=0). The reservoir filled to predetermined water levels of 20, 30, and 40 cm above the false bed, corresponding to water impoundment volumes of 0.805, 1.208, and 1.611 m³, respectively. As illustrated in Figure 49, the reservoir is wider in the upstream area to accommodate a larger water volume in a limited flume length. To determine the aspect ratio of the reservoir length to water impoundment depth (L_{eq}/d_0), the equivalent length was calculated as L_{eq}=10.6 m. For impoundment water depths (d_0) of 20, 30, and 40 cm, the equivalent aspect ratios (L_{eq}/d_0) were calculated to be 53, 35.3, and 26.6, respectively. These values significantly exceed the recommendations of Lauber and Hager (1998) for generating an ideal tsunami bore, highlighting the unique experimental conditions of this setup.

The generated tsunami-like bore propagated along the flume, crossed over the canal, and after impacting the column, was dropped through a vertical drain at the end of the flume. Four ultrasonic distance sensors were placed at certain locations along the flume to monitor the bore depth variations. Additionally, a 6-axial load cell mounted on top of the column recorded the time history of the bore induced forces exerted on the column. Five GoPro Hero5 video cameras were employed

to monitor the propagation of the bore along the flume, its behavior before and after entering the canal, and around the column. Further details of the experiments can be found in Arefi et al. (2025).

4.3 Numerical Modeling

For decades, numerical models have been employed to address complex engineering problems. Due to the rapid development of computers and their power of calculation, the use of numerical models is increasing every day. In this study, to analyze the effects of water-filled canals to reduce tsunami-like bore induced forces on a structure located behind the canal, a series of numerical modeling was performed using FLOW-3D. This software was selected because of its robustness in simulating coastal engineering problems (Vasquez and Walsh, 2009; Alemi and Maia, 2018; Le Quéré et al., 2020; Lo et al., 2020; Wang et al., 2024; Yang et al., 2025), and has been applied by many researchers to study hydrodynamic forces on structures (Thanyamanta et al., 2011; Yoshida et al., 2018; Ghasemi et al., 2023).

4.3.1 Governing equations

FLOW-3D solves the Navier-Stokes momentum equations in all directions, allowing a fully nonhydrostatic solution methodology for the flow. The continuity and momentum equations, which are solved in all Cartesian directions, are expressed as

$$\frac{\partial u_i}{\partial x_i} = 0 \tag{1}$$

$$\frac{\partial u_i}{\partial t} + \frac{\partial u_i u_j}{\partial x_j} = -\frac{1}{\rho}\frac{\partial P}{\partial x_i} + \frac{\partial}{\partial x_j}\left[(\nu + \nu_t)\left(\frac{\partial u_i}{\partial x_j} + \frac{\partial u_j}{\partial x_i}\right)\right] + F_i \tag{2}$$

where u_i and u_j are the velocity vectors, t is the time, x_i and x_j are the position vectors, P is the pressure, ρ is the fluid density, ν is the eddy viscosity, and F_i represents the external force.

Using the fractional area/volume method (FAVOR), FLOW-3D is capable of modeling complex geometric regions within a rectangular grid (Zhang et al., 2021). To ensure simulation stability and convergence, an automatic time-step adjustment mechanism was implemented (Yang et al., 2025). In addition, sharp free surfaces can be captured using the Volume of Fluid (VOF) method.

4.3.2 Numerical setup

The computational domain was considered the same as in the experimental setup. The false floor and column were created by introducing boxes with dimensions like those used in the experiments. All boundaries were defined as zero gradient pressure boundaries except the downstream boundary, where a constant pressure boundary (z=-10 m) was applied, allowing the water to exit the numerical domain with no reflection and changes in the water level during the simulation. The mesh design employs a graded approach with varying cell sizes to ensure both computational efficiency and accuracy, which is achieved by using different mesh blocks throughout the computational domain (Figure 50). The finest mesh was utilized in the vicinity of the column to capture the detailed flow interactions and hydrodynamic forces accurately.

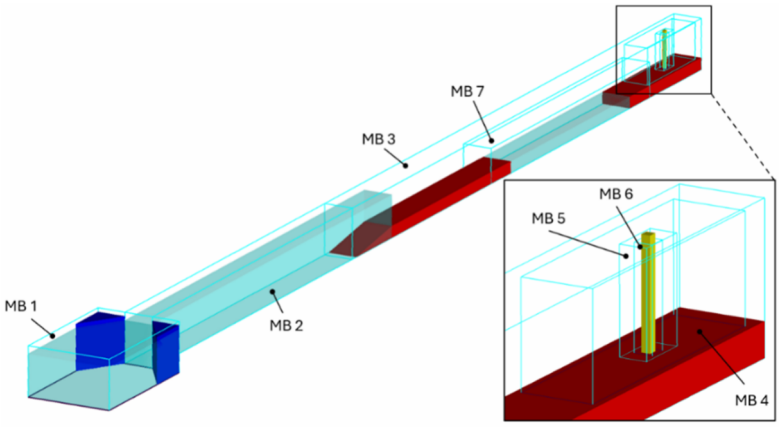

Figure 50: Mesh design based on experimental tests

Table 10: The positions of each mesh block in the x, y, and z directions and relative mesh size

Mesh Block	Region	Extent of mesh blocks						Mesh size (-)
		x-direction (m)		y-direction (m)		z-direction (m)		
MB1	Reservoir	-7.8	-6.04	-0.56	0.56	-0.15	0.5	6M*
MB2	Upstream flume	-6.04	-1	-0.19	0.19	-0.15	0.5	5M
MB3	Downstream flume	-1	7.8	-0.19	0.19	-0.15	0.5	3M
MB4	Around column (1)	6.5	7.7	-0.16	0.16	0	0.47	M
MB5	Around column (2)	7.1	7.34	-0.06	0.06	0	0.46	0.6M
MB6	Around column (3)	7.18	7.26	-0.04	0.04	0	0.45	0.25M
MB7	Around canal	2.5	6.5	-0.19	0.19	-0.15	0.3	M

* M is the mesh size of MB4 and MB7 which will be determined based on mesh sensitivity analysis

4.3.3 Mesh sensitivity analysis

Mesh sensitivity analyses are essential for balancing the accuracy and efficiency of numerical modeling. In this study, four different models were tested using 2,350,000 (M=0.5 cm), 1,200,000 (M=1 cm), 550,000 (M=1.3 cm), and 150,000 (M=2 cm) meshes. Figure 51 presents the time history of the horizontal force exerted on the column for a test without a canal and with a water impoundment depth of 40 cm. In all models, a square column (4 cm × 4 cm) was placed at x=720 cm. Based on the results, the model with 1,200,000 cells (M = 1 cm) was selected, as it provided reliable accuracy while maintaining computational efficiency. As illustrated in Figure 51, further increasing the number of mesh elements did not lead to a significant improvement in the results.

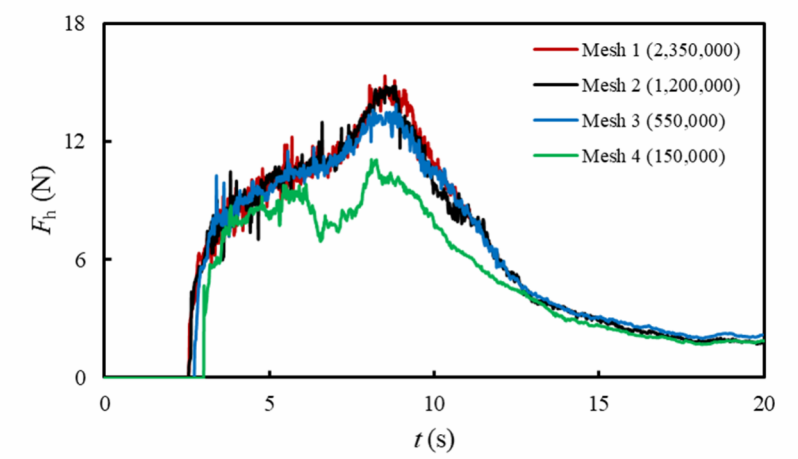

Figure 51: Mesh sensitivity analysis for four different models (the value in the parenthesis indicates the number of mesh cells)

4.3.4 Turbulence model

The turbulence model is essential for simulating the turbulent regime caused by the interaction of a tsunami-like bore with a water-filled canal and column. After evaluating different turbulence models available in FLOW-3D, based on the time histories of bore depth and horizontal force on the column, the Smagorinsky model was selected, as it provided the best results compared with experimental data despite computational limitations in resolving boundary layer. Figure 52 and Figure 53 show a comparison of the water surface profiles resulting from these interactions for both the numerical simulations and experimental tests at different time steps. As shown in these figures, the numerical model reasonably captures the essential details of this complex flow regime.

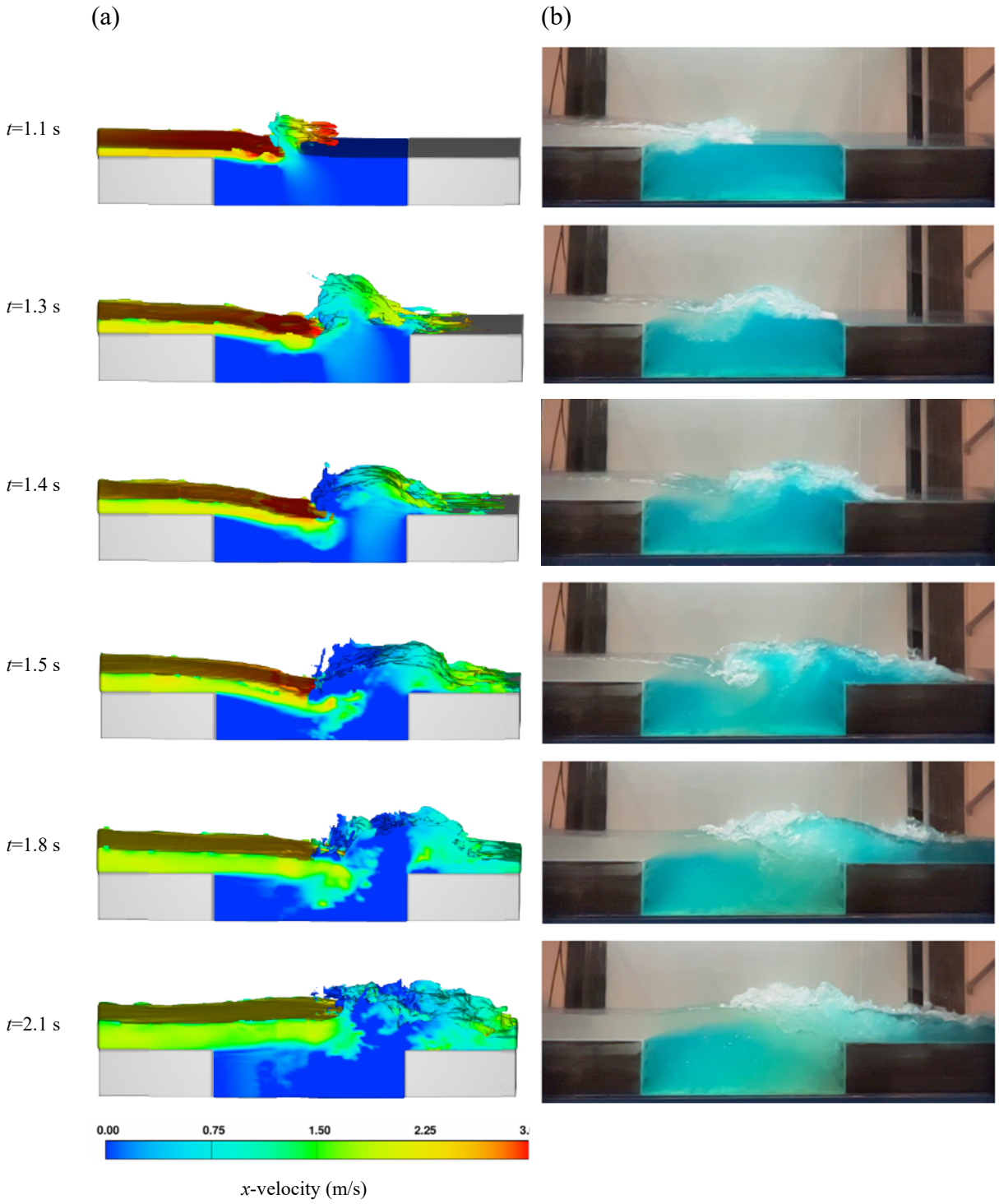

Figure 52: Tsunami-like bore interaction with water-filled canal at different time steps for (a) numerical modeling with x-velocity pattern, and (b) experimental test (d_0=40 cm, w_c=60 cm, d_c=15 cm)

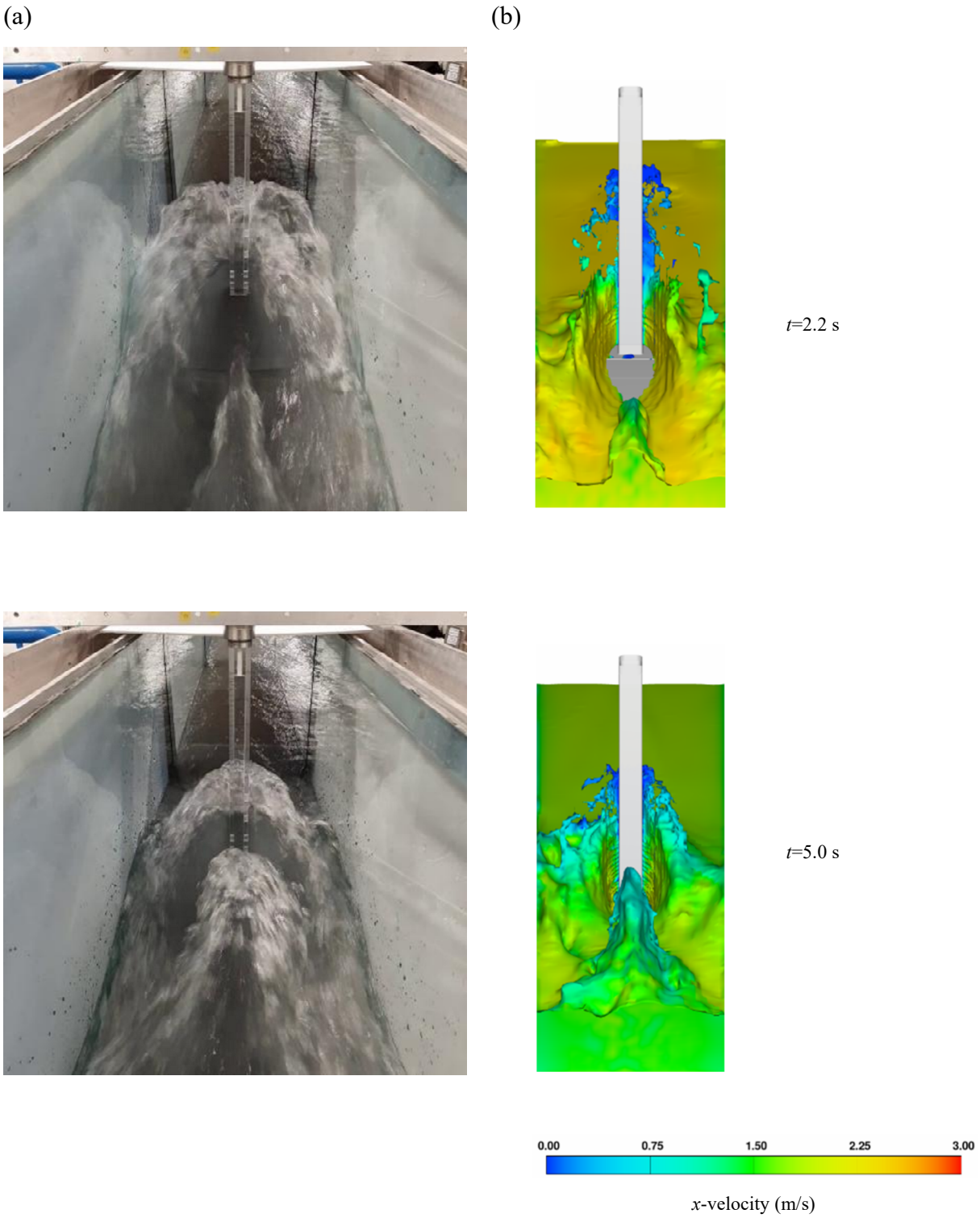

Figure 53: Bore interaction with column at different time steps for (a) experimental test, and (b) numerical modeling (Test without canal, d_0=40 cm, and the column is located at x=720 cm)

4.3.5 Validation

Figure 54 and Figure 55 present the comparisons of time histories of the horizontal force for two test scenarios: a test without a canal where the column was located at x=420 cm (Without canal-With column), and a test involving a canal 300 cm wide and 15 cm deep, with the column positioned at x=660 cm (With canal-With column). In both cases, a 40 cm deep impoundment was considered upstream of the gate. The results demonstrate good agreement between the numerical and experimental data, with NRMSE of 5.6 and 6.2%. Additionally, bore depth comparisons are shown in Figure 56 and Figure 57 for a test without a canal and column (Without canal-Without column), and a test with a 60 cm wide, 15 cm deep canal and no column (With canal-Without column). NRMSE for these comparisons were 2.9 and 7.2%, further confirming the accuracy of the model.

In summary, the numerical model demonstrated a good agreement with the experimental data across multiple configurations. This level of accuracy was achieved without parameter tuning, relying only on the use of a sufficiently refined mesh to capture complex hydrodynamic behavior. This successful validation provides a solid foundation for using the model to explore additional scenarios and assess the effectiveness of water-filled canals as a tsunami force mitigation countermeasure.

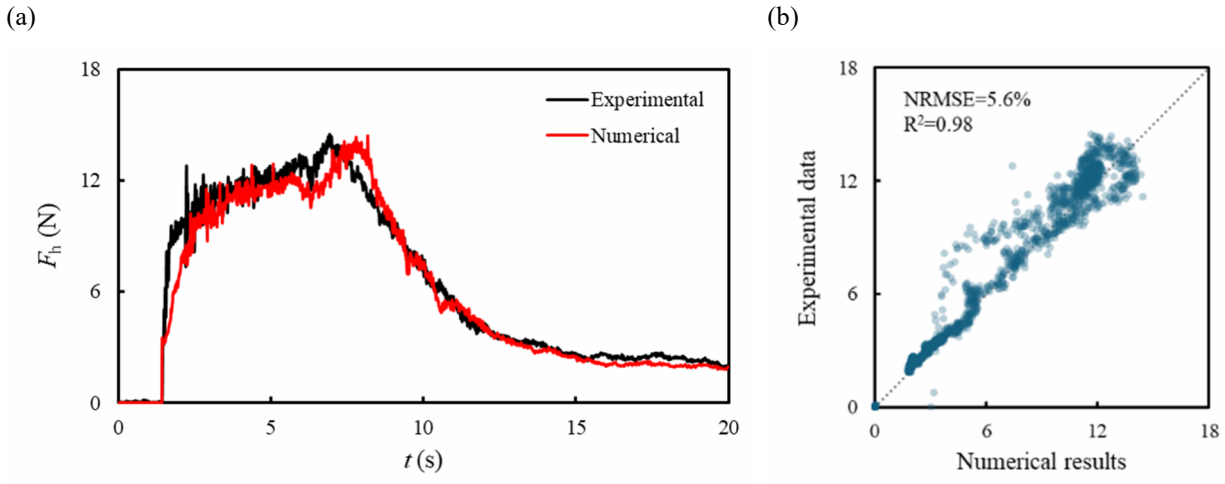

Figure 54: (a) Comparison of horizontal force on column for numerical modeling results and experimental data, and (b) scatter plot and NRMSE for the test Without canal-With column

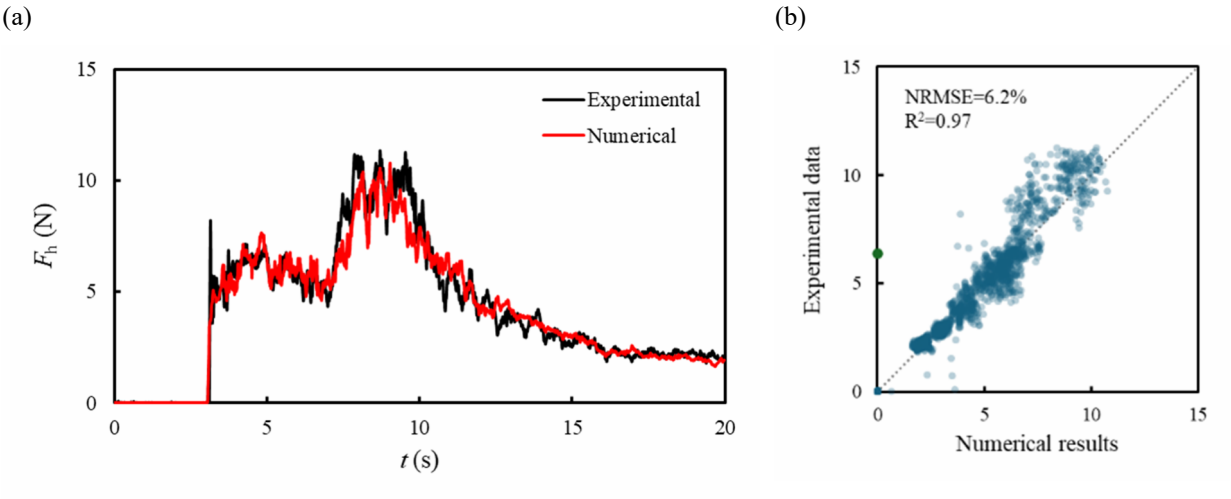

Figure 55: (a) Comparison of horizontal force on column for numerical modeling results and experimental data, and (b) scatter plot and NRMSE for the test With canal-With column

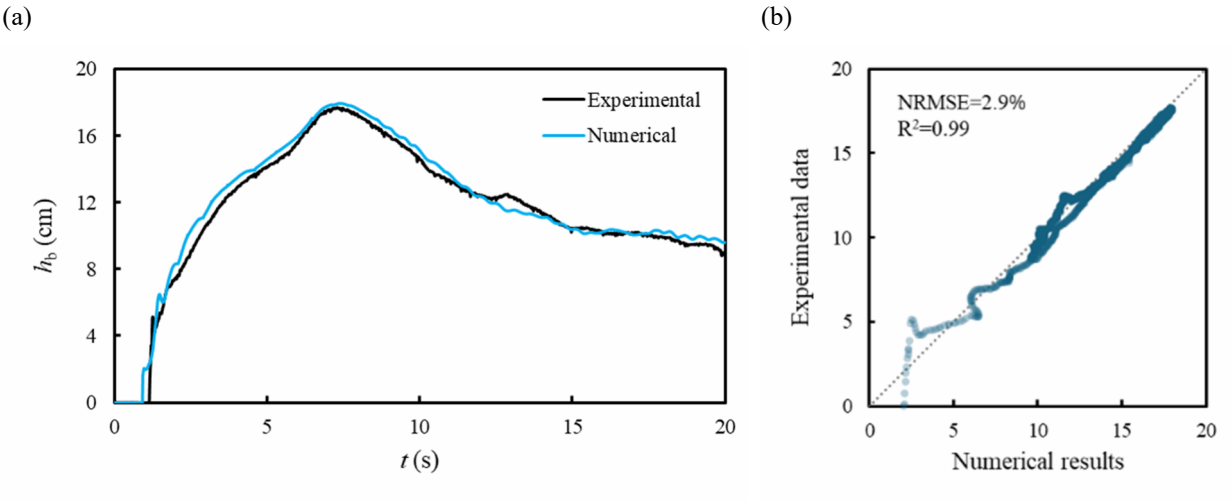

Figure 56: (a) Comparison of bore depth at x=2.7 m for numerical modeling results and experimental data, and (b) scatter plot and NRMSE for the test Without canal-Without column

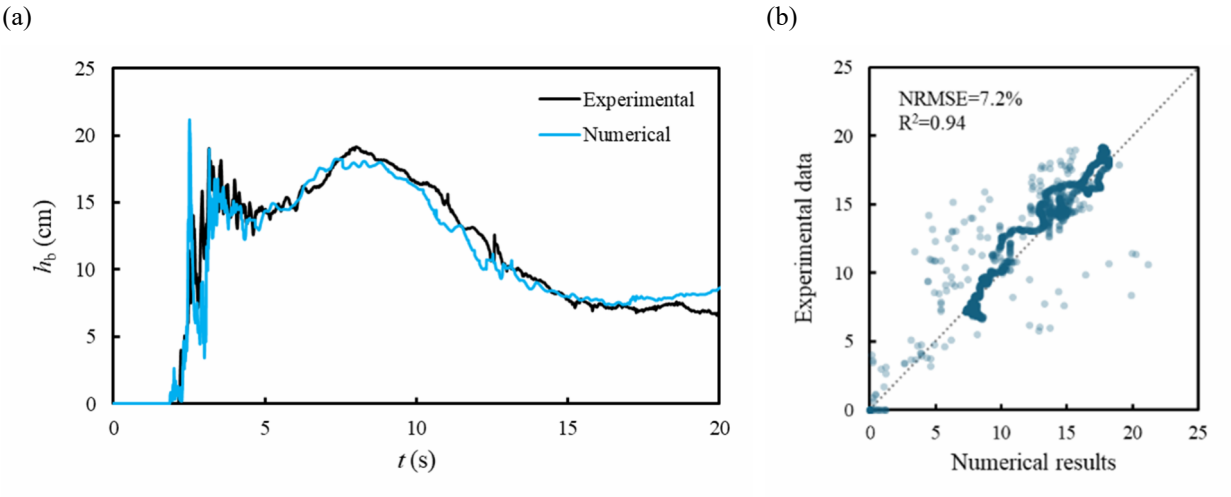

Figure 57: (a) Comparison of bore depth at x=3.9 m for numerical modeling results and experimental data, and (b) scatter plot and NRMSE for the test With canal-Without column

4.4 Flume limitations in experimental tests

4.4.1 Scale effect

Unlike physical experiments constrained by laboratory size, numerical models can be conducted without spatial or temporal limitations. While small-scale models provide valuable insights into complex phenomena, scaling down introduces distortions in the dynamic and flow parameters that are challenging to replicate accurately.

The physical experiments in this study, conducted at a 1:10 Froude scale, highlighted phenomena that may not scale perfectly. These discrepancies can result in variations in the flow dynamics and force measurements when extrapolated to full scale. By employing 1:1 numerical modeling, these scale effects are inherently avoided, ensuring a more accurate representation of the true physical behavior. In this regard, the results of numerical simulations conducted at the experimental scale (1:10) with those at the prototype scale (1:1) were compared. In both cases, the water impoundment depth was set to 4 m, and the column was positioned at x=72 m, and in the scenario with canal, a 60 m wide and 1.5 m deep canal was implemented (all dimensions in prototype scale).

As illustrated in Figure 58, the results of the 1:1 numerical model exhibit good agreement with those of the 1:10 numerical model. The comparison of the horizontal force exerted on the column as well as the bore depth 2 m in front of the column for the tests with and without canal demonstrated good agreement between the 1:1 and scaled 1:10 numerical results. It should be noted that the scale effect on force in the presence of canal is more pronounced, although it is still reasonable. For the scaled model, the bore depth, time, and force were scaled by $1/\lambda$, $1/\lambda^{0.5}$ and $1/\lambda^{3}$ respectively, where λ is the scale ratio and is equals to 0.1.

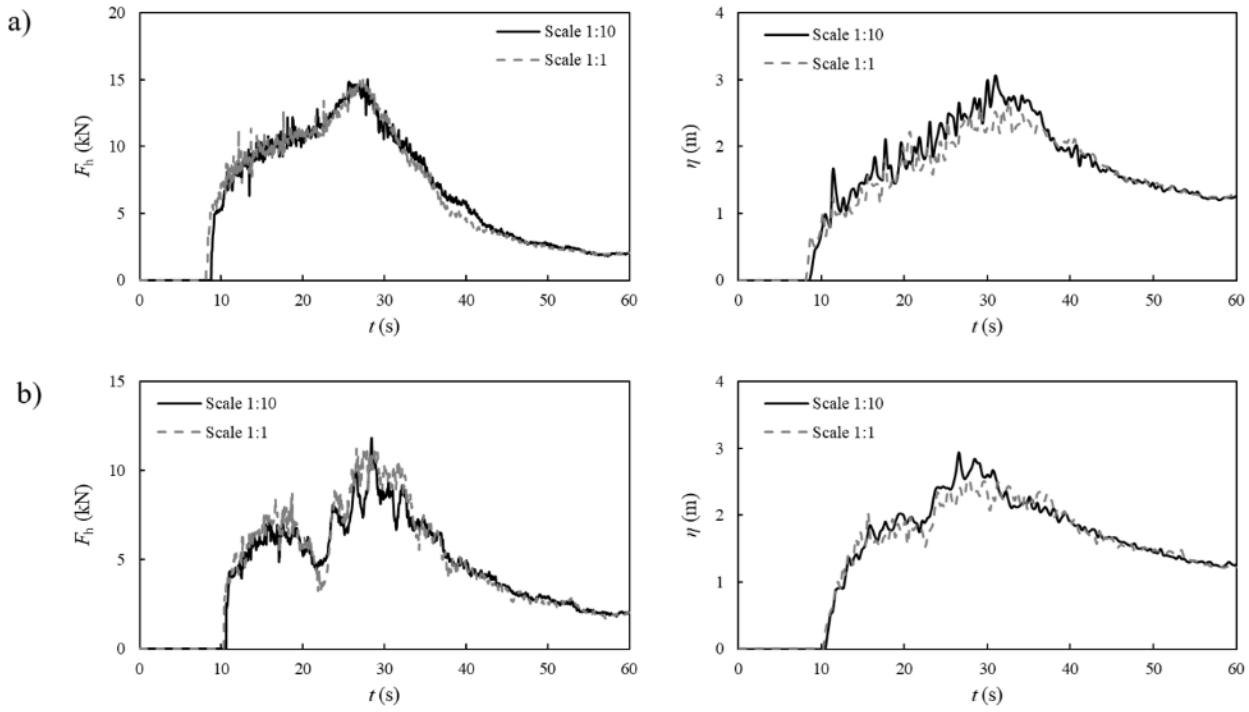

Figure 58: Comparison of the horizontal force on column (left panel) and the bore depth at 2 m front of the column (right panel) for scales of 1:1 and 1:10 for tests. Results are shown for tests without a canal (top row), and with a canal (bottom row)

4.4.2 Length of flume

For a dam-break problem, the reservoir length is crucial for ensuring a stable bore front during water propagation. A longer reservoir maintains a steady flow, which is essential for stable bore formation (Shugan et al., 2020), where an insufficient reservoir length can cause rapid emptying, leading to unstable bore characteristics (Liu et al., 2020). In addition, the pressure exerted on

surfaces varies significantly with bore shape and stability, which is contingent on reservoir length (Issakhov et al., 2020).

In this section three different models with reservoir lengths of 100, 200, and 500 m were chosen, and the time histories of the horizontal forces on the columns were compared. As shown in Figure 59, by increasing the length of the reservoir, the maximum horizontal force on the column remained constant. While a reservoir length of 100 m was sufficient to capture the peak horizontal force exerted on the column, a 500 m long reservoir was ultimately selected to ensure an accurate analysis of the hydrodynamic processes and ensured that the reservoir would not be fully depleted during the 100-second simulation.

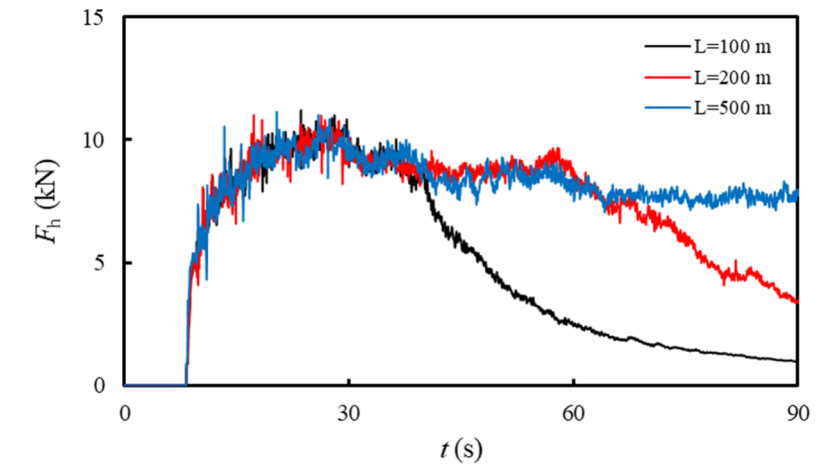

Figure 59: The effect of the reservoir length on horizontal force exerted on the column

4.4.3 Width of flume

Another limitation of the experimental modeling was related to the flume width. In this regard, wider flumes with widths of 6 m and 10 m were selected, and the flow around the column and the horizontal force on the column were compared with the results of the model with a flume width equal to 3.8 m.

The time history of the horizontal force was plotted for different flume widths to analyze the effects of the flume width on the force exerted on the column. As shown in Figure 60, the maximum horizontal force differs by less than 1% between widths of 3.8 m and 6 m, and the time history of the force shows negligible variations. Increasing the width to 10 m does not significantly affect the results. Therefore, a width of 3.8 m was selected for the numerical modeling tests.

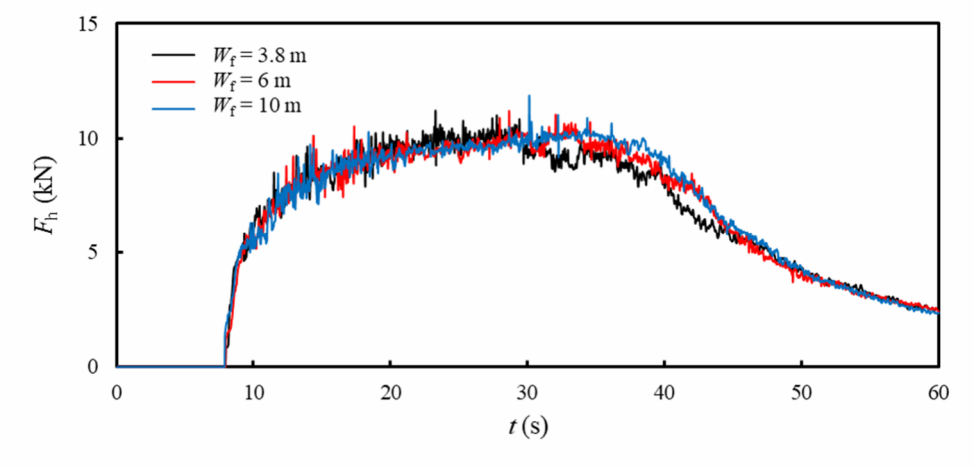

Figure 60: The effect of the reservoir width on horizontal force on the column (test without canal)

4.5 Results

The primary objective of this study is to investigate the effects of a rectangular water-filled canal on the horizontal force induced by a tsunami bore on a column located behind a canal. By overcoming the constraints of laboratory-scale experimental modeling, numerical simulations were conducted at a prototype scale (1:1) using a flume with a width of 3.8 m, and reservoir length of 500 m. A square column of 40 cm on each side was fixed at x=72 m for all the tests. Different dimensions of the canal were considered, and the downstream edge of the canal was positioned at x=60 m. The bore was generated by releasing a water impoundment at a depth of 4 m, resulting in a tsunami-like bore with a maximum flow depth of 2.5 m, flow velocities ranging from 4 to 8 m/s. These conditions are representative of the moderate tsunami events that may occur in coastal areas. Consequently, the flow velocities in the model were higher than those typically observed in real-world tsunamis with the same flow depth.

By keeping all parameters constant for all tests, except for the canal dimensions, the test designations were selected based on the width and height of the mitigation canal. For instance, test w30-d1.5 refers to a scenario in which a mitigation canal with a width (w_c) of 30 m and depth (d_c) of 1.5 m.

4.5.1 Bore interaction with column

The interaction between tsunami bores and a structural column involves complex hydrodynamic regions around the column, and subsequently, forces and pressure distributions on it. Various studies have utilized numerical simulations and experimental setups to analyze these interactions (St-Germain et al. 2014, Nouri et al., 2010). Tsunami bores are characterized by high velocity and turbulent flow, which can exert substantial forces on structures. The bore depth and velocity are crucial factors that influence the pressure exerted on columns (Asadollahi et al., 2019; Chuang et al., 2020).

As illustrated in Figure 61, the time history of the bore depth and depth-averaged velocity for the test without a canal and at x=70 m reveals that the bore front initially propagates with a significantly high velocity, which gradually decreases over time. Conversely, the bore depth exhibits an increasing trend as the bore propagates. A combination of high velocity and low bore depth results to a high Froude number (Fr=$\overline{U}/\sqrt{gh_b}$), which creates a supercritical region with a Fr of approximately 8. It should be noted that calculating the Fr at the moment of wave arrival is challenging and highly susceptible to numerical errors. By increasing the bore depth and decreasing the bore velocity during this time, Fr drops to lower than 1 around $t(g/d_0)^{0.5}$=60, which means that the flow regime changes from supercritical to subcritical.

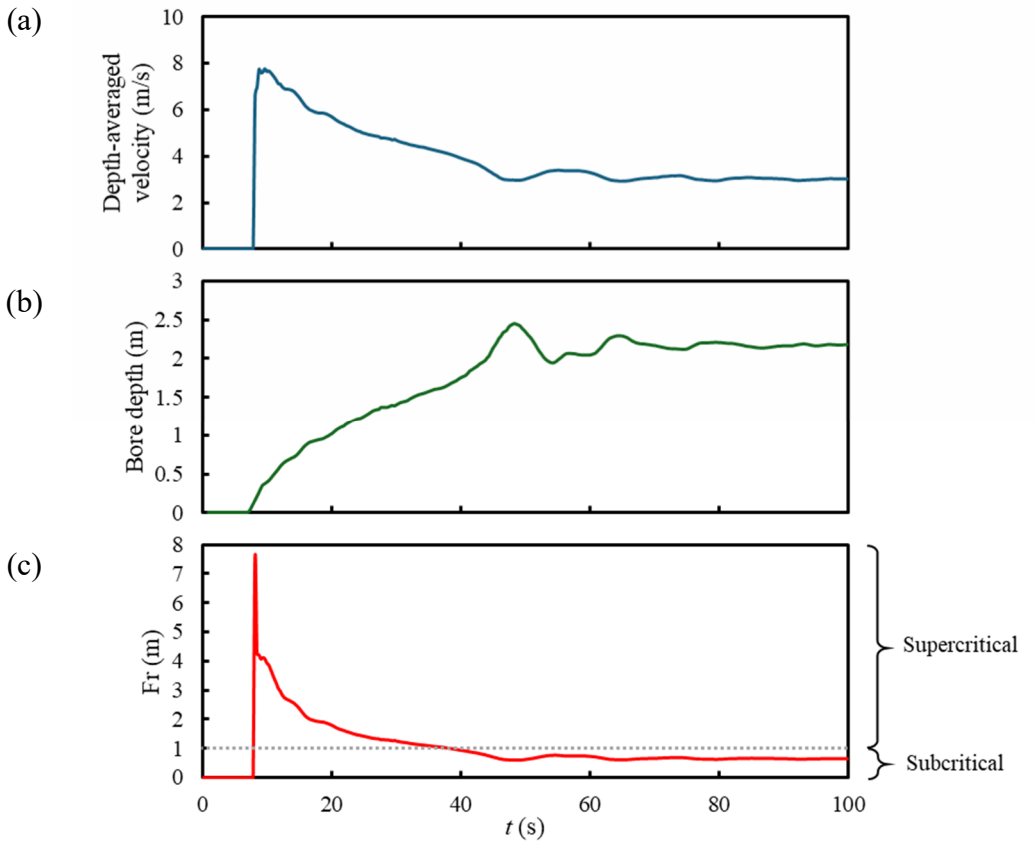

Figure 61. Time history of (a) bore depth, (b) depth-averaged velocity, and (c) *Fr* at x=70 m for the test without canal and column

The interaction between a tsunami-like bore and a column creates a highly turbulent and complex flow region, which has been the subject of extensive research (Harish et al., 2025; Nouri et al., 2010; Al-Faesly et al., 2012). The presence of the column significantly influences the surrounding flow pattern. Figure *62* presents the *x*-velocity distribution along the centerline of the flume (y=0) at t=26 s, corresponding to the moment when the horizontal force on the column reaches its peak. As shown in this figure, the presence of the column reduces the *x*-direction velocity in the region immediately in front of the structure. By analyzing the *x*-direction velocity along the depth at various locations upstream of the column, it is evident that the column's influence extends approximately 2 m upstream (Figure 63). Because of the obstruction caused by the column, part of the flow is diverted laterally in the *y*-direction, while another portion moves upward, leading to a run-up on the front face of the column, where the *x*-velocity remains relatively low.

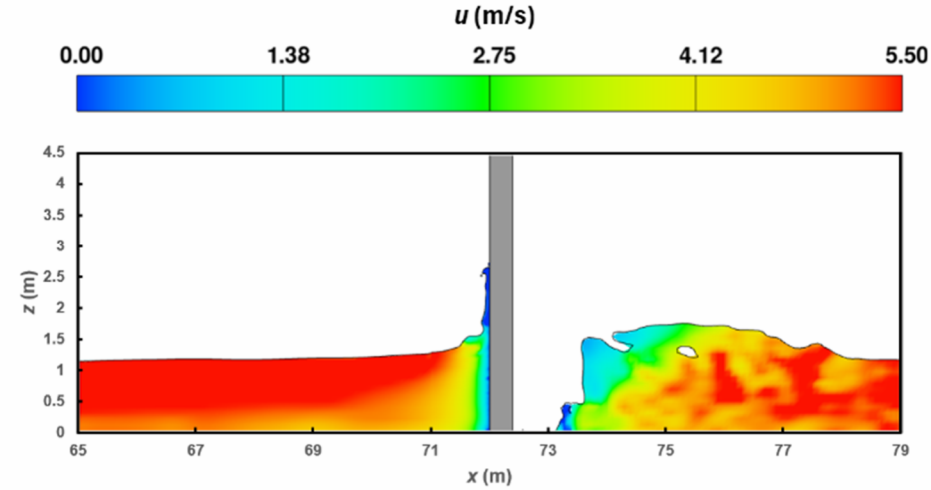

Figure 62. Snapshot of x-velocity pattern around the column at t=26 s and y=0 (centerline) for the test without canal (NC)

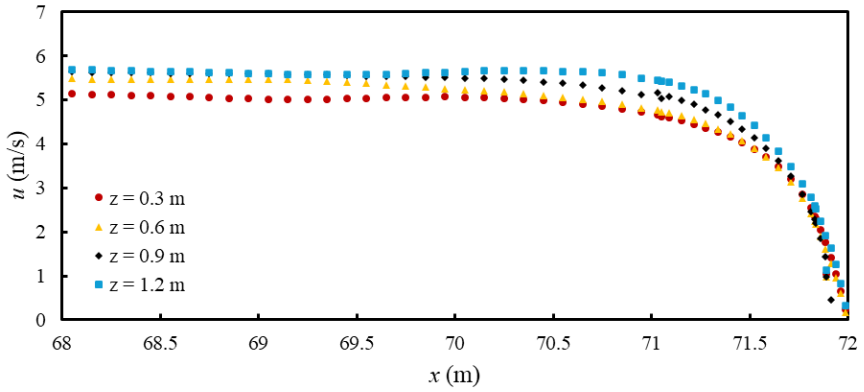

Figure 63. x-direction velocity at different z-levels, t=26 s and y=0 for the test without canal (NC)

4.5.2 Bore interaction with canal

The crossing of a tsunami-like bore over a water-filled canal generates large free-surface fluctuations and velocity variations, which can be described as hydraulic jumps (Henderson, 1996; Elsheikh et al, 2020). By reaching the bore to the water-filled canal, it penetrates the canal, which creates a high-turbulence regime, and the interaction of the front bore with the canal causes a reduction in the high velocity of the bore front. Figure 64 shows snapshots of the tsunami-like bore interactions with a rectangular water-filled canal for test w30-d1.5. As shown in this figure, by entering the bore into the canal, a large volume of water goes out, which makes the bore propagate, but at a smaller velocity.

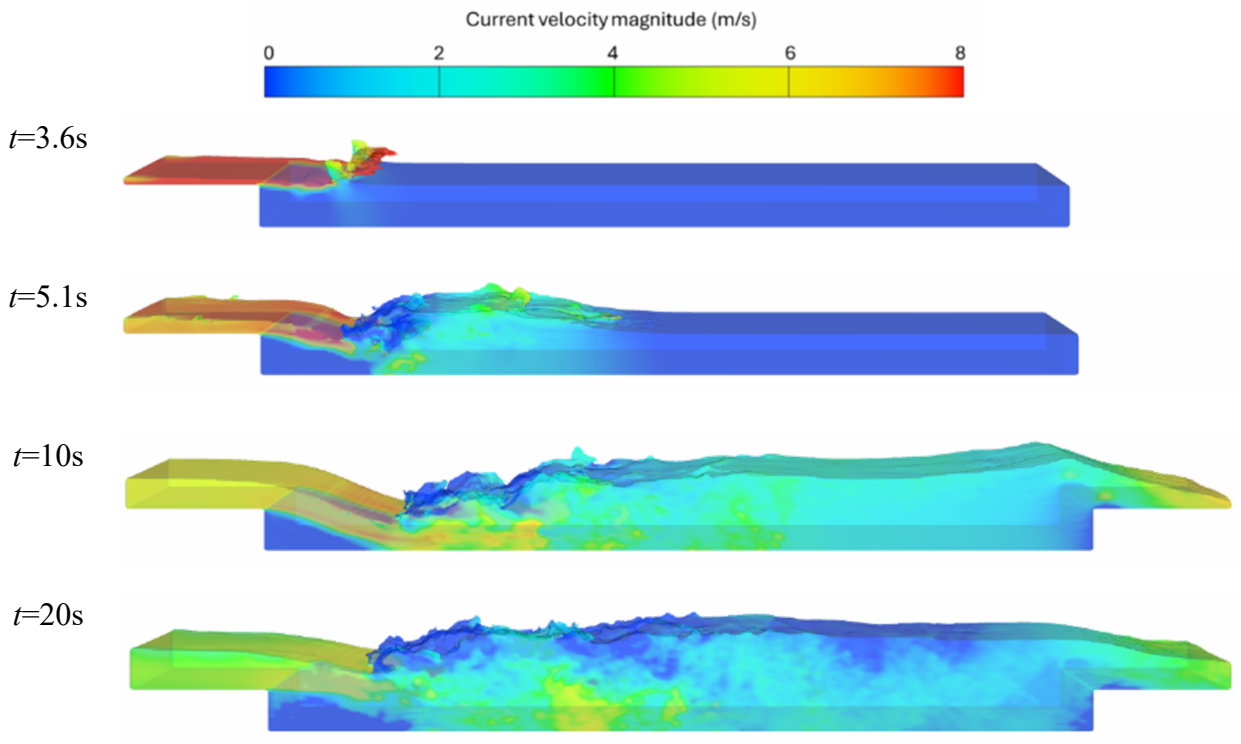

Figure 64: Snapshots of bore interaction with rectangular water filled canal (Test: w30-d1.5)

Figure 65 shows the time history of the *x*-direction velocity at *z*=0, taken after the canal (*x*=65 m) in test w30-d1.5. These results were compared to those of a test without the presence of a canal (Test NC). The findings reveal that the inclusion of a canal with a width of 30 m and a depth of 1.5 m resulted in a reduction in bore front velocity by approximately 13%. While the presence of the canal increased the arrival time of the bore front, it is important to note that this delay is not significant enough to meaningfully enhance evacuation times during a tsunami event.

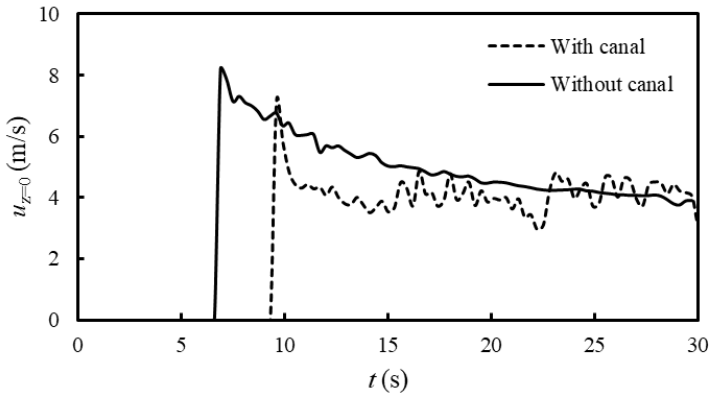

Figure 65: Effect of canal on reducing the bore front velocity at *z*=0 (Test: w30-d1.5 for the test with canal)

While the presence of the canal increased the arrival time of the bore front, it is important to note that this delay is not significant enough to meaningfully enhance evacuation times during a tsunami event.

4.5.3 Effect of the canal on flow patterns around the column and forces exerted on the column

The interactions between tsunami-like bores and structures have been widely investigated using both experimental (Nistor et al., 2009; Nouri et al., 2010; Al-Faesly et al., 2012) and numerical approaches (Wei et al., 2015; Sarjamee et al., 2017; Spröer et al., 2025), providing crucial insights into the forces exerted during such events. However, limited research has been conducted on the interaction of tsunami-like bores with water-filled canals (El-sheikh et al., 2022a, b; El-sheikh et al., 2020; Rahman et al., 2017).

Figure 66 presents the time history of x-velocity at 0.5 m above the bed for different combinations of canal and column presence at x = 70 m (2 m in front of the column). The presence of canal caused to velocity reduction, accompanied by some oscillations, and significantly reduces the bore front velocity, which is a crucial factor in certain cases, where it contributes to the maximum force exerted on the structures. The presence of the column reduces the flow velocity in the x-direction due to wave reflection, as evidenced by the comparison of the time history of velocity, which the velocity profiles for the case with the column (red and green lines) consistently lie below those for the case without the column (black and blue lines).

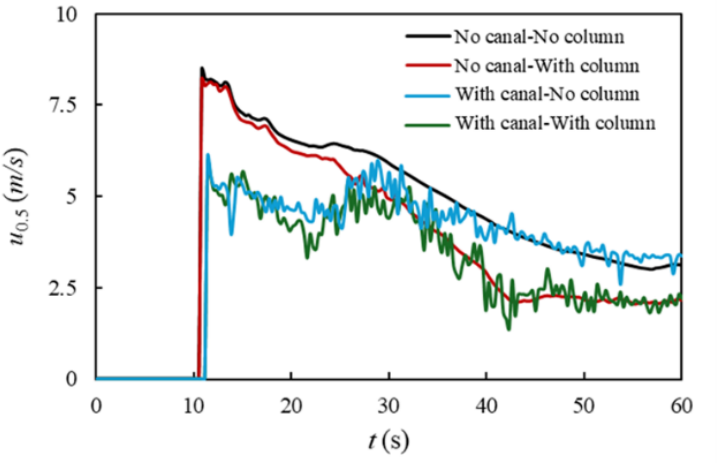

Figure 66: Effect of canal and column existence on x-velocity at z=0.5 m, y=0, and x=70 m (2 m front of the canal)

Figure 67 illustrates the snapshots of the bore front impacting the column, with and without the presence of a 30 m wide and 1.5 m deep canal. For a better comparison, the bore-front arrival time to the column was selected as the origin of the time in this figure. The presence of the canal reduces the bore-front velocity and results in smaller splashes and run-up both in front of and downstream of the column, while simultaneously causing the bore to reach the column with a higher water depth.

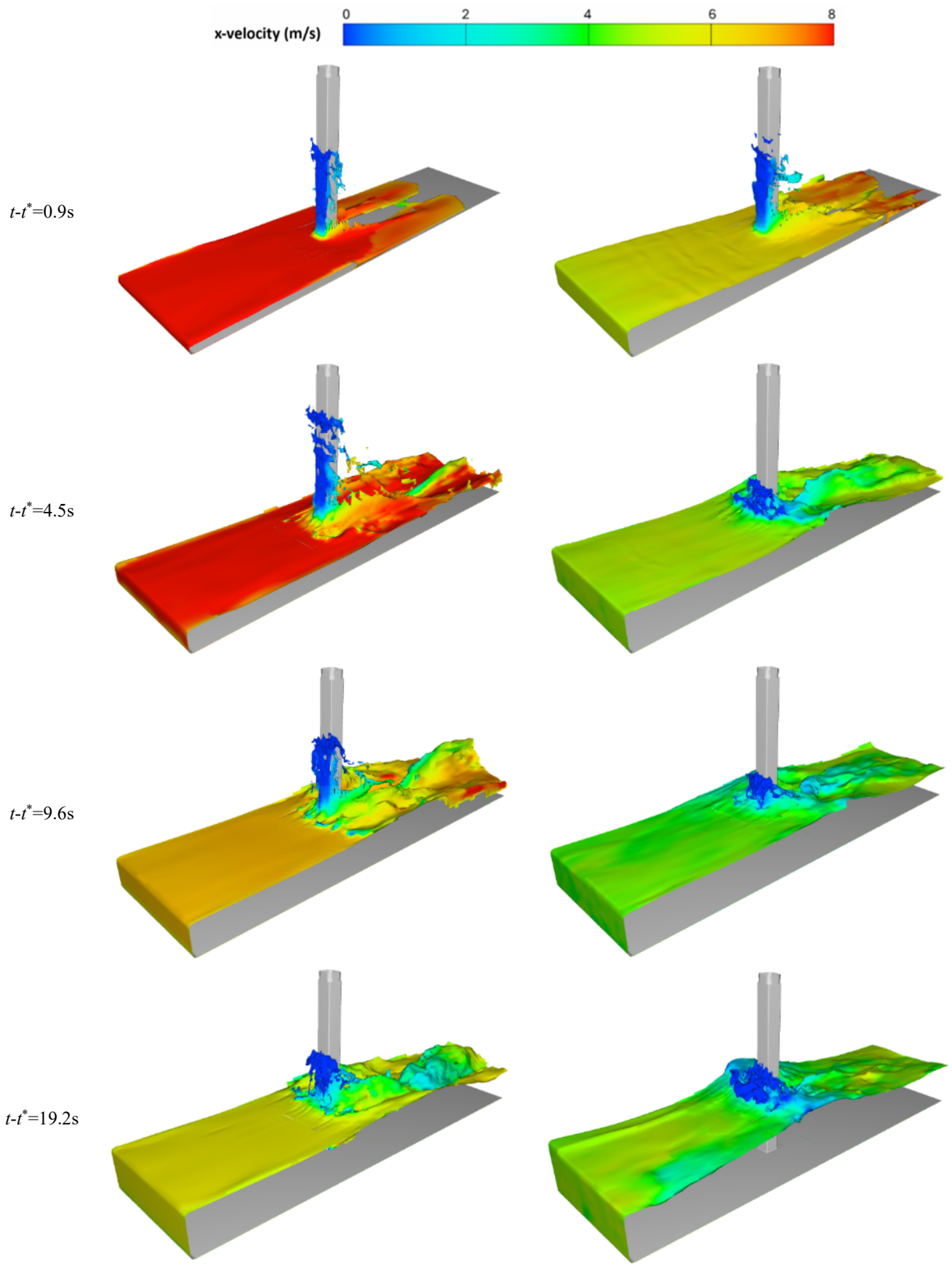

Figure 67: Snapshots of the bore front impact on the column without presence of the canal (left panel) and with presence of canal (right panel) at different time steps (t^* is bore arrival time to the column)

To quantitatively compare the effect of the canal, Figure 68 shows the time histories of the bore height, depth-averaged velocity, momentum flux at x=70 m (2 m in front of the column), and horizontal force exerted on the column. These graphs illustrate that the canal increases the bore front depth while decreasing the depth-averaged velocity in front of the column, which are two main factors determining the momentum flux, and therefore the force on the column, which means the canal influences them in opposite ways. In particular, the canal's reduction of the x-velocity (which is squared in the momentum flux calculation) outweighs its effect on increasing the bore front depth, ultimately resulting in a decrease in the overall momentum flux. For better comparison, the graphs plotted based on arrival time using t-t^* on the horizontal axis.

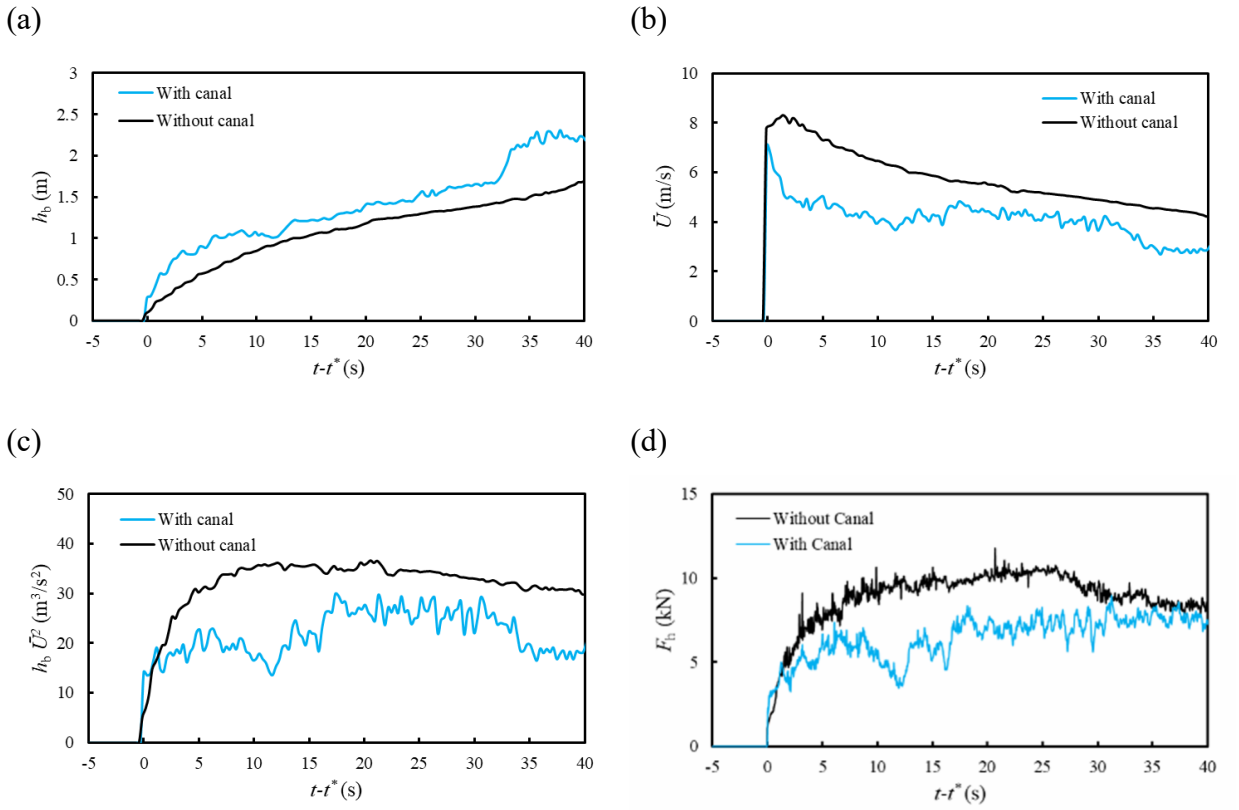

Figure 68: Time history of (a) the bore depth (h_b), (b) the depth-averaged velocity ($\bar{U}$), (c) the momentum flux density per unit width ($h_b\bar{U}^2$), and (d) the horizontal force exerted on the column at x=70 m, with (blue line) and without (black line) presence of a 30 m wide and 1.5 m deep canal

The pressure distribution in front of the column with and without the presence of a canal is shown in Figure 69. The canal causes some oscillations in the water surface level, leading to a more fluctuating pressure distribution, as shown in Figure 69b (with the canal present), compared

to the smoother distribution without the presence of the canal (Figure 69a). However, the most important note from the comparison in Figure 69 is the lower pressure observed during the initial impact of the bore on the column (between t=10 s and 20 s) in the presence of the canal. The presence of the canal reduces the maximum pressure exerted on the column during the first 15 seconds of bore impact, with a reduction ranging from 20% to 50%. Studies by Arikawa (2008) and Ramsden and Raichlen (1990) revealed that under specific bore and structure conditions, the force exerted on structures during the initial impact of a tsunami bore can exceed the quasi-steady force due to the sudden and intense collision of the bore front with the structure. This reveals that the reduction in bore pressure, and consequently the force on the column during the initial impact of a tsunami-like bore, due to the presence of canals, has a significant effect on protecting coastal infrastructure.

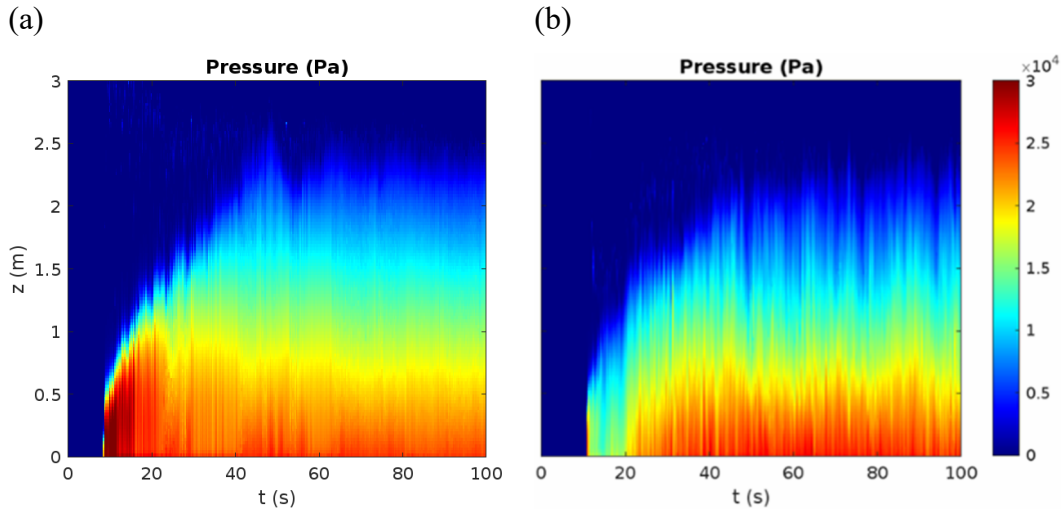

Figure 69: Pressure distribution on the column, (a) without canal (test NC), and (b) with canal (test w30-d3)

Figure 70 illustrates the flow pattern around the column and the influence of the canal presence on these patterns. The figure compares the flow around the column with and without a canal with a width of 30 m and depth of 3 m at t=26 s (when the force is at its maximum) and z=0. As shown in this figure, the shorter vectors in the test with the canal indicate that the canal creates a calmer region, particularly behind the column and along its edges. This reduction in flow velocity is a critical factor in mitigating scouring around the column, which is one of the main contributors to structural failure. The absence of black vectors behind the column indicates the formation of a wake, which creates an empty region. However, in the presence of the canal, this area is not empty, as the canal helps to calm the flow and reduce the wake effect.

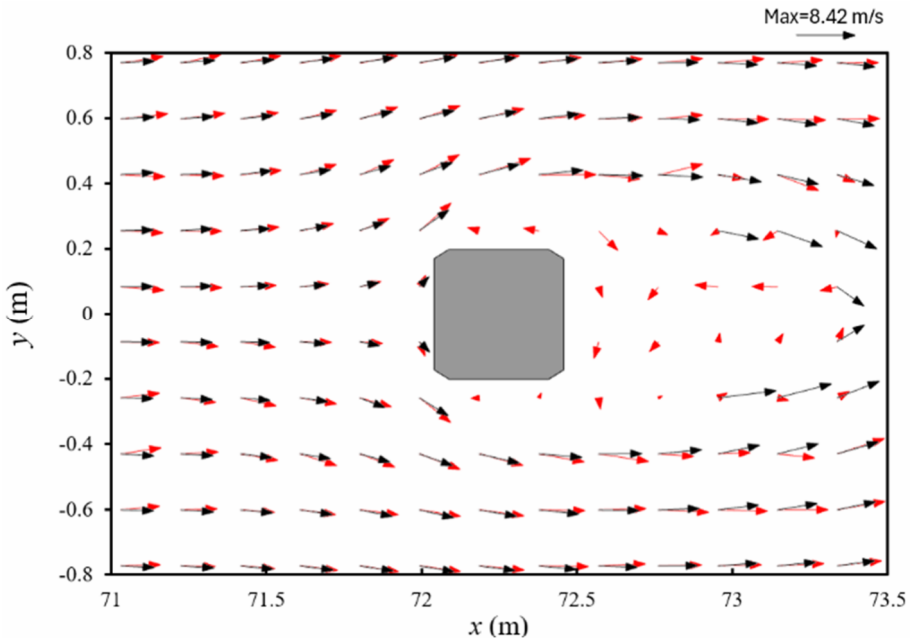

Figure 70: Velocity vectors around the column at t=26 s and z=0 without (black) and with (red) presence of a 30 m wide and 3 m deep canal

4.5.4 The effects of canal dimensions

To study the effects of canal dimensions on the attenuation rate of the horizontal force exerted on the column, a series of numerical modeling with different widths and depths of canals was performed. As mentioned previously, the test designations were determined based on the canal width (d_c) and canal depth (w_c). All tests were performed with the same water impoundment depth of 4 m and the upstream edge of the canal and column located at x=20 m and at x=72 m, respectively.

Table 9 lists the configuration parameters in the numerical simulations. In the first test, no canal was considered (NC), and in the next tests, canals with depths of 0.5, 1.5, 3, and 4.5 m and widths of 10, 20, 30, and 40 m were considered.

Table 11. Numerical modeling tests

Test No.	Test name	w_c (m)	d_c (m)
1	No Canal (NC)	-	-
2	w10-d3	10	3
3	w20-d3	20	3
4	w30-d3	30	3
5	w40-d0.5	40	0.5
6	w40-d1.5	40	1.5
7	w40-d3	40	3
8	w40-d4.5	40	4.5

Figure 71 and Figure 72 illustrate the time history of the horizontal force exerted on the column for different canal dimensions. For better understanding, the bore arrival time was considered for the horizontal axis. By comparing the time histories, it is clear that the presence of the canal reduces the force exerted on the column, which increases the rate of attenuation by increasing the depth or width of the canal. Although, as shown in these figures, the canal's presence effects are significant in the initial impact and run-up regions (t-t_0<40 s), the presence of the canal causes fluctuations in the horizontal force, which makes it more difficult to study the effects of the canal dimensions on the reduction factor by comparing the maximum amount of the force exerted on the column, especially in the quasi-steady region (t-t_0>50 s). In this regard, the average of the force during the first 25 s was selected, and the effects of the dimensions of the canal were studied and compared, as depicted in Figure 73.

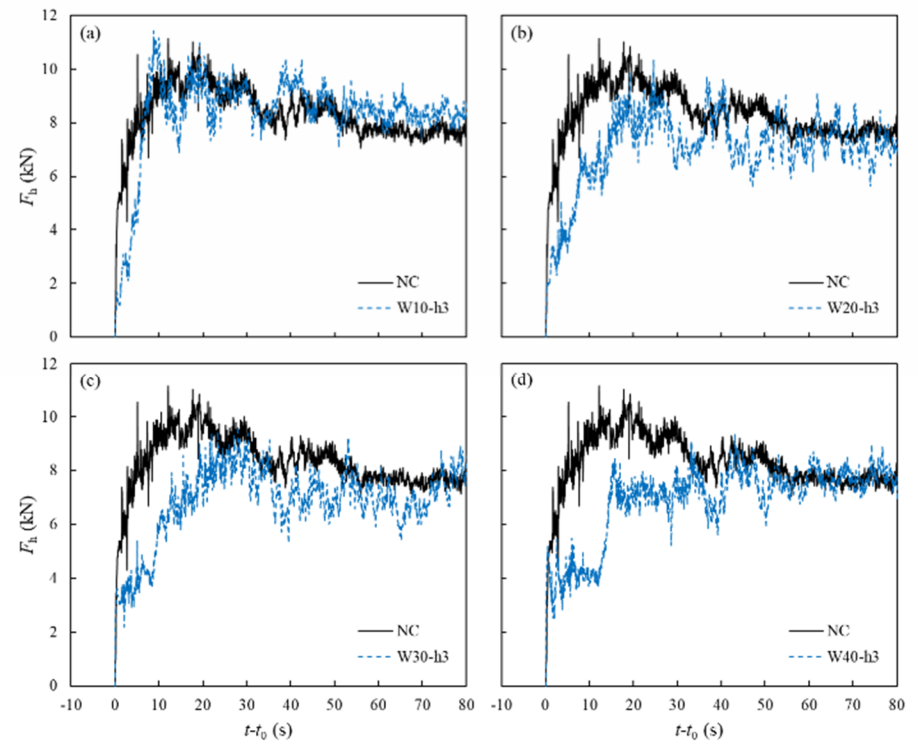

Figure 71: Comparison of the time history of the horizontal force exerted on the column for a canal with a depth of 3 m and various width of (a) 10, (b) 20, (c) 30, and (4) 40 m with a test without canal (NC)

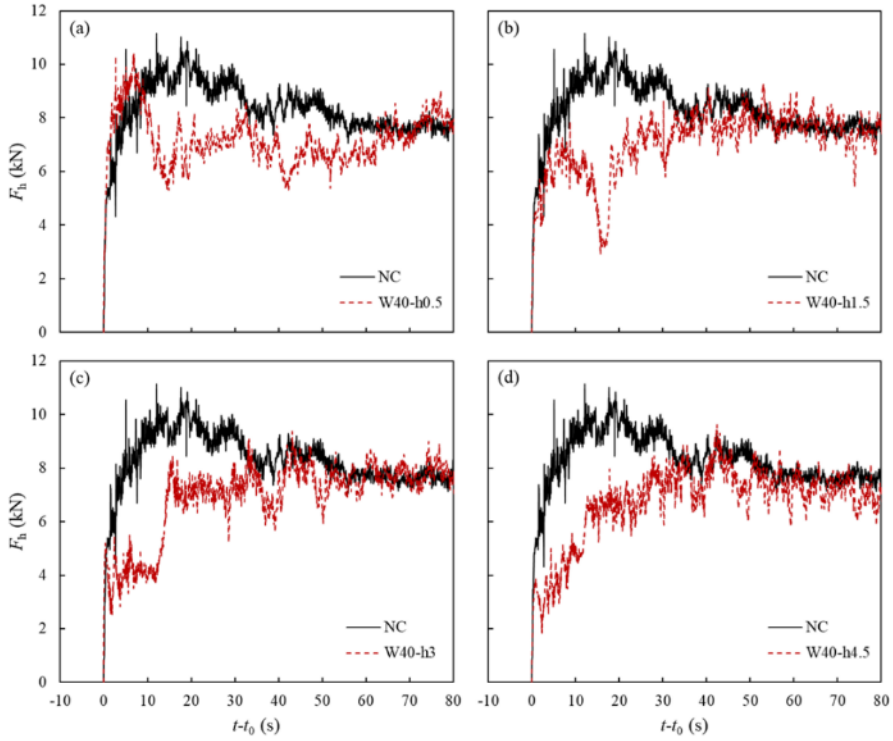

Figure 72: Comparison of the time history of the horizontal force exerted on the column for a canal with a width of 40 m and various depth of (a) 0.5, (b) 1.5, (c) 3, and (4) 4.5 m with a test without canal (NC)

As shown in Figure 73(a), increasing the canal depth beyond a certain threshold did not lead to a significant improvement in the force reduction factor. For example, in the case of a tsunami-like bore generated by a 4 m dam break, when the canal width is fixed at 40 m, the threshold depth is approximately 3 m. This indicates that further increasing the canal depth to 4.5 m results in a negligible additional reduction in the force exerted on the column.

Conversely, Figure 73(b) clearly illustrates that increasing the canal width substantially enhanced the reduction in horizontal forces on the column. For a canal with a constant depth of 3 m, increasing the width from 10 to 40 m significantly increased the reduction rate from approximately 11% to 37%. This indicates that canal width plays a more dominant role than depth in mitigating tsunami-like bore forces, emphasizing the importance of lateral expansion in canal design for improved energy dissipation, as reported by Rahman et al. (2017) and Elsheikh et al. (2022a, b).

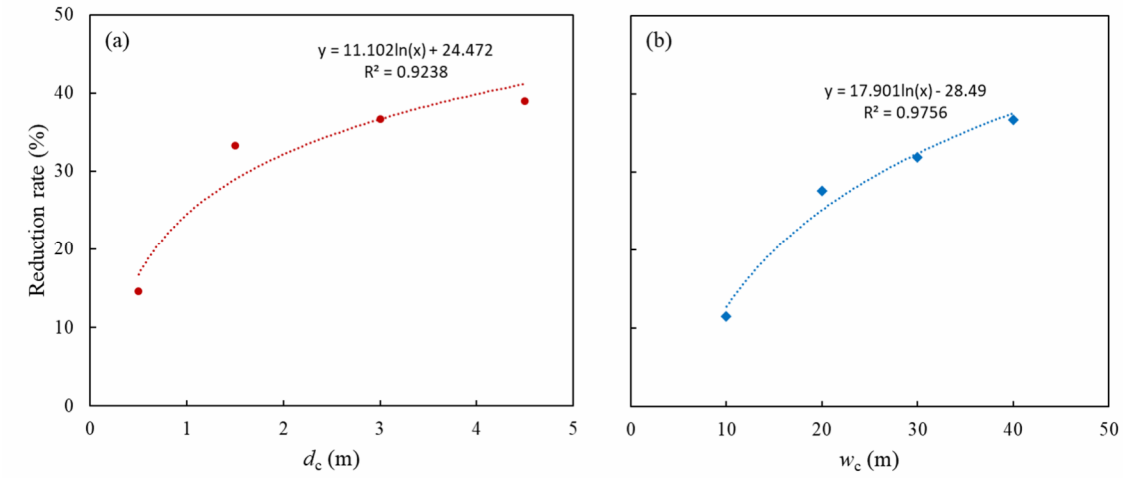

Figure 73: Effects of canal's dimensions on the reduction rate of horizontal force exerted on column due to the presence of canal with (a) different depth of canal with a width of 40 m, and (b) different width of canal for a canal with a depth of 3 m

4.6 Discussion

Tsunamis are rare events that are difficult to study through field experiments. Therefore, most studies on tsunami propagation and its interactions with structures on affected coastlines rely on laboratory experiments and numerical simulations. To reduce these impacts, both nature-based and engineered solutions have been implemented. Among these, water-filled canals aligned parallel to

coastlines have shown the potential for dissipating tsunami energy and reducing the intensity of coastal inundation.

This study investigated the role of a rectangular water-filled canal in reducing the force exerted by a tsunami-like bore on a vertical column located in front of the canal. A series of calibrated numerical simulations using FLOW-3D were performed to evaluate how the canal affects bore dynamics and its interaction with both the canal and column. To overcome the limitations of small-scale experiments, full-scale numerical models have been developed using realistic tsunami parameters and practical canal and column dimensions. The results showed that scaling effects had negligible influence on the results of the time history of the bore depth and force exerted on the column. However, full-scale modeling better captured the high-turbulence zone generated by the interaction of the bore with the canal and the column.

In the laboratory experiments, due to the limited flume length, a reservoir with a wider width than the flume was constructed behind the gate to hold enough water volume. However, the non-rectangular geometry of the reservoir influenced the bore characteristics and resulting forces. To simulate different canal depths in the experimental tests, some boxes were placed on the flume bed, while a 1:6 sloped bed was added upstream of the gate to suppress vortex formation. These features were removed from the numerical models, which assumed the same level of bed throughout the domain, producing results that are more representative of real tsunami behavior. The extended reservoir length (up to 500 m) in the simulations prevented depletion over the 100 s runtime, ensuring continuous and realistic bore evolution. The flume width was kept the same as in the experiments because changes showed no significant effect.

The turbulence generated as the bore passed through the water-filled canal played a key role in dissipating the energy and reducing the force exerted on the column. Notably, the canal significantly changed the flow regime and reduced the bore velocity, especially the bore front velocity. Time-history comparisons confirmed that the canal had a stronger influence on reducing the initial impact force than on reducing the later quasi-steady force.

The findings of this study are consistent with those of Rahman et al. (2017), who also investigated canals as tsunami mitigation measures. Their results indicated that while canals could partially absorb tsunami energy, they also caused reflected waves that led to variations in inundation depth compared with cases without canals. Their experiments showed that deeper and

wider canals resulted in greater reductions in the wave impact. Similarly, Elsheikh et al. (2022) found that wider canals were more effective at reducing the momentum of tsunami bores, while deeper canals absorbed more energy as the bore passed through. Their experimental and numerical results also indicated that canals led to an increased maximum bore depth landward of the canal while reducing the bore's velocity. These findings align closely with those of the present study, in which increased canal width and depth led to energy dissipation, velocity reduction, and force mitigation. However, it appeared that canal depth had a threshold for a certain tsunami event which beyond a certain point, increasing depth and width did not lead to further reductions in force. In the present study, for a canal width of 40 m, the threshold depth is approximately 3 m, beyond which further increases in canal depth do not significantly change the reduction factor.

Despite these promising results, several limitations of this study remain to be acknowledged. Sediment transport, debris flow, and scour effects were not modeled, although they are crucial in real tsunami scenarios. The studied structure was limited to a single square column.

Future research should explore:

- The incorporation of finer gird, more advanced turbulence models, and wider range of simulation parameters,
- Larger full-scale domains and more canals configurations,
- The influence of canal location and its distance from the structure,
- The performance of canals in multi-column arrangements,
- The inclusion of debris impact, sediment transport, and scour,
- Cost-benefit analysis and feasibility of implementing water-filled canals in real-world coastal cities.

Overall, the findings of this study contribute to the understanding of using engineered water-filled canals as a tsunami mitigation measure and emphasize the need for further investigation to develop practical design guidelines for protecting coastal infrastructure.

4.7 Conclusion

This study investigated the effectiveness of a rectangular water-filled canal as a potential mitigation measure to reduce the energy of a tsunami-like bore impacting a column using a series of numerical modeling simulations. FLOW-3D was employed as a robust tool capable of simulating complex fluid-structure interactions. To calibrate the numerical model, experimental tests were conducted in the Water Resources Engineering Laboratory at the University of Ottawa, Canada, using a flume measuring 15.60 m in length, 0.38 m in width, and 0.60 m in depth. In the experimental tests, various canal configurations were tested with depths of 5, 10, and 15 cm and widths of 60, 160, and 300 cm. The results from the numerical simulations were compared with the experimental data in terms of the bore depth before and after the canal, as well as the force exerted on the column. The numerical domain was designed to replicate the experimental flume. Among the turbulence models available in FLOW-3D, the Smagorinsky model was chosen due to its ability to capture the complex interaction between the tsunami-like bore, the water-filled canal, and the column.

To overcome certain limitations of the physical experiments, numerical simulations were conducted at the prototype scale, and the reservoir length was extended to 500 m to ensure a sufficient volume of water behind the gate, allowing the simulations to run for 100 seconds without depletion, thereby maintaining consistent bore characteristics. The flume width was set to 3.8 m, matching the laboratory flume size, and the study showed that increasing the width had no significant effect on the results. The calibrated model at real-world scale was then used to analyze the performance of the water-filled canal as a tsunami mitigation strategy. The propagation of the tsunami-like bore and its interaction with the canal and the column were thoroughly examined. The column size was set to 40 cm, which is comparable to that of a typical residential building column in the real world. Comparisons of the time histories of the bore depth and impact force on the column demonstrated a good agreement between the numerical and experimental results.

In the present study, various canal widths and lengths were analyzed. Although increasing both the width and depth of the canal enhanced energy dissipation and consequently reduced the force on the column, the results suggest that there is a limit to the reduction factor. Beyond this limit, which depends on the characteristics of the tsunami bore, further increases in canal dimensions do

not lead to significant additional force reduction. For a tsunami-like bore generated by the sudden release of a 4 m water impoundment behind a gate, the horizontal force reduction factor was approximately 40% for a canal with a width of 40 m and a depth of 4.5 m. Notably, increasing the canal width had a more significant effect on force reduction than increasing the depth. However, there is a threshold for both depth and width of the canal which further depth and width increases had a minimal impact.

Overall, this study confirms that water-filled canals can reduce tsunami-induced forces on structures located near coastlines by approximately 40%. These findings suggest that such canals are viable passive mitigation measures. Further studies are recommended to develop practical design guidelines for determining the optimal dimensions of protective water-filled canals for infrastructure in tsunami-prone coastal zones.

Chapter 5. Conclusions and Recommendations

5.1 Summary of Key Findings

This study investigated the effectiveness of rectangular water-filled canals as a mitigation measure for tsunami-like bore forces on coastal structures. Findings are based on a combination of literature review (Chapter 2), physical modeling experiments at a 1:10 scale (Chapter 3), and prototype-scale numerical simulations using FLOW-3D (Chapter 4). The key findings are summarized as follows:

- Reduction of Structural Forces: Both experiments and numerical simulations demonstrated that water-filled canals can significantly reduce the horizontal force exerted by tsunami-like bores on downstream structures. Force reduction reached up to 40% for a canal with a width of 40 m and depth of 4.5 m under a 4 m-deep dam-break bore scenario. Experimental measurements indicated reductions of at least 25%, highlighting the effectiveness of water-filled canals in mitigating initial impact forces.
- Influence of Canal Geometry: Canal width was found to have a greater influence on force reduction than canal depth, although both parameters contribute to overall mitigation performance. A threshold exists beyond which increasing canal dimensions does not provide significant additional benefits, suggesting that optimized design is more effective than simply increasing size.
- Modification of Bore Characteristics: The presence of a canal altered the hydrodynamic behavior of the tsunami-like bore. Canal interaction increased the bore depth while reducing bore front velocity, which in turn reduced the momentum flux impacting the structure.
- Time-History of Forces and Bore Depth: Experimental and numerical data revealed the dynamic nature of force mitigation. Analysis of time histories showed that energy dissipation occurred primarily at the initial stage of bore-structure interaction, emphasizing the importance of early energy attenuation.

- Consistency Between Experiments and Simulations: Both approaches provided complementary insights. Physical experiments allowed direct measurement and observation of force reduction, while numerical simulations enabled analysis of prototype-scale scenarios, elimination of laboratory limits, and exploration of additional canal configurations.

This thesis provides a comprehensive assessment of rectangular water-filled canals as a tsunami mitigation measure:

- Effectiveness: Water-filled canals reduce horizontal forces on downstream structures, with reductions up to 40% observed in prototype-scale simulations.
- Geometry Matters: Canal width is more influential than depth in reducing bore-induced forces, though both dimensions are critical.
- Threshold Effect: There is a point beyond which increasing canal dimensions does not significantly improve mitigation, highlighting the need for optimized design.
- Hydrodynamic Alteration: Canals modify bore depth, velocity, and momentum flux, reducing peak forces during the initial impact phase.
- Experimental and Numerical Complementarity: Physical experiments and numerical simulations together provide a robust framework to evaluate canal performance and inform real-world design.

5.2 Implications for Coastal Engineering Design

The findings of this study offer several practical insights for engineering design in tsunami-prone areas.

First, water-filled canals can serve as an effective component of integrated coastal protection systems, reducing structural loads on buildings, piers, and other coastal infrastructure. Their ability to attenuate peak forces before they reach critical structures is particularly valuable in reducing damage during the first impact.

Second, careful geometric optimization is essential. For a given scenario, wider canals generally provide greater force reduction than deeper canals, though both dimensions contribute to performance. Designers should therefore evaluate both absolute size and width-to-depth ratios to maximize energy dissipation.

Third, canal placement may be crucial for maximizing mitigation benefits. Positioning a canal to intercept the bore during its initial high-energy phase ensures that the most severe loads are reduced before reaching downstream structures.

Fourth, numerical modeling tools such as FLOW-3D are indispensable for evaluating site-specific hydrodynamics, exploring extreme scenarios, and analyzing complex flow behavior that cannot be fully captured in laboratory experiments.

Finally, while canals are effective, they are best integrated with other mitigation measures, such as natural features, hybrid solutions, or structural defenses, to create multilayered protection systems capable of performing under diverse tsunami conditions.

5.3 Recommendations for Coastal Design

- Integrate water-filled canals in coastal mitigation schemes where structural load reduction is critical.
- Optimize width-to-depth ratios and consider placement relative to infrastructure.
- Use numerical simulations for site-specific design and assessment of extreme events.

  Consider combined mitigation strategies for enhanced protection.

5.4 Recommendations for Future Research

Future research should therefore explore:

- Investigate non-rectangular canal geometries (e.g., trapezoidal) and assess the influence of different initial water levels within the canal on tsunami-like bore attenuation and force reduction.

- Apply machine learning and data-driven approaches to identify the optimal canal width-to-depth ratio as a function of tsunami-like bore characteristics. This approach would require an expanded experimental and numerical database covering a wide range of canal geometries and flow conditions.
- Since the presence of a canal can significantly reduce near-bed flow velocity, future studies should examine the potential reduction of seabed scouring downstream of canals through detailed sediment transport measurements and coupled hydro-morphodynamic modeling.
- Extend the analysis to wet-bed conditions, with particular emphasis on the second and subsequent tsunami bores, which may more destructive due to increased bore depth and momentum.
- Investigate the effectiveness of water-filled canals in reducing debris impact and debris loading on coastal infrastructure, given that canals can substantially decrease bore momentum and the intensity of the initial impact.
- Consider a broader range of structural configurations, including different column shapes, sizes, spacing, and arrangements, as well as varying distances from the canal, to evaluate the robustness and scalability of canal-based mitigation strategies.
- Future studies are recommended to employ OpenFOAM as an alternative open-source computational fluid dynamics (CFD) platform to further investigate tsunami bore–canal–structure interactions. This would allow comparison of numerical performance, turbulence modeling approaches, and computational efficiency with commercial solvers such as FLOW-3D.
- The presence of the water-filled canal induces non-uniform vertical velocity profiles downstream of the canal. Therefore, the use of Ultrasonic Velocity Profilers (UVP) in future experimental studies is strongly recommended to obtain high-resolution velocity measurements along the water depth and to improve understanding of post-canal flow hydrodynamics and momentum redistribution.

- Utilize PIV measurements to capture detailed velocity fields and turbulence characteristics of tsunami-like bores interacting with water-filled canals, enabling improved validation of numerical models and refined interpretation of force-reduction mechanisms.

Advancing these research areas will strengthen the technical basis for canal-based tsunami mitigation and support more reliable, practical applications in coastal engineering. Progress in these topics will ultimately enhance coastal resilience and improve the protection of communities and infrastructure.

References

Adityawan, M. B., & Tanaka, H. (2016). Investigating the 2011 Tsunami Impact on the Teizan Canal and the Old River Mouth in Sendai Coast. *Springer Link*, 125–136. doi: 10.1007/978-3-319-28528-3_9

Al-Faesly T, Palermo D, Nistor I, Cornett A (2012) Experimental modeling of extreme hydrodynamic forces on structural models. Int J Prot Struct 3:477–505. https:// doi. org/ 10. 1260/ 2041- 4196.3. 4. 477

American Society of Civil Engineers (ASCE). (2022). *Minimum design loads and associated criteria for buildings and other structures (ASCE/SEI 7-22)*. Reston, VA: American Society of Civil Engineers.

Asadollahi, N., Nistor, I., & Mohammadian, A. (2019a). Numerical investigation of tsunami bore effects on structures, part I: drag coefficients. *Natural Hazards*, 96(1), 309–330. https://doi.org/10.1007/s11069-018-3542-2

Asadollahi, N., Nistor, I., & Mohammadian, A. (2019b). Numerical investigation of tsunami bore effects on structures, part II: effects of bed condition on loading onto circular structures. *Natural Hazards*, 96(1), 331–351. https://doi.org/10.1007/s11069-018-3544-0

Aureli, F., Maranzoni, A., Petaccia, G., & Soares-Frazão, S. (2023). Review of experimental investigations of dam-break flows over fixed bottom. *Water*, 15(6), 1229. https://doi.org/10.3390/w15061229

Bremm, G. C., Goseberg, N., Schlurmann, T., & Nistor, I. (2015). Long wave flow interaction with a single square structure on a sloping beach. *Journal of Marine Science and Engineering*, *3*(3), 821–844. https://doi.org/10.3390/jmse3030821

Burcharth, H.F., Hughes, A.S. (2003). Types and functions of coastal structures. In: Coastal engineering manual, vol. 6, Coastal Engineering Research Center, pp VI-2-i–VI-2–44.

CCH (City and County of Honolulu). (2000). "City and County of Honolulu building code." Chapter 16, Article 11, Honolulu, HI.

Chanson, H. (2006). Tsunami surges on dry coastal plains: Application of dam break wave equations, Coastal Engineering J. 48(4), 355-370.

Chanson, H. (2009). "Application of the method of characteristics to the dam break wave problem." J. Hydraul. Res., 47(1), 41–49.

Chock, G., Robertson, I., Kriebel, D., Francis, M., & Nistor, I. (2013). *Tohoku, Japan, Earthquake and Tsunami of 2011: performance of structures under tsunami loads*. American Society of Civil Engineers.

Dao. N.X., Adityawan, M.B., Tanaka, H., Lin, P., (2013a). Effectiveness of a Shore-parallel Canal to Reduce Tsunami Impact. *Proceedings of the 35th IAHR World Congress (Chengdu, 2013).*

Dao. N.X., Adityawan, M.B., Tanaka, H. (2013b). Sensitivity Analysis of Shore-parallel Canal for Tsunami Wave Energy Reduction. Journal of Japan Society of Civil Engineers, Ser. B3 (Ocean Engineering), Vol. 69, No. 2, I_401-I_406, 2013.

Dias, P., Dissanayake, R., Chandratilake, R., 2006. Lessons Learned from Tsunami Damage in Sri Lanka. pp. 74–81.

Dias, F., Dutykh, D., O'Brien, L., Renzi, E., & Stefanakis, T. (2014). On the modelling of tsunami generation and tsunami inundation. *Procedia IUTAM*, *10*, 338–355. https://doi.org/10.1016/j.piutam.2014.01.029

Elsheikh, N., Azimi, A. H., Nistor, I., & Mohammadian, A. (2020). Experimental Investigations of Hydraulic Surges Passing over a Rectangular Canal. *Journal of Earthquake and Tsunami*, *14*(5). https://doi.org/10.1142/S1793431120400047

Elsheikh, N., Nistor, I., Azimi, A. H., & Mohammadian, A. (2022a). Tsunami-Induced Bore Propagating over a Canal, Part I: Laboratory Experiments and Numerical Validation. *Fluids*, *7*(7). https://doi.org/10.3390/fluids7070213

Elsheikh, N., Azimi, A. H., Nistor, I., & Mohammadian, A. (2022b). Tsunami-Induced Bores Propagating over a Canal, Part II: Numerical Experiments Using the Standard *k-ε* Turbulence Model. *Fluids*, *7*(7). https://doi.org/10.3390/fluids7070214

Esteban, M., Thao, N. D., Takagi, H., Jayaratne, R., Mikami, T., & Shibayama, T. (2015). Stability of breakwaters against Tsunami attack. In *Handbook of Coastal Disaster Mitigation for Engineers and Planners* (pp. 293–323). Elsevier Inc. https://doi.org/10.1016/B978-0-12-801060-0.00015-0

FEMA. (2001). "Coastal construction manual: Principles and practices of planning, siting, designing, constructing, and maintaining residential buildings in coastal regions." FEMA 55, Washington, DC.

FEMA P-646. Guidelines for Design of Structure for Vertical Evacuation from Tsunamis, Third ed. (2019); Federal Emergency Management Agency: Redwood, CA, USA.

Fraser, S., Leonard, G., Matsuo, I., Murakami, H., 2012. Tsunami Evacuation: Lessons from the Great East Japan Earthquake and Tsunami of March 11th, 2011. GNS Science.

Ghodoosipour, B., Stolle, J., Nistor, I., Mohammadian, A., & Goseberg, N. (2019). Experimental study on extreme hydrodynamic loading on pipelines. Part 1: Flow hydrodynamics. *Journal of Marine Science and Engineering*, *7*(8). https://doi.org/10.3390/jmse7080251

Goltz J, Yamori K (2020). Tsunami preparedness and mitigation strategies. In: Goltz J, Yamori K (eds) Oxford research encyclopedia of natural hazard science. Oxford University Press. https://doi.org/10.1093/acrefore/9780199389407.013.324

GoPro, Inc. (2025). GoPro Quik [Mobile app]. Available from https://gopro.com/en/ca/shop/quik-app-video-photo-editor

Hanzawa, M., Matsumoto, A. (2015). Stability and disaster mitigation effect of wave-dissipating concrete blocks of detached breakwaters against tsunami waves. In: Esteban M, Takagi H, Shibayama T (eds) Handbook of coastal disaster mitigation for engineers and planners. Elsevier, pp 325–347. https://doi.org/10.1016/B978-0-12-801060-0.00016-2

Hayashi, S., Koshimura, S., 2013. The 2011 Tohoku tsunami flow velocity estimation by the aerial video analysis and numerical modeling. J. Disaster Res. 8 (4), 561–572.

Huang, J. X., Qu, K., Li, X. H., & Lan, G. Y. (2022). Performance Evaluation of Seawalls in Mitigating a Real-World Tsunami Wave Using a Nonhydrostatic Numerical Wave Model. *Journal of Marine Science and Engineering*, *10*(6). https://doi.org/10.3390/jmse10060796

Inagaki, N., Nishida, Y., Mikami, T., Nakamura, R., Nistor, I., Soltanpour, M., Goseberg, N., & Shibayama, T. (2025). Field survey of the 2024 Noto Peninsula Earthquake and Tsunami in Japan: Characteristics of damage patterns to coastal communities. *Ocean Engineering*, *316*. https://doi.org/10.1016/j.oceaneng.2024.119765

Jaffe, B.E., et al., 2012. Flow speed estimated by inverse modeling of sandy tsunami deposits: results from the 11 March 2011 tsunami on the coastal plain near the Sendai Airport, Honshu, Japan. Sediment. Geol. 282, 90–109.

Kathiresan K, Rajendran N (2005) Coastal mangrove forests mitigated tsunami. Estuar Coast Shelf Sci 65:601–606. https://doi.org/10.1016/j.ecss.2005.06.022

Larsen, B. E., Fuhrman, D. R., Baykal, C., & Sumer, B. M. (2017). Tsunami-induced scour around monopile foundations. *Coastal Engineering*, *129*, 36–49. https://doi.org/10.1016/j.coastaleng.2017.08.002

Lauber, G., & Hager, W. H. (1998). Experiments to dambreak wave: Horizontal channel. *Journal of Hydraulic Research*, *36*(3), 291–307. https://doi.org/10.1080/00221689809498620

Matsutomi, H., Sakakiyama, T., Nugroho, S., Matsuyama, M., (2006). Aspects of inundated flow due to the 2004 indian ocean tsunami. Coast. Eng. J. 48 (2), 167–195.

Matsutomi, H., and Okamoto, K. (2010). “Inundation flow velocity of tsunami on land.” Isl. Arc, 19(3), 443–457.

Matuo, H. (1934). Experimental investigation on prevention of damage of tsunami. Tokyo Daigaku Jishin Kenkyusho Iho (Bull Earthq Res Inst Univ Tokyo) Suppl. 1:65–76

McGovern, D. J., Allsop, W., Rossetto, T., & Chandler, I. (2023). Large-scale experiments on tsunami inundation and overtopping forces at vertical sea walls. *Coastal Engineering*, *179*. https://doi.org/10.1016/j.coastaleng.2022.104222

Mikami, T., Kinoshita, M., Matsuba, S., Watanabe, S., Shibayama, T. (2015). Detached breakwaters effects on tsunamis around coastal dykes. Proc Eng 116:422–427. https://doi.org/10.1016/j.proeng.2015.08.307

Murty, T. S. (1977). Seismic sea waves: Tsunamis, Dept. of Fisheries and the Environment Fisheries and Marine Service, Ottawa.

Nateghi, R., Bricker, J.D., Guikema, S.D., Bessho, A. (2016). Statistical analysis of the effectiveness of seawalls and coastal forests in mitigating tsunami impacts in Iwate and Miyagi prefectures. PLoS ONE 11:e0158375. https://doi.org/10.1371/journal.pone.0158375

National Geophysical Data Center / World Data Service: NCEI/WDS Global Historical Tsunami Database. NOAA National Centers for Environmental Information. doi:10.7289/V5PN93H7

Nistor, I., Palermo, D., Nouri, Y., Murty, T., & Saatcioglu, M. (2009). Tsunami-induced forces on structures. In *Handbook of Coastal and Ocean Engineering* (pp. 261–286). World Scientific Publishing Co. https://doi.org/10.1142/9789812819307_0011

Nouri, Y., Nistor, I., Palermo, D., & Cornett, A. (2010). Experimental investigation of tsunami impact on free standing structures. *Coastal Engineering Journal*, *52*(1), 43–70. https://doi.org/10.1142/S0578563410002117

Oetjen, J., Sundar, V., Venkatachalam, S., Reicherter, K., Engel, M., Schüttrumpf, H., & Sannasiraj, S. A. (2022). A comprehensive review on structural tsunami countermeasures. In *Natural Hazards* (Vol. 113, Issue 3, pp. 1419–1449). Springer Science and Business Media B.V. https://doi.org/10.1007/s11069-022-05367-y

Palermo, D., Nistor, I., Nouri, Y., & Cornett, A. (2009). Tsunami loading of near-shoreline structures: A primer. *Canadian Journal of Civil Engineering*, *36*(11), 1804–1815. https://doi.org/10.1139/L09-104

Rahman, S., Akib, S., Khan, M. T. R., & Shirazi, S. M. (2014). Experimental study on tsunami risk reduction on coastal building fronted by sea wall. *The Scientific World Journal*, *2014*. https://doi.org/10.1155/2014/729357

Rahman, M.M., Schaab, C., Nakaza, E., (2017). Experimental and numerical modeling of tsunami mitigation by canals. J Waterw Port Coast Ocean Eng 143:4016012. https://doi.org/10.1061/(ASCE)WW.1943-5460.0000355

Ramalingeswara, R. B., Vijayaraghavan, D., Sarma, S. D., and Satyanarayanan, M. (2005). "Buckingham Canal saved people in Andhra Pradesh (India) from the tsunami of 26 December

2004." Paper to be presented at the Asia Oceania Geosciences Society, 2nd Ann. Meeting and Conf., Suntec, Singapore (June 20–24, 2005).

Rao, B.R., (2005). Buckingham Canal saved people in Andhra Pradesh (India) from the tsunami of 26 December 2004. Curr Sci 89:12–13

Reuters (2018) Seven years after tsunami, Japanese live uneasily with seawalls. URL: https://www.reuters.com/article/us-japan-disaster-seawalls/seven-years-after-tsunami-japanese-live-uneasily-with-seawalls-idUSKCN1GL0DK. (Accessed 05 February 2020)

Ritter, A. (1892). "Die fortpflanzung der wasserwellen." Zeitschrift des Verein Deutscher Ingenieure, 36, 947–954.

Röbke, B. R., & Vött, A. (2017). The tsunami phenomenon. In *Progress in Oceanography* (Vol. 159, pp. 296–322). Elsevier Ltd. https://doi.org/10.1016/j.pocean.2017.09.003

Rossetto, T., et al., 2007. The Indian Ocean tsunami of December 26, 2004: observations in Sri Lanka and Thailand. Nat. Hazards 42 (1), 105–124.

Samarasekara RSM, Sasaki J, Esteban M, Matsuda H (2017) Assessment of the co-benefits of structures in coastal areas for tsunami mitigation and improving community resilience in Sri Lanka. Int J Disaster Risk Red 23:80–92. https://doi.org/10.1016/j.ijdrr.2017.04.011

Shafiei, S., Melville, B. W., & Shamseldin, A. Y. (2016). Experimental investigation of tsunami bore impact force and pressure on a square prism. *Coastal Engineering*, *110*, 1–16. https://doi.org/10.1016/j.coastaleng.2015.12.006

Suppasri, A., et al., 2012. Damage charachteristic and field survey of the 2011 great east Japan tsunami in Miyagi prefecture. Coast. Eng. J. 54 (1), 1250005-1–1250005-30.

Tanaka, N., Igarashi, Y., & Zaha, T. (2021). Numerical investigation of the effectiveness of vegetation-embankment hybrid structures for tsunami mitigation introduced after the 2011 Tsunami. *Geosciences (Switzerland)*, *11*(11). https://doi.org/10.3390/geosciences11110440

Teh, S. Y., Koh, H. L., Liu, P. L. F., Ismail, A. I. M., & Lee, H. L. (2009). Analytical and numerical simulation of tsunami mitigation by mangroves in Penang, Malaysia. *Journal of Asian Earth Sciences*, *36*(1), 38–46. https://doi.org/10.1016/j.jseaes.2008.09.007

Usman F, Murakami K, Kurniawan EB (2014) Study on reducing tsunami inundation energy by the modification of topography based on local wisdom. Procedia Environ Sci 20:642–650. https://doi.org/10.1016/j.proenv.2014.03.077

Watanabe, S., Mikami, T., & Shibayama, T. (2016). Laboratory study on tsunami reduction effect of Teizan Canal. In Proceedings of the 6th International Conference on the Application of Physical Modelling in Coastal and Port Engineering and Science (Coastlab16), Ottawa, Canada, May 10–13, 2016, pp. 1–6.

Wüthrich, D., Pfister, M.; Nistor, I., & Schleiss, A. J. (2018a). Experimental Study of Tsunami-Like Waves Generated with a Vertical Release Technique on Dry and Wet Beds. J. Waterway, Port, Coastal, Ocean Eng. https://doi.org/10.1061/(ASCE)WW.1943

Wüthrich, D., Pfister, M., Nistor, I., & Schleiss, A. J. (2018b). Experimental study on the hydrodynamic impact of tsunami-like waves against impervious free-standing buildings. *Coastal Engineering Journal*, *60*(2), 180–199. https://doi.org/10.1080/21664250.2018.1466676

Appendix A: Supplementary Discussion on Physical Modelling

A.1 Introduction

This appendix provides supplementary material to complement Chapter 3 of the thesis, addressing several important topics that require further elaboration.

A.2 Similarity Laws and Dimensional Analysis

Physical hydraulic models of tsunami events are almost universally governed by Froude similarity. The Froude number (Fr) is the ratio of inertial to gravitational forces and is defined as:

$$Fr = U / \sqrt{(g \cdot h)}$$

where U is the flow velocity, g is gravitational acceleration, and h is the local flow depth. Froude similarity ensures that the ratio of inertial forces to gravity forces is preserved between model and prototype. This is the appropriate governing criterion for free-surface, gravity-driven flows such as tsunami bores, where gravitational effects dominate the wave propagation dynamics. In this study, experiments were conducted at a geometric scale of λ = 1:10. Under Froude scaling, the relationships for the primary physical quantities are as follows:

Length: $L_m = L_p / \lambda$

Velocity: $U_m = U_p / \lambda^{0.5}$

Time: $T_m = T_p / \lambda^{0.5}$

Force: $F_m = F_p / \lambda^3$

Depth: $h_m = h_p / \lambda$

Discharge: $Q_m = Q_p / \lambda^{(5/2)}$

where the subscripts m and p denote model and prototype quantities, respectively. These relationships were applied to scale the experimental water impoundment depth (40 cm in the model) and canal dimensions to their prototype equivalents (4 m impoundment depth; canal widths 10-40 m; canal depths 0.5-4.5 m).

A definition relevant to surge propagation is the surge Froude number, which accounts for the surge front celerity as observed from the channel bank:

$$Fr_s = (V + U) / \sqrt{(g \cdot D)}$$

where V is the depth-averaged flow velocity in the channel, U is the surge front celerity (speed of the bore front), and D is the surge depth. A fully developed positive surge of this type is also known as a hydraulic jump in translation. These definitions are consistent with classical surge theory (Chanson, 2006) and provide a physically meaningful non-dimensional characterisation of the bore that can be directly compared between model and prototype scales, and across studies conducted at different scales.

Reynolds number similarity, which preserves the ratio of inertial to viscous forces ($Re = UL/\nu$, where ν is the kinematic viscosity of water), cannot be simultaneously satisfied with Froude similarity in a scaled physical model unless the model fluid properties are adjusted, which is impractical for water-based experiments.

The most significant scale effect in this study relates to the dissipation of turbulent kinetic energy within and downstream of the canal. In the physical model, the Reynolds number during bore-canal interaction was of the order $Re \approx 10^4$–10^5, while at prototype scale it would be $Re \approx 10^6$–10^7. At lower Reynolds numbers, the turbulent energy cascade is compressed and dissipation occurs more rapidly, meaning that the model may slightly overestimate energy losses compared to the prototype. The practical consequence is that prototype-scale canals may exhibit somewhat less energy dissipation per unit volume than suggested by the scaled experiments alone, a conservative outcome from a design perspective.

The numerical comparison between 1:10 and 1:1 scale simulation presented in Section 4.4.1 of the thesis provides direct quantitative evidence of scale effects. The results demonstrated good agreement between scales, with the most notable discrepancy occurring for bore depth and force time histories in the presence of the canal. These differences are attributed primarily to the scale-dependent turbulent dissipation associated with bore-canal interaction and are consistent with expected Reynolds number effects.

A.3 Comparison with Previous Experimental Studies

A systematic comparison of the results of this study with those of previous experimental investigations provides important context for evaluating the physical findings and situating the contributions within the existing body of knowledge.

A.3.1 Bore Propagation and Velocity

The bore front velocities measured in this study are consistent with those reported by Nouri et al. (2010) and Al-Faesly et al. (2012). The relationship between bore front velocity and water impoundment depth follows the theoretical dam-break solution (Chanson, 2006), with a coefficient α of approximately 1.2 in this study, consistent with the range compiled from multiple studies in the literature.

A.3.2 Force on a Square Column

The time history of bore-induced force on a square column measured in this study is qualitatively consistent with the force pattern described by Nistor et al. (2009). The magnitude of the peak force per unit bore depth and velocity squared is consistent with values reported by Shafiei et al. (2016) and Wuthrich et al. (2018b) for similar square prism geometries and comparable bore Froude numbers. Although a considerable number of studies have investigated tsunami bore interaction with structural columns, a direct comparison between the present results and those of individual studies was not feasible due to the large number of differing parameters involved, including the bore generation method, column shape, wet or dry bed conditions, and the distance of the column from the gate. Nevertheless, a general qualitative and quantitative comparison has been carried out where possible, and a more detailed comparison focusing specifically on bore propagation characteristics and hydrodynamic conditions is presented in this thesis.

A.3.3 Effect of the Canal

The primary quantitative finding of this study, that a water-filled canal reduces the peak force on a downstream column by 25–40%, is broadly consistent with the results of Rahman et al. (2017) and Elsheikh et al. (2022a, b), who also investigated tsunami bore interaction with water-filled canals. Rahman et al. (2017) reported wave height reductions of 15–30% downstream of model canals in their experimental flume, depending on canal depth and width. Elsheikh et al. (2022a) reported significant reduction in bore momentum and depth-averaged velocity downstream of the canal, with wider and deeper canals producing greater reductions, consistent with the present findings.

Appendix B: Supplementary Discussion on Numerical Modelling

This appendix provides supplementary material to complement Chapter 4 of the thesis, addressing topics in numerical modelling that require more detailed exposition than was possible within the main body of the thesis.

B.1 LES

The Large Eddy Simulation (LES) approach to turbulence modelling originated from atmospheric flow modelling. The underlying principle is that turbulent flow structures large enough to be resolved by the computational grid are computed directly, while only the sub-grid scale (SGS) motions, those too small to be captured by the mesh, are approximated through a turbulence model (Smagorinsky, 1963). It is important to note that LES is inherently three-dimensional and time-dependent, and that turbulent fluctuations must be appropriately initialised and specified at inflow boundaries. While this increases the computational cost relative to Reynolds-averaged approaches, primarily because finer meshes are required, LES provides more information about the flow field.

The mathematical foundation of LES rests on the concept of spatial filtering, which provides a formal framework for separating the resolvable large-scale turbulent motions from the unresolvable small-scale (sub-grid scale) motions. A spatial filter is applied to the instantaneous flow variables (velocity, pressure, and other transported quantities) to decompose them into a resolved (filtered) component and a residual (sub-grid scale) component.

For any flow variable $\varphi(x, t)$, the filtered (resolved) component is defined by the convolution integral:

$$\bar{\varphi}(x, t) = \int G(x - x', \Delta)\, \varphi(x', t)\, dx'$$

where $G(x - x', \Delta)$ is the filter kernel, x' is the integration variable in physical space, and Δ is the filter width, which characterises the spatial scale of the filtering operation. The residual (sub-grid scale) component is then defined as:

$$\varphi'(x, t) = \varphi(x, t) - \bar{\varphi}(x, t)$$

so that the instantaneous field is always recovered as the sum of the filtered and residual components: $\varphi = \bar{\varphi} + \varphi'$.

In practice, when LES is implemented in a finite-volume solver such as FLOW-3D, an explicit filter is not always applied. Instead, the computational grid itself acts as an implicit filter: the numerical discretization naturally cannot represent flow structures smaller than the grid cell size, so the grid spacing effectively defines the filter width. The filter width Δ is typically taken as the geometric mean of the local grid cell dimensions:

$$\Delta = (\Delta x \cdot \Delta y \cdot \Delta z)^{(1/3)}$$

This implicit grid filtering approach is the most widely used in engineering LES computations and was adopted in the present study.

Applying the spatial filter to the incompressible continuity and Navier-Stokes equations yields the LES-filtered governing equations. For an incompressible Newtonian fluid, the filtered continuity equation is:

$$\partial \bar{u}_i / \partial x_i = 0$$

and the filtered momentum equation is:

$$\partial \bar{u}_i/\partial t + \partial(\bar{u}_i\, \bar{u}_j)/\partial x_j = -(1/\rho)\, \partial \bar{p}/\partial x_i + \nu\, \partial^2 \bar{u}_i/\partial x_j \partial x_j - \partial \tau_{ij}/\partial x_j$$

where $\bar{u}_i$ is the filtered velocity vector, $\bar{p}$ is the filtered pressure, ρ is the fluid density, and ν is the kinematic viscosity. The term τ_{ij} is the sub-grid scale (SGS) stress tensor, defined as:

$$\tau_{ij} = \bar{u}_i \bar{u}_j - \bar{u}_i\, \bar{u}_j$$

This term arises directly from the filtering operation and represents the effect of the unresolved sub-grid scale motions on the resolved large-scale flow. It is important to note that τ_{ij} is not directly computable from the resolved field alone, it constitutes the closure problem of LES and must be modelled using a SGS model. The physical interpretation of τ_{ij} is that it represents the transfer of momentum and energy between the resolved large eddies and the unresolved small eddies, a process that in reality occurs through the nonlinear interactions of the turbulent velocity field across all scales.

Since the SGS stress tensor τ_{ij} cannot be computed directly from the resolved velocity field, it must be modelled. The most widely used SGS model, and the one employed in FLOW-3D, is the Smagorinsky (1963) eddy viscosity model. This model is based on the Boussinesq hypothesis,

which assumes that the deviatoric part of the SGS stress tensor is proportional to the resolved strain rate tensor:

$$\tau_{ij} - (1/3)\delta_{ij}\,\tau_{kk} = -2\nu_{SGS}\,\bar{S}_{ij}$$

where δ_{ij} is the Kronecker delta, ν_{SGS} is the SGS kinematic eddy viscosity, and $\bar{S}_{ij}$ is the filtered strain rate tensor:

$$\bar{S}_{ij} = (1/2)(\partial\bar{u}_i/\partial x_j + \partial\bar{u}_j/\partial x_i)$$

The isotropic part $(1/3)\delta_{ij}\,\tau_{kk}$ is absorbed into the modified filtered pressure and does not appear explicitly in the momentum equation. The SGS eddy viscosity is modelled as:

$$\nu_{SGS} = (C_s \cdot \Delta)^2 \cdot |\bar{S}|$$

where C_s is the Smagorinsky coefficient, typically in the range 0.1 to 0.2, and $|\bar{S}| = \sqrt{(2\bar{S}_{ij}\,\bar{S}_{ij})}$ is the magnitude of the filtered strain rate tensor. The product $C_s \cdot \Delta$ represents a mixing length at the sub-grid scale, analogous to the mixing length concept in classical turbulence theory. The SGS eddy viscosity ν_{SGS} is then incorporated into the effective dynamic viscosity used throughout FLOW-3D in the same manner as for the Reynolds-averaged turbulence transport models:

$$\mu_{eff} = \rho(\nu + \nu_{SGS})$$

The Smagorinsky model has the desirable property that $\nu_{SGS} \to 0$ as the local strain rate $\to 0$, meaning that no artificial diffusion is introduced in regions of low turbulence intensity. However, the model is known to be overly dissipative in transitional flow regions and near solid walls, where the value of C_s typically needs to be reduced. In the present study, the standard value of $C_s = 0.1$ was used, consistent with previous LES studies of free-surface hydraulic flows (Chanson, 2006; Nouri et al., 2010).

B.2 Volume of Fluid (VOF) Method

The Volume of Fluid (VOF) method is the free-surface tracking approach employed in FLOW-3D. It was originally proposed by Hirt and Nichols (1981) and remains one of the most widely used interface-capturing methods in computational hydraulics. The VOF method defines a scalar function *F* (x, t), called the fluid fraction or volume fraction, which represents the fraction of each computational cell occupied by the primary fluid (water):

$F = 1$ (cell fully occupied by water)

$0 < F < 1$ (cell contains the water-air interface)

$F = 0$ (cell fully occupied by air)

The volume fraction F is transported with the flow according to the advection equation:

$$\partial F/\partial t + u_i \, \partial F/\partial x_i = 0$$

This equation states that F is conserved following a fluid parcel. In FLOW-3D, a specialised FAVOR™ (Fractional Area/Volume Obstacle Representation) technique is used in conjunction with VOF to accurately represent complex solid boundaries within the Cartesian mesh. The FAVOR approach defines fractional open areas and volumes for each cell face and cell body, allowing accurate representation of curved or inclined solid surfaces without requiring body-fitted meshes.